

Spring 2015

Large scale modeling, model reduction and control design for a real-time mechatronic system

Qiong Li
Purdue University

Follow this and additional works at: https://docs.lib.purdue.edu/open_access_dissertations



Part of the [Electrical and Computer Engineering Commons](#), and the [Mechanical Engineering Commons](#)

Recommended Citation

Li, Qiong, "Large scale modeling, model reduction and control design for a real-time mechatronic system" (2015). *Open Access Dissertations*. 502.
https://docs.lib.purdue.edu/open_access_dissertations/502

This document has been made available through Purdue e-Pubs, a service of the Purdue University Libraries. Please contact epubs@purdue.edu for additional information.

PURDUE UNIVERSITY
GRADUATE SCHOOL
Thesis/Dissertation Acceptance

This is to certify that the thesis/dissertation prepared

By Qiong Li

Entitled

LARGE SCALE MODELING, MODEL REDUCTION AND CONTROL DESIGN
FOR A REAL -TIME MECHATRONIC SYSTEM

For the degree of Doctor of Philosophy

Is approved by the final examining committee:

Haiyan H.Zhang

Chair

Richard M.French

Xiumin Diao

Ayhan Ince

To the best of my knowledge and as understood by the student in the Thesis/Dissertation Agreement, Publication Delay, and Certification Disclaimer (Graduate School Form 32), this thesis/dissertation adheres to the provisions of Purdue University's "Policy of Integrity in Research" and the use of copyright material.

Approved by Major Professor(s): Haiyan H.Zhang

Approved by: Kathryne A Newton

Head of the Departmental Graduate Program

4/16/2015

Date

LARGE SCALE MODELING, MODEL REDUCTION AND CONTROL DESIGN
FOR A REAL –TIME MECHATRONIC SYSTEM

A Dissertation
Submitted to the Faculty
of
Purdue University
by
Qiong Li

In Partial Fulfillment of the
Requirements for the Degree
of
Doctor of Philosophy

May 2015
Purdue University
West Lafayette, Indiana

For my parents

ACKNOWLEDGEMENTS

I would never have been able to finish my dissertation without the guidance of Professor Haiyan Zhang and other committee members, help from friends, and support from my family.

I would like to express my deepest gratitude to my advisor, Professor Haiyan Zhang, for his excellent guidance based on his broad knowledge in multiple disciplines, caring in helping me to find funding to support my research, and patience to encourage me to make progress. I would also like to thank Professor Mark French and Professor Nancy Denton for their helps in my PhD study in the past several years. Special thanks go to Professor Ayhan Ince and Professor Xiumin Diao, who are willing to join my defense committee at the last minute.

I would want to present my great appreciation to the Pence family, who treated me as their family member and provided me a wonderful experience in my life. At last, I would like to thank my parents who gave me the biggest support and encouragement in my way to pursuit the PhD degree.

TABLE OF CONTENTS

	Page
LIST OF TABLES	vii
LIST OF FIGURES	viii
ABSTRACT	xi
CHAPTER 1. INTRODUCTION.....	1
1.1 Definition of Mechatronics	1
1.2 Large Scale Modeling of Mechatronic System	3
1.3 Modeling for Two-wheeled Self-balancing Scooter	4
CHAPTER 2. VARITIONAL METHOD FOR MULTIDISCIPLINARY SYSTEM ..	7
2.1 Systematic Modeling Methods	7
2.2 Effort Variable and Flow Variable	9
2.3 Stored Energy and Co-Energy.....	10
2.4 Energy Dissipators.....	14
2.5 Energy Converters and Energy Couplers.....	15
2.6 Compatibility and Continuity Constraints for Multiphysics System.....	17
2.7 Variational Method Used in The Unified Energy Based Framework	19
CHAPTER 3. MATHEMATICAL MODELING OF TWO-WHEELED SELF-BALANCING SCOOTER.....	27
3.1 Mechanical System Modeling	28
3.1.1 Tractive force	30
3.1.2 Rolling resistance	33
3.1.3 Grading resistance	39
3.1.4 Resistance to acceleration.....	43
3.2 Dynamic modeling by variational method.....	50

	Page
3.3 Electrical System Modeling	53
3.3.1 Modeling of motor drive.....	53
3.3.2 Modeling of motor.....	59
3.3.3 Modeling of Inertial Measurement Unit	63
3.3.3.1 Modeling of accelerometers.....	64
3.3.3.2 Modeling of Gyroscope	69
3.3.4 Sensor fusion.....	73
3.3.5 Modeling of electromagnetic relay	77
3.3.6 Modeling of optical encoder	80
3.3.7 Modeling of microprocessor system	82
3.3.7.1 Modeling of microprocessor	82
3.3.7.2 Modeling of DAC.....	85
3.3.7.3 Modeling of ADC.....	87
3.3.7.4 CompactRio system.....	90
3.4 State space modeling for scooter drivetrain system	94
CHAPTER 4. MODEL ORDER REDUCTION TECHNIQUE.....	106
4.1 Introduction	106
4.2 Continued fraction expansions	107
4.2.1 Caucer First Form.....	109
4.2.2 Caucer Second Form	110
4.2.3 Routh approximation technique	110
4.3 Generalized Routh Algorithm	117
4.4 State space formulation of routh algorithm and other related forms.....	121
4.5 Model Reduction for Two-wheeled Self-balancing Scooter.....	128
4.6 Determination of scooter parameters.....	131
CHAPTER 5. SIMULATION, EXPERIMENT AND CONCLUSION	136
5.1 Simulation and experiment	136
5.2 Conclusion.....	140

	Page
LIST OF REFERENCES.....	142
VITA.....	146

LIST OF TABLES

Table	Page
2.1 Effort accumulation and flow accumulation variables in various systems	19
4.1 α (Routh) Table	112
4.2 β (Routh) Table	113
4.3 The expansion of Routh array	118

LIST OF FIGURES

Figure	Page
1.1 Mechatronics: synergetic integration of multiple disciplines	1
2.1 Ideal energy source elements	10
2.2 Stored energy and co-energy	12
2.3 Stored energy and co-energy	16
2.4 Flow and effort laws	18
2.5 Parallel system.....	21
3.1 CAD model of two-wheeled self-balancing scooter.....	29
3.2 Analysis of tractive force	31
3.3 Deformation vs. force curve.....	34
3.4 The deflection and rolling resistance analysis on rigid road surface.....	36
3.5 Two dimensional roadway model.....	40
3.6 Force analysis of rolling wheel on slope.....	42
3.7 The force and torque at acceleration moment of driving wheel.....	44
3.8 Force and torque at acceleration moment of cart and rider.....	46
3.9 Modeling of scooter-rider system on slope.....	51
3.10 30A8DD analog servo drive.....	54
3.11 Block diagram of 30A8DD analog servo drive.....	55
3.12 H-bridge motor drive circuit.....	55

Figure	Page
3.13 The drain current flow i_D VS the drain-to-source voltage V_{DS}	57
3.14 The drain current flow i_D versus the gate-to-source voltage V_{GS}	58
3.15 Large-signal equivalent circuit model of n-channel MOSFET in saturation region .	59
3.16 T-64 NPC DC motor.....	60
3.17 Schematic diagram of DC motor	60
3.18 Torque-speed characteristic of DC motor	63
3.19 ADXL203/ADXRS300 Combo IMU board	64
3.20 Mechanical model of accelerometer	64
3.21 Functional block diagram of ADXL203	67
3.22 Structure of differential capacitor	67
3.23 Mechanical model of vibrational gyroscope	69
3.24 Block diagram with external components of ADXRS300.....	71
3.25 RATEOUT vs. RATEIN Curve for ADXRS300	72
3.26 Block diagram of complementary filter for accelerometer and gyroscope.....	74
3.27 Bode plot and phase over frequency diagram for Low and high pass filter	76
3.28 Simple schematics of electromagnetic relay schematics	77
3.29 Basic structure of incremental encoder.....	81
3.30 Encoder wave form for clockwise and counter-clockwise rotation.....	82
3.31 Basic structure and data exchange for general microprocessor.....	83
3.32 Simplified block diagram of n bits DAC	86
3.33 Ideal transfer curve of DAC	87
3.34 Simplified block diagram of n bits ADC	88

Figure	Page
3.35 Ideal transfer curve of ADC	90
3.36 NI cRIO-9014 Real-time controller	91
3.37 Reconfigurable FPGA chassis	91
3.38 I/O modules	91
3.39 Architecture of the CompactRIO system of two-wheeled self-balancing scooter	93
3.40 Architecture of the Comprehensive system of two-wheeled self-balancing scooter.	94
4.1 Block digram of feedback system	121
4.2 Detailed block digram of feedback system	122
4.3 Generalized block diagram in Cauer third form.....	123
4.4 Block diagram for $n=4$	123
4.5 Real structure and dimensions of rob and wheels (side views).....	131
5.1 Inside structure of two-wheeled self-balancing scooter.....	136
5.2 Scooter FPGA program panel on Labview	137
5.3 Scooter host program panel.....	138
5.4 Encoder for wheels	138
5.5 Gyro rate and acceleration input.....	139
5.6 PWM output	139
5.7 Host program block digram.....	139
5.8 Riding on the scooter	140

ABSTRACT

Li, Qiong . Ph.D., Purdue University, May 2015. Large Scale Modeling, Modeling Reduction and Control Design for a Real-time Mechatronic System. Major Professor: Haiyan H. Zhang.

Mechatronics is the synergistic integration of the techniques from mechanical engineering, electrical engineering and information technology, which influences each other mutually. As a multidisciplinary domain, mechatronics is more than mechanical or electronics, and the mechatronic systems are always composed of a number of subsystems with various controllers. From this point of view, a lot of such systems can be defined as large scale system. The key element of such systems is integration. Modeling of mechatronic system is a very important step in developing control design of such products, so as to simulate and analyze their dynamic responses for control design, making sure they would meet the desired requirements. The models of large scale systems are always resulted in complex form and high in dimension, making the computation for modeling, simulation and control design become very complicated, or even beyond the solutions provided by conventional engineering methods. Therefore, a simplified model obtained by using model order reduction technique, which can preserve the dominant physical parameters and reveal the performance limiting factor, is preferred.

In this dissertation, the research have chosen the two-wheeled self-balancing scooter as the subject of the study in research on large scale mechatronic system, and

efforts have been put on developing a completed mathematical modeling method based on a unified framework from variational method for both mechanical subsystem and electrical subsystem in the scooter. In order to decrease the computation efforts in simulation and control design, Routh model reduction technique was chosen from various model reduction techniques so as to obtain a low dimensional model. Matlab simulation is used to predict the system response based on the simplified model and related control design. Furthermore, the final design parameters were applied in the physical system of two-wheeled self-balancing scooter to test the real performance so as to finish the design evaluation. Conclusion was made based on these results and further research directions can be predicted

CHAPTER 1. INTRODUCTION

1.1 Definition of Mechatronics

Mechatronics is the synergistic integration of the techniques from mechanical engineering, electrical engineering and information technology, which influences each other mutually. Figure 1.1 describes the interrelationship between these areas. As is shown, it consists of three overlapping circles and the junction area in the middle forms mechatronics.

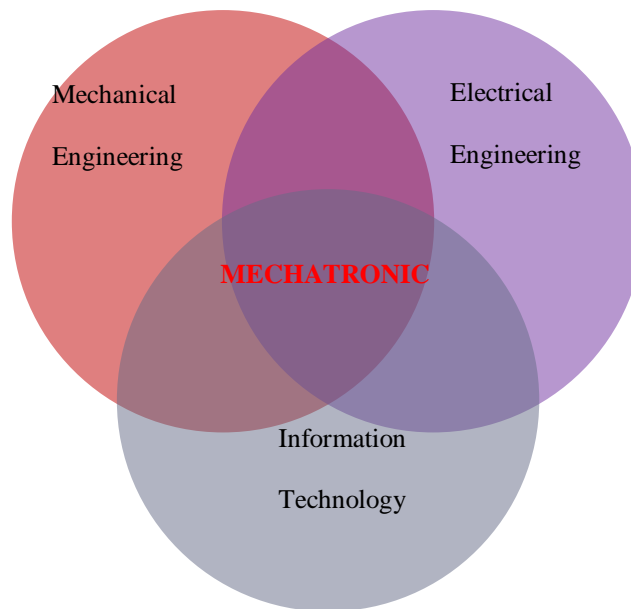


Figure 1.1 Mechatronics: synergetic integration of multiple disciplines

In general, mechanical engineering focuses on the analysis of motions, forces or torques to figure out variables such as displacements, velocities or forces. Simple feedforward and feedback control systems have been developed long time ago by using analog devices to manipulate designed variables, but it can only realize very limited control functions. With the introduction of digital computers into control systems, not only the system becomes more flexible and more comprehensive to be able to deal with various control functions can be processed, but also the precision of system is highly improved.

The following example can explain how the mechatronic system can be formed. Generally speaking, a machine set is mainly composed of two parts: a power-generating machine and a power-consuming machine. The power electronics, commonly called actuators enables the manipulated input of energy flow feed into the power-generating machine, such as a DC motor, while the drive train builds the connection between the power-generating machine and power-consuming machine, obtaining the desired energy output measured by corresponding sensors. There are basically three types of energy flows handled: electrical energy, mechanical energy and hydraulic energy. If this system is integrated with information processing subsystem enabling the communication between the input and output, automatically handling data based on the manipulated variables and measured variables in a feedback or feedforward way, a mechatronic system is formed.

The term mechatronics was coined by a Japanese engineer Tetsuro Mori in 1969, by combining the mecha-from mechatronic and –tronics from electronics to describe the electronic control systems for mechanical factory equipment built by Yaskawa Electric

Corporation. Different literatures gave several definitions for this new term, and all of them pointed out that mechatronics is a multidisciplinary field of mechanical engineering, electrical engineering and information technology. Moreover, the first mechatronic systems appeared in 1980s, with the realization of integrating the mechanical system, sensors, actuators and microcontrollers. Examples of first generation mechatronic products are the anti-lock braking systems, cameras, printers and disk storage, etc.

1.2 Large Scale Modeling of Mechatronic System

As a multidisciplinary domain, mechatronics is more than mechanical or electronics, and the mechatronic systems are always composed of a number of subsystems with various controllers. From this point of view, a lot of such systems can be defined as large scale system. The key element of such systems is integration, consisting both horizontal integration from various disciplines and vertical integration from design to manufacturing. Thus, a simultaneous engineering is recommended for mechatronic system design, and an overall integrated multidisciplinary modeling has to take place, in order to create sophisticated control functions.

Modeling of mechatronic system is a very important step in developing control design of such products, so as to simulate and analyze their dynamic responses, making sure they would meet the desired requirements. The physical mechatronic system basically includes sensors, actuators, electrical components, and embedded digital control systems. The focus of the modeling method is on the development of a unified framework for the multidisciplinary system in recent years. In 1950s and 1960s, the

network-based modeling method was applied in mechanical domain, which is originally used in electrical circuit. Meanwhile, variational modeling method, such as Lagrangian and Hamiltonian function, was extended to electrical networks from mechanical domain. Evolving from this, the network representation of subsystems builds up the basics mechatronic systems modeling methods in current days.

The models of large scale systems are always resulted in complex form and high in dimension, making the computation for modeling, simulation and control design become very complicated, or even beyond the solutions by conventional engineering methods. Furthermore, as a simultaneous engineering design, system optimization is required to find out the best way to realize all the design specification from various disciplines. In order to make optimized control design for mechatronic system. Therefore, a simplified model obtained by using model order reduction technique, which can preserve the dominant physical parameters and reveal the performance limiting factor, is preferred.

1.3 Modeling for Two-wheeled Self-balancing Scooter

In this dissertation, the two-wheeled self-balancing scooter is chosen as a real-time mechatronic system for the research object. In recent years, it has drawn great interests in both robotics field and mechatronic filed. The first two-wheeled self-balancing robot was proposed in 1986 in Japan. Because of this inspiration, nowadays, similar robots are designed, and they trends to be compact and smart mechatronic system.

Commercial available product of such system is developed by Segway, which can be used in transportation, entertainment, and automation.

As a naturally unstable system, it is very similar to an inverted mobile pendulum in its main mechanical structure. Therefore, a simplified model for the two-wheeled self-balancing scooter is broadly used for modeling, simulation and control design, based on the simplification of the scooter mechanical structure, in which the scooter is treated as an inverted pendulum structure system in mathematical modeling. In such modeling method, the tires of the scooter are considered as rigid objects without deformation, and all the dynamics in electrical subsystem is neglected. Various control methods have been proposed, such as fuzzy control, Lyapunov control and linear state feedback control. Generally speaking, these conventional methods focus on modeling of the main mechanical parts and corresponding control design so as to compensate the imperfection of the modeling process.

Thus the unified modeling method combined both mechanical subsystems and electrical subsystems has not been raised much attention. Moreover, since the resulted model from such method is way more complicated and high in dimension, the research on its corresponding model reduction technique for such model is still a blank area.

In this dissertation, the the two-wheeled self-balancing scooter has been chosen as the subject of the study in research on the large scale mechatronic system, and efforts have been put on developing a completed mathematical modeling method based on a unified framework from variational method for both mechanical subsystem and electrical subsystem in the scooter. In order to decrease the computation efforts in simulation and control design, Routh model reduction technique was chosen from various model

reduction techniques so as to obtain model with lower dimension than the original model Matlab simulation is used to predict the system responses based on the simplified model and corresponded control design. Furthermore, the experiment of the final design in the real physical system of two-wheeled self-balancing scooter was conducted to verify the accuracy of the model through the real performance so as to finish the design evaluation. Conclusion was made based on these results and limitations and directions for future research were discussed in detail.

CHAPTER 2. VARITIONAL METHOD FOR MULTIDISCIPLINARY SYSTEM

2.1 Systematic Modeling Methods

Mathematical modeling is an important tool to describe the dynamic behaviors of a system using a number of important principles with physical variables, such as velocity and force, angular speed and torque in mechanical systems, current and voltage in electrical system, flow rate and pressure in hydraulic system.

There are several systematic modeling methods, including network method, which is rooted in electrical circuit studies, variational method, which stems from Hamilton and Lagrange equations of motion, and bond graph methods, which graphically illustrate the system energy interactions. All of these methods are based on energy analysis, and each of them has its own uniqueness. Network method establishes systems by connected linear graphs using oriented line segments as system elements, which represent the power flow of energy sources. Based on the interconnective constraints, such as flow continuity constraint and energy compatibility constraint, it builds up different constraint matrices to complete the state space modeling of systems. From the graph formed with connected lines, the system modeling can be derived with Kirchoff's Laws. As another graphical method, bond graph method is very similar to network method. However, it presents the interactive energy relationships in energy bonds to

couple the energy ports of basic components. Variational method has advantages over the forementioned methods in the case in which the complicated interconnective system constraints are dealt, and in the solution procedure of variational method there is no need to explicitly formulate the tedious flow continuity constraint and energy compatibility constraint. It is a suitable method to handle multidisciplinary energy couplings for the physical system with lumped parameters. Among the three methods, variational method is the only one directly describing systems with algebraic forms through the use of the techniques from Halmilton and Lagrange to present the internal connections and constraints, so as to form the dynamical modeling. [Wellstend, 2005]

No matter which method is chosen to construct the mathematical formulation of the physical system, the generalized variables and the basic system elements should be identified before the model is derived. As mentioned above, all of the three methods are energy analysis approaches, which depict the system as an energy manipulator to handle the energy flow in and out through energy ports. From this point of view, the generalized system variables could be sorted according to their physical properties of energy during the energy generation, restore, conversion, transmission, and dissipation of the physical object. In mechanical, electrical, magnetic, hydraulic and thermal disciplines, their systems are expressed with different physical variables. However, there are conceptual similarities among these variables in various disciplines, and the variables in a discipline can find their analogous correspondents in other disciplines.

For a physical system, its energy flow at inlet / outlet ports is created by a couple of variables, i.e., effort variable and flow variables, whose product is the power. These variables are related to energy transfer, and they can be divided into a pair of abstract

quantities effort, denoted as e , and flow, denoted as f , in general forms, delivering the instantaneous power. In this way, the different variables, either flow variables or effort variables, for energy transfer from a wide range of physical systems can be governed in a unified framework.

2.2 Effort Variable and Flow Variable

In general, there are two analogy rules, i.e., mobility analogy and classical analogy, can be utilized to assign the variables into these two categories: effort variable and flow variable.

Under the mobility analogy rule, the effort is considered to be an across variable, which is measured across two data points from each terminal of the elements; and the flow is considered to be a through variable, which can be measured through only one data point. In this sense, the velocity in mechanical system, voltage in electrical system, and pressure in hydraulic system are the effort variables, while the force in mechanical system, current in electrical system, and flow rate in hydraulic system are the flow variables.

In comparison, under the classical analogy rule, the assignments of variables are opposite to those in the mobility analogy. Theoretically speaking, the assignment of effort and flow variables could be arbitrary, because the different assignments produce the same mathematical model. In this dissertation, the mobility analogy rule is followed for the system modeling of the two-wheeled self-balancing scooter.

Similar to the classification of system variables, the system elements could be categorized to reflect their distinct energy handling functions. Generally, there are five

basic energy manipulation elements: energy sources (flow sources and effort sources), energy stores (flow stores and effort stores), and energy dissipators.

Theoretically, the ideal energy sources could supply or absorb unlimited power or energy to the physical systems. Depending on the form of the energy sources, they can be either flow source or effort source. Mostly, these two types of sources are the functions of time, and they are independent of each other. The flow sources in various energy domains are the force source in mechanical system, current source in electrical system, and flow rate source in hydraulic system, while the effort sources are velocity source, voltage source, and pressure source in these three domains, respectively. The symbols of these two sources are in Figure 2.1. [Wellstead, 2005]

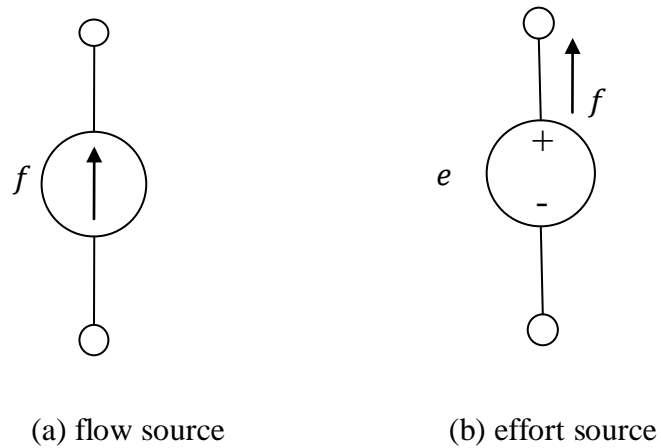


Figure 2.1 Ideal energy source elements

2.3 Stored Energy and Co-Energy

Energy store E within an element can be calculated through the integral of the power P , the product of flow variable f and effort variable e :

$$E = \int_{t_0}^t P dt = \int_{t_0}^t e f dt = \int_{t_0}^t e d f_a = \int_{t_0}^t f d e_a \quad (2.1)$$

Equation (2.1) shows that the energy stores relate to the time integral of flow variable. $f_a = \int_{t_0}^t f dt$, which is flow accumulation, or effort variable $e_a = \int_{t_0}^t e dt$, which is effort accumulation, and consequently they become the function of effort variable or flow variable. This provides the basic criterion to decide the type of energy store elements, since an element is termed to be a flow store when its stored energy is the function of effort and it is defined as an effort store when its stored energy is the function of flow.

An example of mechanical mass undergoing translational movement is used to illustrate how the energy store is expressed. The momentum p of this translational mass can be calculated as below.

$$p = \int_{t_0}^t F dt + p(t_0) \quad (2.2)$$

where F is the force applied to the mass. The above Equation (2.2) shows that the momentum p is analogous to the flow accumulation in the mobility analogy. Moreover, this flow accumulation is the function of the effort produced by the force source at the output of the element which can be concluded by the following equation.

$$p = mv \quad (2.3)$$

The above two equations provide the internal relationship between the flow accumulation and the effort, which can be expressed as a linear function $f_a = f(e)$, and can be illustrated below in Figure 2.2.

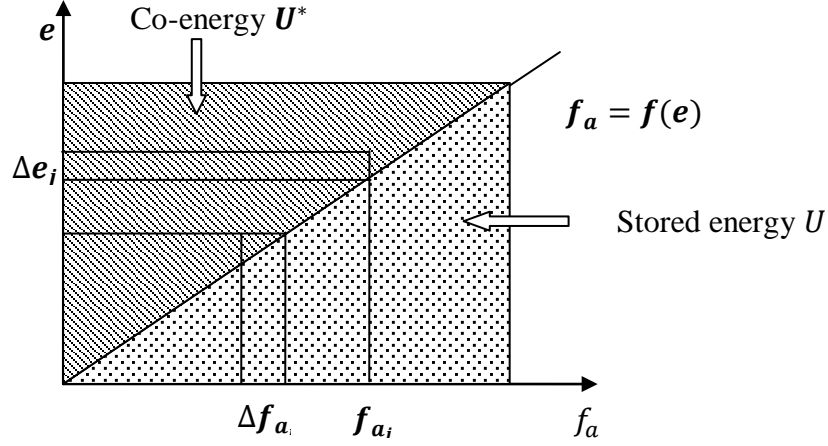


Figure 2.2 Stored energy and co-energy

Thus the corresponding stored flow energy U can be derived

$$U = \lim_{n \rightarrow \infty} \sum_{i=1}^n e_i \Delta f_{a_i} = \int_0^{f_a} e df_a = \frac{1}{2} mv^2 \quad (2.4)$$

In Figure 2.2, the dotted region under the relationship curve represents the stored energy U . At the same time, the left hatched area above the curve can be calculated from the function below.

$$U^* = \lim_{n \rightarrow \infty} \sum_{j=1}^k f_{a_j} \Delta e_j = \int_0^e f_a de = \frac{1}{2} mv^2 \quad (2.5)$$

where U^* is the stored co-energy, which is the complementary energy. The co-energy analysis is suitable to linear conservative systems. To some extent it can be used in systems with minor nonlinearities, if the relationship $U = U^*$ is satisfied. In general, the relationship $U = U^*$ is assured most commonly in linear systems, also it can be observed in minor nonlinear systems, but it rarely exist in highly nonlinear cases.

Equations (2.2) and (2.3) explain the constitutive relation of the flow accumulation f_a and the effort, as shown in Equation (2.5), while Equation (2.4) indicates that the stored flow energy U is the function of the effort variable-velocity, so in this case, the translational mass is the flow store.

Likewise, the effort store deals with the effort accumulation e_a . This concept could be illustrated by a mechanical spring under translational movement as an example of effort store in mechanical system. Because the displacement of the spring from its free state is expressed as,

$$x = \int_{t_0}^t v dt + x(t_0) \quad (2.6)$$

Equation (2.6) points out that this displacement is analogous to the effort accumulation. The characteristic of the spring material reveals the constitutive relation between spring deformation and applied force, which can be calculated as below.

$$x = \frac{F}{k} \quad (2.7)$$

The stored potential energy T and co-energy T^* are computed as below.

$$T = \int_{t_0}^t e f dt = \int_0^{e_a} f de_a = \frac{1}{2k} F^2 \quad (2.8)$$

$$T^* = \int_0^f e_a df = \frac{1}{2k} F^2 \quad (2.9)$$

Equations (2.6) and (2.7) explain the constitutive relation of the effort accumulation and the flow, while Equation (2.8) indicates that the stored effort energy T is the function of the flow variable F , which is a force, then the translational spring is the effort store in this case.

Similar examples can be also found in other physical systems. The circuit inductance in electrical system, and fluid reservoir/pressurized tank in hydraulic system are typical examples of flow stores, while the capacitance in electrical system, and the moving body of fluid in hydraulic system represent the examples of effort store respectively.

The forementioned part specified some special cases of basic flow store and effort store elements in mechanical, electrical and hydraulic systems. From the similar properties of these energy stores, some conclusion can be drawn:

Energy store elements deal with both flow and effort variables, and flow storage device is termed when the stored energy in it is related to the flow accumulation, while the effort storage device is defined when the stored energy in it is related to the effort accumulation.

Furthermore, the constitutive relationship between the flow accumulation and effort or effort accumulation and flow are usually nonlinear, thus the energy and co-energy are not always equal to each other.

2.4 Energy Dissipators

Although both energy sources and energy stores can be divided into two categories –flow related and effort related, this rule doesn't fit the case of energy dissipators. There is only one kind of basic device for energy dissipation. And the dissipated energy is gained as below.

$$ef = \int_0^f edf + \int_0^e fde \quad (2.10)$$

In mechanical system, the dissipative effects happen in the devices which need steady force to keep their movement, such as the friction force. In electrical system, the resistance is the dissipation device which consumes the stored energy and transforms it into thermal energy. Moreover, the dissipation exists when the viscous forces is generated in hydraulic system.

2.5 Energy Converters and Energy Couplers

Although these elements are sufficient to represent most of the systems, exceptions exist when describing the energy transformation process or systems coupled with subsystems, because the basic five system elements are limited to represent one-port / two terminals devices in the same energy domain, while the coupled systems and energy transformation always include multi-ports elements to describe the energy change in various energy domains. The most interested multi-port elements are two-port elements, including both energy converters and energy couplers.

Energy converters, with which the energy conversion is performed in the same field, are used to model the energy transformation devices, in which the same factor is used to relate two sets of variables, input flow and output flow, output effort and input effort, or gyration devices, in which other two sets of variables are related, input flow and output effort, output flow and input effort. On the other hand, energy couplers made the energy from different energy domains interchangeable. The graphical representation of the general two-port element is in Figure 2.3.

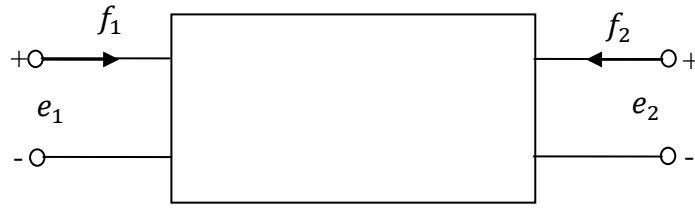


Figure 2.3 Stored energy and co-energy

Figure 2.3 shows that the general two-port element has four terminals with both the flow and effort variables in each of the port, and they may be defined in different energy disciplines. In order to fully understand the principles of energy converters and energy transducers, some detailed examples in mechanical system are discussed in the following part.

In mechanical system, the gear box is a simple example of energy converter, which changes the ratio of the flow and effort variable, but the product of the two variables remains the same, so the power or the energy is unchanged. More examples could be pulleys, levers and electrical transformer. The ideal energy converters do not store or dissipate any energy and these variables are linearly correlated by constant coefficient, so the relationship between the two pairs of variables can be expressed in the following matrix form, where the matrix elements a_{11} , a_{12} , a_{21} and a_{22} are all constants.

$$\begin{bmatrix} v_1 \\ f_1 \end{bmatrix} = \begin{bmatrix} a_{11} & a_{12} \\ a_{21} & a_{22} \end{bmatrix} \begin{bmatrix} v_2 \\ f_2 \end{bmatrix} \quad (2.11)$$

And if $a_{11} = -1/a_{22}$ and $a_{12} = a_{21} = 0$, the converter is termed energy transformation device, while if $a_{21} = -1/a_{12}$ and $a_{11} = a_{22} = 0$, it is called energy gyration device.

The energy couplers process energy in more than one energy domain, and they always exist in the transducers and motors. The most common case is the couplers in the motor, which transform the electrical energy into mechanical energy. For ideal energy converters and couplers, the most distinguish characteristics are the power conserving features, i.e., there is no power stored or dissipated.

2.6 Compatibility and Continuity Constraints for Multiphysics System

The above analysis developed a uniform framework for the modeling of a broad range of physical systems, in which energy is picked as the suitable unifying concept. According to this framework, most systems are reduced to a set of one-port elements, transferring energy through two-port power conserving elements. When a system is simplified under this framework, its structure will determine the interaction among these elements, thus build up the relationships among system variables. Furthermore, these interconnections will establish a group of constraints on these variables to describe the system dynamics. For one-port elements, they can be connected in two ways: parallel and series, and the way how they are connected will introduce the constraints for the efforts and flows: if the elements are connected in series, the total effort across these elements is the sum of individual efforts from each element, and the flow through all these elements remains the same, and it is the other way round if the elements are connected in parallel.

Just like the Kirchhoff laws in the electrical systems, these relationships in other physical systems can be graphically illustrated as shown in Figure 2.4.

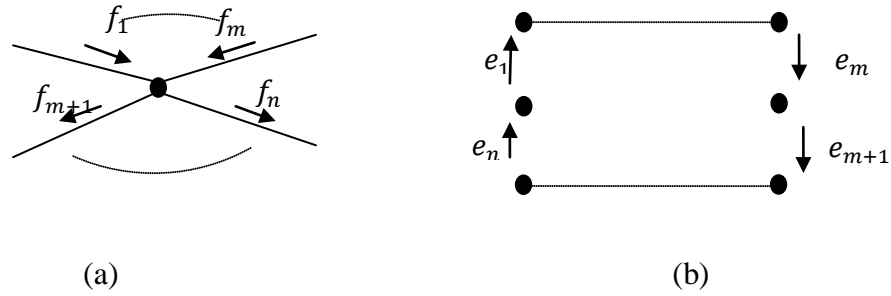


Figure 2.4 Flow and effort laws

Figure 2.4(a) shows the point rule or junction rule, which implies that the sum of flows flowing into the node equals to the sum of flows flowing out from the node, and this principle is expressed as:

$$\sum_{k=1}^n f_k = 0 \quad (2.12)$$

On the other hand, the effort law is called loop rule or mesh rule, and this rule states that the sum of efforts in any closed loop is zero, and its mathematical expression is as below.

$$\sum_{k=1}^n e_k = 0 \quad (2.13)$$

In general, the constraints set on effort variables are always called compatibility effort constraints, and those upon flow variables are termed as continuity flow constraints.

The unified framework structure of system elements provides a uniform basis for multidisciplinary physical system analysis. On this basis, for the given different physical systems, a specific modeling method can be formulated under the energy based uniform framework, using the state space equations or differential equations.

2.7 Variational Method Used in The Unified Energy Based Framework

Variational method is the extension to the research on infinitesimal alternations, and it mainly focuses on the admissible variations, which are infinitesimal alternations under compatibility or continuity constraints. When applying the variational method in the unified energy based framework, the alternation variables should relate to generalized variables in this framework, which are effort and flow, then the corresponding constraints are effort compatibility constraint and flow continuity constraints. Generally, the effort accumulation and flow accumulation variables are used as the admissible variations, which are listed as below.

Table 2.1 Effort accumulation and flow accumulation variables in various systems

	effort accumulation variable	flow accumulation variable
Mechanical system	displacement x	momentum p
Electrical system	flux linkages λ	electrical charge q
Hydraulic system	fluid pressure momentum Γ	volumetric flow V

Moreover, choosing the appropriate constraint depends on the structure of the system. In a series connected system composed of one-port elements, such as effort store, flow store, and dissipater, the flow continuity constraint needs to be employed, which means that the variations in flow accumulation variables through each system elements are equal, while in a parallel connected system, the effort compatibility constraint is set for it, in which the variations in effort accumulation variables are equal for all the elements joined at both terminals.

In order to describe the interactions in the system, a set of variational variables have to be figured out for further analysis. In this energy based framework, a bunch of effort accumulation and flow accumulation variables can be calculated and used for the system dynamics study. Although these variational variables may be found out for each of the system elements, only those together providing the full description of the admissible variation for all the system elements are required to be utilized, and are said to be a complete set of variational variables. In addition, these variables are always independent, and the number of the complete set of independent variational variables defines the degree of freedom of the system. Usually, the generalized coordinates are called instead of these complete set of variational variables when they are related to a number of variations in a system. It is notable that different numbers of degree of freedom of the same system can be resulted in choosing different coordinates as description.

In order to qualify the usage of variational method, there is another requirement needs to be met, that the system have to be holonomic, and the mathematical expression of this holonomic constraint on the generalized coordinate system is as below.

$$h(q_1, q_2 \dots q_n) = \text{constant} \quad (2.14)$$

where $q_1, q_2 \dots q_n$ are the system coordinates, and variation form of Equation (2.14) is expressed in the following equation.

$$\delta q_1 \frac{\partial h}{\partial q_1} + \delta q_2 \frac{\partial h}{\partial q_2} + \dots + \delta q_n \frac{\partial h}{\partial q_n} = 0 \quad (2.15)$$

The analysis of system dynamics through variational method can be studied through a variational indicator, which is constructed to be a scalar function based on the

configuration of admissible variations. In the energy based framework, the effort accumulation and flow accumulation are used to build the variational indicators, which lead to two types of variational indicators, nodal variational indicator and loop variational indicator.

The nodal variational analysis is related to the flow accumulation variables under flow continuity constraints. For example, in a parallel system with a flow source, an effort store, a flow store and a dissipater, there are two nodes connecting these four elements, as shown in Figure 2.5.

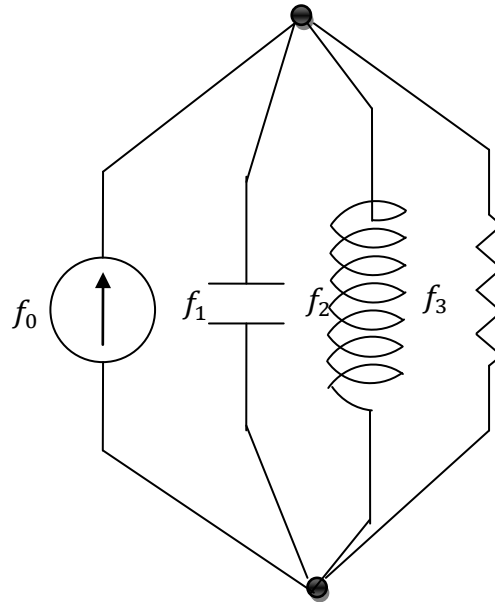


Figure 2.5 Parallel system

The energy increment in any one of the nodes follows the description in the equation showed below.

$$\begin{aligned}
\delta E &= (\delta E_0 - \delta E_1 - \delta E_2 - \delta E_3) \\
&= \delta q * f_0 - \delta q * f_1 - \delta q * f_2 \\
&\quad - \delta q * f_3
\end{aligned} \tag{2.16}$$

Where δE and δq is the variation in energy and effort accumulation variables, and f_0 , f_1 , f_2 , f_3 are the flow variables through flow source, effort store, flow store and dissipator.

$$\delta q * f_0 - \delta q * f_1 - \delta q * f_2 - \delta q * f_3 = 0 \tag{2.17}$$

From the flow continuity constraints, the aforementioned relationship between effort accumulation and flow will provide more in-depth analysis for Equation (2.17).

$$\delta q * f_1 = \delta T \tag{2.18}$$

$$\delta q * f_2 = \frac{d}{dt}(p_2 \delta q) - p_2 \delta \dot{q} = \frac{d}{dt}(p_2 \delta q) - \delta U^* \tag{2.19}$$

$$\delta q * f_3 = \frac{\partial J}{\partial \dot{q}} \delta q \tag{2.20}$$

where T is the energy from effort stores, U^* is the co-energy in the flow stores, and J is the total co-content in the dissipators.

Equations (2.18) to (2.20) show that the energy increment in these elements relate to the store energy and co-energy, when combining them with Equation (2.16), as showed in below:

$$\delta E = \delta U^* - \delta T - \left[\frac{\partial J}{\partial \dot{q}} - f_0 \right] * \delta q - \frac{d}{dt}(p \delta q) \tag{2.21}$$

From the differentiation of Equation (2.21), the admissible variation concerned in system dynamics δQ can be expressed below:

$$\delta Q = \int_{t_1}^{t_2} \left[\delta U^* - \delta T - \left[\frac{\partial J}{\partial \dot{q}} - f_0 \right] * \delta q - \frac{d}{dt}(p\delta q) \right] dt \quad (2.22)$$

From Hamilton's principle, these admissible variations are set to be zero. Then the extended Lagranges' equation can be derived.

For simplicity, a new function $L(q, \dot{q})$ is introduced to denote as below.

$$L(q, \dot{q}) = \delta U^* - \delta T \quad (2.23)$$

$$\begin{aligned} \int_{t_1}^{t_2} \delta U^* dt &= \int_{t_1}^{t_2} \frac{\partial U^*}{\partial \dot{q}} \delta \dot{q} dt = \int_{t_1}^{t_2} \frac{\partial L(q, \dot{q})}{\partial \dot{q}} \delta \dot{q} dt = \\ \int_{t_1}^{t_2} \frac{\partial L(q, \dot{q})}{\partial \dot{q}} \frac{d(\delta q)}{dt} dt &= \int_{t_1}^{t_2} \frac{\partial L(q, \dot{q})}{\partial \dot{q}} d(\delta q) = \\ - \int_{t_1}^{t_2} \frac{d}{dt} \left(\frac{\partial L(q, \dot{q})}{\partial \dot{q}} \right) \delta q dt \end{aligned} \quad (2.24)$$

$$\delta T = \frac{\partial T}{\partial \dot{q}} \delta \dot{q} = - \frac{\partial L(q, \dot{q})}{\partial \dot{q}} \delta \dot{q} \quad (2.25)$$

Combining Equations (2.22) through (2.25),

$$\delta Q = \int_{t_1}^{t_2} \left[\frac{\partial L(q, \dot{q})}{\partial q} - \frac{d}{dt} \left(\frac{\partial L(q, \dot{q})}{\partial \dot{q}} \right) - \frac{\partial J}{\partial \dot{q}} + f_0 \right] \delta q dt \quad (2.26)$$

Because $\delta Q = 0$,

$$\frac{\partial L(q, \dot{q})}{\partial q} - \frac{d}{dt} \left(\frac{\partial L(q, \dot{q})}{\partial \dot{q}} \right) - \frac{\partial J}{\partial \dot{q}} + f_0 = 0 \quad (2.27)$$

Equation (2.27) is the extended Lagranges' equations. Furthermore, this equation can be applied to systems with more than one generalized effort accumulation coordinates. And the expressions for the complicated systems can be written as a set of Lagranges' equations.

$$\frac{d}{dt} \left(\frac{\partial L(q_i, \dot{q}_i)}{\partial \dot{q}_i} \right) - \frac{\partial L(q_i, \dot{q}_i)}{\partial q_i} + \frac{\partial J}{\partial \dot{q}_i} = F_i \quad (2.28)$$

where q_i is the i th generalized coordinate which is related to effort accumulation and F_i is the flow utilized in the i th generalized coordinate.

When it concerns with the flow accumulation variables, the loop variational analysis should be used instead of the nodal variational analysis. This method can be explained in a series system composed of an effort source, an effort store, a flow store and a dissipator, which together make a close loop for the energy flows. Similar to the nodal analysis method, the variation in energy and flow accumulation variables are considered, which are named as δG and δp .

$$\delta W = \delta p * e_0 - \delta p * e_1 - \delta p * e_2 - \delta p * e_3 \quad (2.29)$$

where e_0, e_1, e_2 and e_3 are the effort variables through effort source, effort store, flow store and dissipator. Because of the flow continuity constraints,

$$\delta W = 0 \quad (2.30)$$

Using the similar process in Equation (2.18), (2.19) and (2.20), the following equation can be derived:

$$\delta W = \delta T^* - \delta U - \left[\frac{\partial G}{\partial \dot{p}} - e_0 \right] * \delta p - \frac{d}{dt} (q \delta p) \quad (2.31)$$

where T^* is the co-energy from effort stores, U is the energy from flow stores, G is the energy dissipated by the dissipator.

The differentiation of Equation (2.31) gives the dynamic indicator of the system:

$$\delta V = \int_{t_1}^{t_2} \left[\delta T^* - \delta U - \left[\frac{\partial G}{\partial \dot{p}} - e_0 \right] * \delta p - \frac{d}{dt}(q\delta p) \right] dt \quad (2.32)$$

Using the similar deduction in Equations (2.24) through (2.27), the extended Lagrange's equation in the loop variational analysis is as below.

$$\frac{\partial L^*(p, \dot{p})}{\partial p} - \frac{d}{dt} \left(\frac{\partial L^*(p, \dot{p})}{\partial \dot{p}} \right) - \frac{\partial G}{\partial \dot{p}} + e_0 = 0 \quad (2.33)$$

where $\partial L^*(p, \dot{p}) = \delta T^* - \delta U$, is the system co-Lagrangian.

For system with more than one generalized coordinates from flow accumulation, the unity functions can be expressed as below.

$$\frac{d}{dt} \left(\frac{\partial L(p_i, \dot{p}_i)}{\partial \dot{p}_i} \right) - \frac{\partial L(p_i, \dot{p}_i)}{\partial p_i} + \frac{\partial G}{\partial \dot{p}_i} = E_i \quad (2.34)$$

where p_i is the i th generalized coordinate which is related to flow accumulation and E_i is the effort utilized in the i th generalized coordinate.

From the expressions in the above equations, it can be found that the nodal variational method deals with generalized effort accumulations leading to a number of Lagrange's equations, while the loop variational method concerns with generalized flow accumulations formulating a set of co-Lagrange's equations. Both of them can model the physical systems in terms of a set of second order differential equations.

To this extent of theoretical analysis, the energy based variational approach for multidisciplinary system modeling has been fully developed. This method will be applied for the complete mathematical modeling of various multiphysics systems. Actually, the motivation behind the theoretical work stated in Chapter 2 is to find the most appropriate way to mathematically describe the complicated dynamics of the two-wheel self-balancing scooter.

CHAPTER 3. MATHEMATICAL MODELING OF TWO-WHEELED SELF-BALANCING SCOOTER

The two-wheeled self-balancing scooter is a typical case of multidisciplinary mechatronic system, because it is a complicated physical system, composed of electrical subsystems and mechanical subsystems. For such a system, the energy based variational method provides a unified approach to describe these two different subsystems, so that a set of equations can be derived for dynamic modeling and control design.

The scooter to be modeled in this chapter is similar to the Segway scooter products, but it has its own uniqueness in its hands-free and self-balancing characteristics, i.e., the balancing of the scooter is based on the Tai Chi poses originated from the Chinese martial arts. To be more specific, the scooter is composed of two driving wheels and a platform with built-in sensors, a real-time microcontroller, motors and their drivers. By shifting the rider's Tai Chi poses, the tilt angle of the platform is changed. The driving direction and speed of the scooter will be determined by collecting and processing the sensor data to make the scooter move as desired via the designed control laws.

Considering this requirement, the energy based variational approach is chosen as the modeling methodology. As the components of the comprehensive mathematical

model, the mechanical system modeling and electrical system modeling for the scooter are presented in the following sections.

3.1 Mechanical System Modeling

The mechanical system modeling should take at least two steps. First of all, it is necessary to simplify the structure of modeling object. The second step is developing the equations of motion under the simplified structure to describe the dynamics of the object.

As mentioned previously, the scooter mainly contains two driving wheels and a platform. But with the purpose of simulating its real-time performance, the rider should also be considered as an essential part for the mechanical system modeling. Figure 3.1 shows a basic structure of the self-balancing scooter. From this figure, the platform can be modeled as a cuboid rotating around the center of the wheels. Moreover, under the hypothesis that there is no relative movement between the rider's feet and the platform, and the rider only shifts its center of mass by moving its legs, human body is simplified as thought a bar with one end hinged to the center of the cuboid platform. In this way, the suggested modeling of the whole system is similar to that of an inverted pendulum.

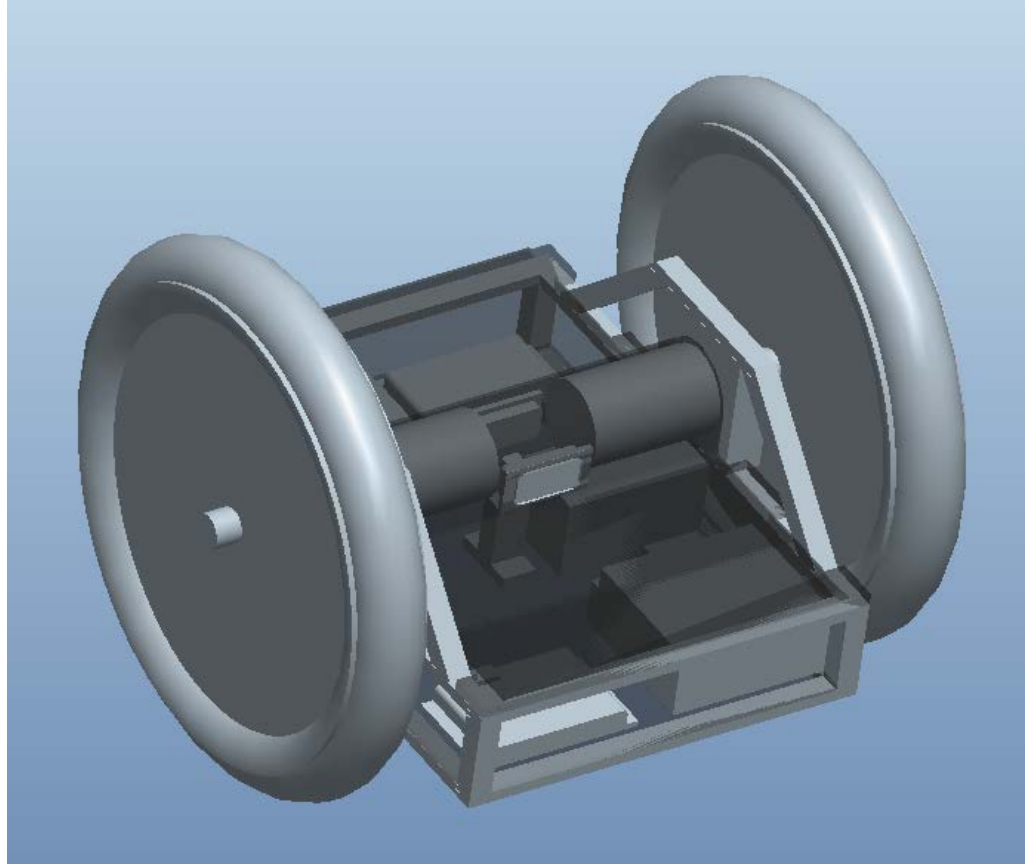


Figure 3.1 CAD model of two-wheeled self-balancing scooter

Besides simplifying the structure of the scooter and rider system, another critical task for the mechanical modeling is to identify the mechanical facts which affect the dynamic characteristics of this scooter, in other words, to figure out the forces so as to build up the equations of motion. Basically, the forces applied to the scooter along its driving direction can be categorized into tractive force and resistance force. And five kinds of forces should be considered acting on the self-balancing scooter, including tractive force, rolling resistance, aerodynamic drag, grading resistance and resistance to acceleration. Except the tractive force, all other four forces are classified as the resistance forces. In the following part, each of these

forces will be discussed in details in order to find out the final equations that describe the motion of the scooter.

Among the resistance forces, aerodynamic drag is termed as the force exerted by the air to the moving body in the direction of motion, which is composed by two parts: drag force due to the air pressure and drag force due to the air friction onto the scooter body. This force is the function of aerodynamic drag coefficient, relative speed, density of air, shape parameters, etc. For commercial vehicles, it would rise with the square of speed, and only when the speed on flat surface surpasses 20 km/h, the air dynamic drag can become the main resistance force. However, for the scooter with little frontal area and relatively low speed discussed in this dissertation, the air drag is neglectable compared to that of the vehicle. Hence, the aerodynamic drag of the scooter is ignored in the following analysis.

3.1.1 Tractive force

Tractive force is defined as the pulling or pushing force. When the wheel torque T_t generated by the motor is transferred through the gear train system to the driving wheel, on the contact area between the tire and road surface, a tangential force will be applied to the ground by the tire, and correspondingly, the reaction force from the ground, which is friction force, is resulted. This friction force enables the forward motion of the wheel. Through this way, the rotational motion of the wheel is converted into the linear motion of the scooter. In the light of actual conditions, the friction force at the interface of the tire and the road comes not only in the longitudinal direction but also in the lateral direction of the tire. Since the scooter

turning is always slow, the lateral friction force is not considered in the modeling process. From the definition of tractive force, the longitudinal friction force is in the direction of the scooter motion, so it is the tractive force F_t for the scooter. As is shown in Figure 3.2, the wheel torque makes the wheel rotation along the clockwise direction, thus the tractive force F_t from the ground is generated pointing to the right direction, making the scooter move to the right.

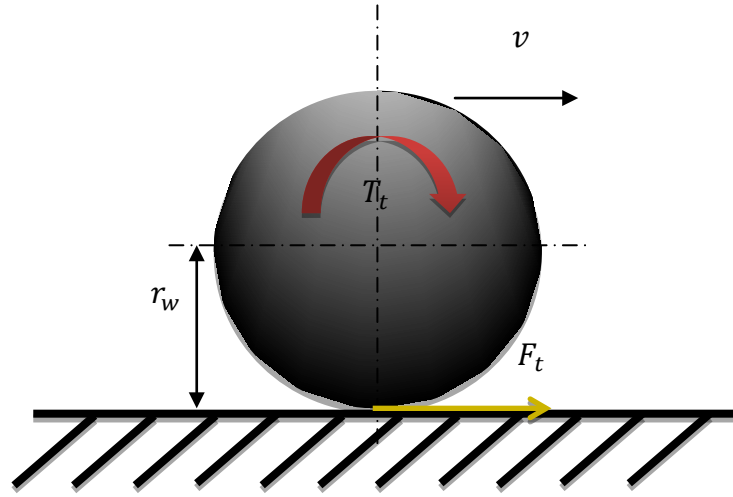


Figure 3.2 Analysis of tractive force

The tractive force F_t is proportional to the wheel torque T_t . Ideally, the value of the tractive force F_t is the result by dividing the wheel torque T_t by the wheel radius r_w , as is shown in Equation (3.1).

$$F_t = \frac{T_t}{r_w} \quad (3.1)$$

It is notable that the tractive force F_t is not always related to the wheel torque T_t , and there is exception which needs to be considered. The value of the tractive force F_t has upper limit, and its maximum value is decided by other facts, which is the road adhesion characteristics, determining the friction coefficient, and current

normal force applied to the driving axle. So the maximum value is the result of multiplication of friction coefficient of the contact road surface and the normal force.

As is said previously, the wheel torque T_t comes from the motor, but it is not the same as the motor torque, and its value is the product of three factors, the motor torque T_{tm} , the gear ratio ζ and the mechanical efficiency η_t showed in Equation (3.2).

$$F_t = T_{tm} \cdot \zeta \cdot \eta_t \quad (3.2)$$

Combining Equations (3.1) and (3.2), the final version for the calculation of tractive force is constructed in Equation (3.3).

$$F_t = \frac{T_t}{r_w} = \frac{T_{tm} \cdot \zeta \cdot \eta_t}{r_w} \quad (3.3)$$

Among these three factors, the motor torque T_{tm} and the gear ratio i are evaluated by the motor property and gear train property respectively. When it comes to the mechanical efficiency η_t , there are many issues that would have an influence on it, and the most common one is the friction loss. Compared to the total transmitted energy, these issues didn't cost too much energy. So in most cases, the mechanical efficiency η_t is between 90% - 95%.

The tractive force F_t is the most fundamental force that would affect the overall dynamic response of the scooter, since it is the only force to enable the linear motion of the scooter, so it is the key concern for the mechanical modeling.

3.1.2 Rolling resistance

The pneumatic tire is designed not only for generating the tractive force F_t to drive the scooter, but also for supporting the cart and the rider of the scooter. Because of normal load from the scooter-rider system acting on the center of the wheel, interaction forces at the contact area between the tire and the road surface are developed, causing the deformation of both the tire and the road surface due to their elastic properties. This deformation makes the tire flattened at the contact area. In addition, during the dynamic motion of rolling, the tire is under repeated cycle of deformation and recovery, in other words, the tire is compressed when it is into the contacts area and trying to relax when it leaves the contact area. The characteristics of the deformation are defined by the relative stiffness between the tire and the road surface. Generally, the distribution of the ground reaction force at the flattened part of the tire on hard road surface and soft road surface needs to be analyzed separately, since the deformation of the soft road surface has to be taken into consideration while that of the hard road surface can be neglected. In this dissertation, the road surface is treated as rigid surface without any deformation, so the discussion will only focus on deformation of the tire.

During the cycle of deformation and recovery, energy is lost and converted into heat because of various internal frictions in the tire material, which means that the energy released at the recovery process is less than the energy stored during the deformation process. As a consequence, the force at the recovery process is smaller than the force applied at the deformation process if the deformed part goes back to its original shape, considering that the energy is the product of force and distance. This

phenomenon is called hysteresis, and correspondingly, the energy loss above is called hysteresis loss. In Figure 3.3, the deformation curve gives a more direct view of hysteresis phenomenon. In this figure, the curve OCA expresses the deformation process while the curve ODA expresses the recovery process. Ideally, these two curves should coincide if there is no energy dissipation, but in actual situation, the recovery curve is always below the deformation curve and they only share two common points at both ends of the curves for the reason that the amount of deflection stays the same for the two processes. From the curves, it can be observed that given the same deformation h , the force F_{n1} at the deformation process is apparently larger than F_{n2} at the recovery process. Besides, the area under the deformation curve OCABO standing for the energy stored at the deformation process is always larger than the area under the recovery curve ODABO standing for the energy released at the recovery process, and the difference of these two areas represents the energy loss.

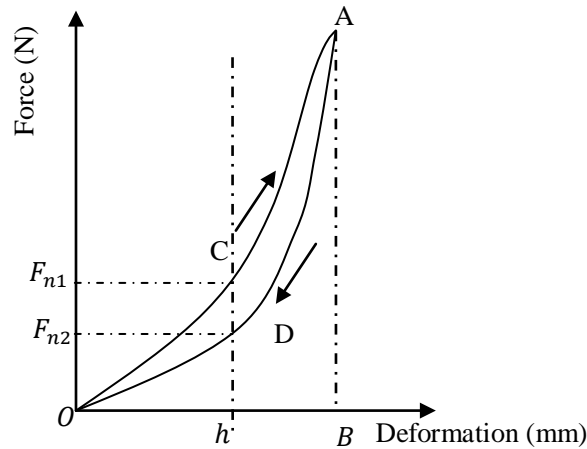


Figure 3.3 Deformation vs. force curve

Because of the hysteresis of the tire material, a resistance moment is produced. More concretely, when the tire is at rest, the distribution of the ground reaction force at the contact area is symmetrically distributed to the normal axis, which is normal axis $n - n'$ in Figure 3.4, because the deformation of it is symmetric, thus the ground reaction force coincides with the normal axis to balance the normal force. But during the motion of rolling, the leading half of the contact area, which is represented as od in Figure 3.4 undergoes deformation process while the trailing half represented by od' is in the transition from compression to relaxation. Owing to the hysteresis of the tire, the force in part od is larger than that in part od' . As the consequence of this phenomenon, asymmetric distribution of normal reaction force is created with the majority of it locating at the leading part of the tire, which is shown in the dashed area in Figure 3.4, resulting in the centroid of the ground reaction force F_n shifting forward from point o which is beneath the normal axis $n - n'$ to point o' . With the shift of the ground reaction force, the pressure on the wheel and the ground reaction normal force is misaligned, causing the instantaneous center of rotation moves forward to from point o to point o' at the same time. Moreover, the shifting distance oo' is determined by the hysteresis loss, which means the more the hysteresis loss, the longer the distance. Compared to the stillness situation, the value of the reaction force F_n keeps unchanged although it shifts to the leading part of the tire, equaling to the normal force F_p , and the directions of these two forces still oppose to each other, the only change is that the two forces are no longer passing through the same line, which is normal axis. As a result, the resistance moment T_r negating the wheel torque T_t is developed.

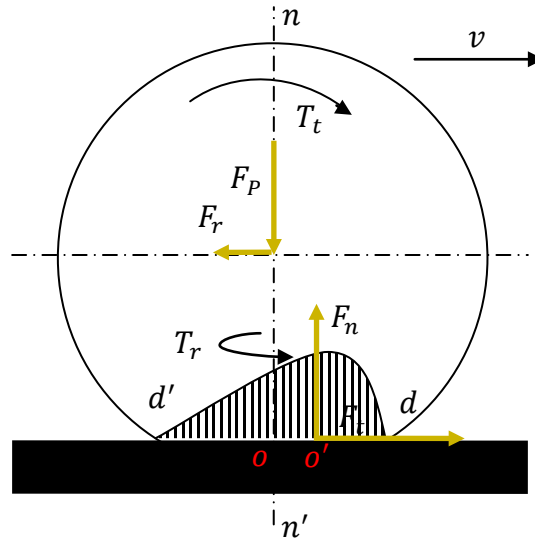


Figure 3.4 The deflection and rolling resistance analysis on rigid road surface

The value of this resistance moment T_r can be calculated as below:

$$T_r = F_n \cdot l_{oo'} \quad (3.4)$$

where $l_{oo'}$ is the distance between o and o' .

Considering that the value of the reaction force F_n equals to that of the normal force F_p , the value of the resistant moment is also expressed as below.

$$T_r = F_p \cdot l_{oo'} \quad (3.5)$$

In order to overcome the resistance moment and keep the wheel rolling as desired, a force is required to compensate this impeding moment. This force should act at the center of the wheel in the direction of the wheel speed. Considering that the force has to create a moment to balance the resistance moment T_r , the value of this force can be determined by the following equation.

$$F = \frac{T_r}{r'} \quad (3.6)$$

where r' is the effective radius of the wheel.

Combining Equations (3.5) and (3.6), the force can also be calculated as below.

$$F = \frac{T_r}{r'} = F_P \cdot \frac{l_{oo'}}{r'} = F_P \cdot C_0 \quad (3.7)$$

where $C_0 = \frac{l_{oo'}}{r'}$, and it is defined as the rolling resistance coefficient. Under the same way, the resistance moment can be also represented equivalently as the ground tangential force F_r shown in Figure 3.4 exerting at the opposite direction of motion, and it is named as rolling resistance, with the same value as F .

$$F_r = F_P \cdot C_0 \quad (3.8)$$

It is noteworthy that the rolling resistance force is only used to replace the resistant moment during analysis, it doesn't exist in real.

From Equation (3.8), the rolling resistance coefficient can also be calculated as below.

$$C_0 = \frac{F_r}{F_P} \quad (3.9)$$

It can be concluded from Equation (3.9) that the rolling resistance coefficient C_0 is the ratio of the rolling resistance force F_r and the normal load F_P . There are many contributing factors affecting the rolling resistance coefficient C_0 , including the tire material, tire radius, tire structure, tire tread property, inflation pressure, road surface property, etc. For example, the tire inflation pressure has a great influence on this coefficient, which will increase significantly with the decrease of the inflation

pressure, since the less the inflation pressure is, the more the deformation of the tire has, and more hysteresis energy loss is. Besides, the forward speed also plays an important role for this coefficient. This coefficient will rise sharply as the speed passing the critical velocity, which is about 200km/h. Compared to normal driving speed of the scooter, this situation is beyond the considerations.

Through certain experiment, the rolling resistance coefficient C_0 on different surface can be figured out. Such as the value of it on concrete or asphalt road is about 0.013, while it is 0.02 on rolled gravel. Typically, the value of the rolling resistance coefficient C_0 is fairly small, with most of it falling in the range of 0.004 and 0.02.

In conclusion, the rolling resistance is mainly caused by the hysteresis of the tire material. The tire is flattened at the contact surface, when it is under the rolling motion, it repeats the cycle of compression and relaxation. The hysteresis of tire made energy loss during the cycle, thus the distribution of ground normal force is no longer symmetric. As a result, the centroid of the force shifts forward, changing the instantaneous center of rotation at the same time. The misalignment of the normal load and the ground reaction force forms a resistance moment opposing the wheel torque. For simple analysis, an equivalent force called rolling resistance force is used to represent the influence by the resistant moment, and it doesn't exist in real. This force is the product of the rolling resistance coefficient and the normal load on the wheel. The tire properties and the road surface properties have influences on this coefficient.

3.1.3 Grading resistance

The previous analysis for the tractive force and the rolling resistance is based on the assumption that the wheel is rolling on level road, and it didn't take the difference of the motion under various roadway conditions into account. Except the motion on level road, the scooter also moves up and down on slopes, which has an obvious impact on both the tractive force and the rolling resistance. For this reason, a completed analysis on the scooter dynamics on slopes has to be proposed.

Before the study of forces under different roadway conditions, there is a must to understand the roadway fundamentals. Since the interest of this study is on the forces along the driving direction, which are not related too much to the horizontal maneuvering of the roadway, the roadway is reduced to a two dimensional model under the hypothesis that it is straight.

Figure 3.5 roughly illustrates this model. In this figure, a tangential coordinate system attaching to the earth is constructed, and the curve stands for the road surface moving with the wheel. Thus the instantaneous center of rotation of the wheel is along this curve, and the direction of gravity is perpendicular to the horizontal axis x . Supposing that the function of the curve is $y = f(x)$, and it is between the points of a and b , hence, the road way position vector $\vec{r}(x)$ is in the form of Equation (3.10).

$$\vec{r}(x) = x \cdot \vec{i} + f(x) \cdot \vec{j} \quad (3.10)$$

Where \vec{i} and \vec{j} are the unit vector along horizontal axis x and vertical axis y .

If Equation (3.10) is expressed as the tangent vector, it will give a more direct view for the direction of motion and simplify the calculation of the travel distance between point a and b . This equation is as below.

$$\vec{T}(x) = \frac{d\vec{r}(x)}{dx} = \vec{i} + \vec{j} \quad (3.11)$$

From Equation (3.11), if the wheel travels from point x_0 to point x_1 , the distance of this travel s shown in Figure 3.5 can be calculated in terms of the tangent vector $\vec{T}(x)$.

$$\begin{aligned} s &= \int_{x_0}^{x_1} \|\vec{T}(x)\| dx = \sqrt{1 + \left(\frac{df(x)}{dx}\right)^2} = \sum_{i=1}^n s_i \\ &= \sum_{i=1}^n \sqrt{(\Delta x_i)^2 + (\Delta y_i)^2} \end{aligned} \quad (3.12)$$

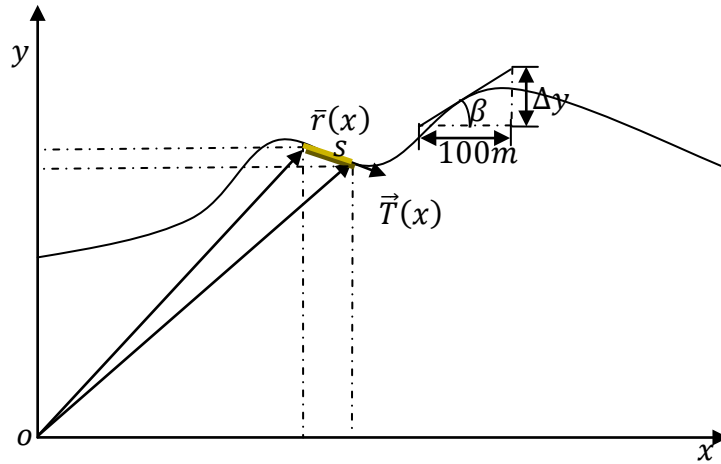


Figure 3.5 Two dimensional roadway model

Moreover, the term $\frac{df(x)}{dx}$ is used to define the roadway percent grade.

$$\beta(x) = \tan^{-1}\left[\frac{df(x)}{dx}\right] \quad (3.13)$$

Generally speaking, the roadway percent grade is the vertical rise per 100 horizontal distance of roadway with both distances expressed in the same unit, as is

shown in Figure 3.5. If the vertical rise per 100 meters is Δy , the slope angle β can also be found from below equation.

$$\tan \beta = \% \text{ grade} = \frac{\Delta y}{100m} 100\% = \Delta y\% \quad (3.14)$$

Obviously, when the scooter is rolling on level road, the percent of grade and the angle β are zeros. But when it moves uphill or downhill, they become nonzero and make the grading resistance as the main resistant force. Furthermore, the change of the roadway slope will change the direction of motion and the resistance force at the same time, influencing the whole dynamics of motion. For this reason, it is essential to find out the relationships between the percent of grade and the angle β of the slope and the resistance forces.

Assuming that the wheel is rolling uphill with slope angle β at a certain moment, the forces applied to the wheel are showed in Figure 3.6. In this case, although the normal load F_P on the wheel stays the same and the direction of the tractive force F_r follows the direction of motion along the tangential direction of the roadway, the contact area is no longer perpendicular to the normal load because of the slope angle. If the normal load F_P is decomposed as the normal force to the contact surface F_{PN} and tangential force to the contact surface F_{PT} , the value of them can be expressed as:

$$F_{PN} = F_P \cos \beta \quad (3.15)$$

$$F_{PT} = F_P \sin \beta \quad (3.16)$$

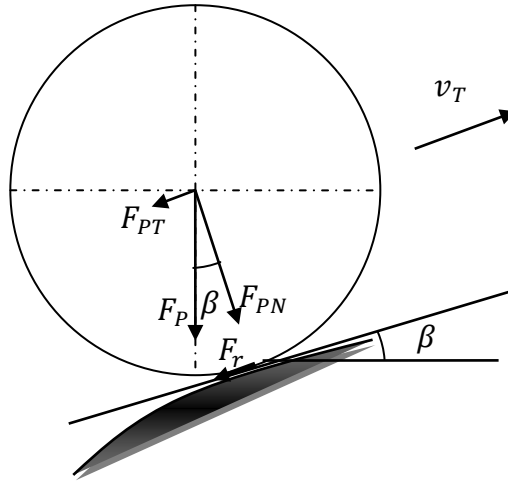


Figure 3.6 Force analysis of rolling wheel on slope

It is not hard to recognize that in Figure 3.6, the tangential force to the contact surface F_{PT} is always pointing to the downward direction, and when the wheel is moving uphill, it is against the direction of motion, thus this force is called grading resistance tangential force to the contact surface. Furthermore, the rolling resistance which is always tangential to the contact surface changes because of the change in the normal force to the contact surface. And the function for calculating the value of it on the roadway with slope angle β is very complicated.

$$F_r = \begin{cases} \text{sgn}[v_T] F_P \cos \beta (C_0 + C_1 v_T^2) & \text{if } v_T \neq 0 \\ F_t - F_{PT} & \text{if } v_T = 0 \text{ and } |F_t - F_{PT}| \leq C_0 F_P \cos \beta \\ \text{sgn}[F_t - F_{PT}] C_0 F_P \cos \beta & \text{if } v_T = 0 \text{ and } |F_t - F_{PT}| > C_0 F_P \cos \beta \end{cases} \quad (3.17)$$

Where C_1 is another rolling resistance coefficient coping with the second order of the vehicle speed.

And the signum function is given as:

$$gn[v_T] = \begin{cases} 0, & \text{if } v_T \geq 0 \\ 1, & \text{if } v_T < 0 \end{cases} \quad (3.18)$$

Where v_T is the tangential velocity of the wheel, and the coefficient $C_1 \ll C_0$. From Equation (3.17), the maximum rolling resistance is $C_0 F_P$, which occurs when the scooter is standstill.

It is worth mentioning that when the slope angle is large enough, the wheel can't climb up the slope, so there is a limit for the slope angle. If it is assumed that the wheel is rolling at a very low constant speed and the rolling resistance can be neglected, the maximum slope angle is decided by the tractive force, which equals to the grading resistance:

$$F_t = F_{PT} = F_P \sin \beta \quad (3.19)$$

$$\beta_{max} = \arcsin\left(\frac{F_t}{F_P}\right) \quad (3.20)$$

The above analysis explains the forces in the direction of motion on the two dimensional roadway model. The roadway fundamentals demonstrate the basic idea about roadway grading, supporting the following analysis of force. Because of the slope angle, a grading force shows up, which is resistance to the uphill motion. In addition, the evaluation of rolling resistance becomes more complicated.

3.1.4 Resistance to acceleration

Resistance to acceleration is defined as the inertia that resists the acceleration of the moving objects. The rolling of the wheel combines the rotational motion and translational motion, thus the acceleration of the rolling motion would bring rotational equivalent of mass to the inertia of motion, which is of great importance for the

dynamic analysis of the scooter. In order to address this concern properly, the analysis for the wheels, the motor, and the combination of cart and rider need to be done separately, since they are under different rotation speeds and accelerations.

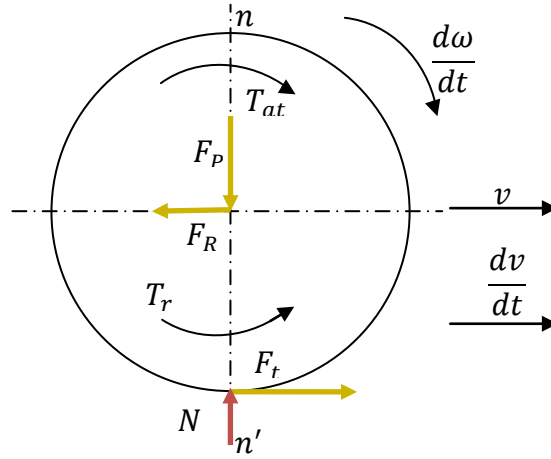


Figure 3.7 The force and torque at acceleration moment of driving wheel

Starting from the analysis for the wheel, both of the wheels on the scooter are the driving wheels, and Figure 3.7 illustrates all the forces and the torque applied to the driving wheel during acceleration. Then from the balance condition, the force balance equation in the direction of velocity and the torque balance equation can be derived below.

$$F_t - F_R = 2m_w \frac{dv}{dt} \quad (3.21)$$

$$F_t r_w = T_{at} - 2I_w \frac{d\omega}{dt} - T_r \quad (3.22)$$

Where T_{at} is the wheel torque applied for the acceleration and its corresponding driving force is F_{at} ; F_R is the total resistance force ; I_w is the moment of inertia of the wheel.

This analysis is based on rolling on level road, F_R equals to the rolling resistance F_r . Whereas when it is rolling uphill, F_R is the sum of rolling resistance F_r and the grading resistance F_{pT} .

Because $T_{at} = F_{at}r_w$, $T_r = F_r r_w$ and $v = \omega r_w$,

$$F_t = F_{at} - 2 \frac{I_w}{r_w^2} \frac{dv}{dt} - F_r \quad (3.23)$$

Use the above equation to replace the parameter F_T in Equation (3.21), then

$$F_R = F_t - 2m_w \frac{dv}{dt} \quad (3.24)$$

$$= F_{at} - 2m_w \frac{dv}{dt} - 2 \frac{I_w}{r_w^2} \frac{dv}{dt} - F_r$$

$$F_{at} = F_R + 2(m_w + \frac{I_w}{r_w^2}) \frac{dv}{dt} + F_r \quad (3.25)$$

Furthermore, the rotational inertia of motion from the motor may also need to be considered. The angular acceleration $\frac{d\omega_m}{dt}$ in the motor is proportional to that of the wheel.

$$\frac{d\omega_m}{dt} = \zeta \cdot \frac{d\omega}{dt} = \frac{\zeta}{r_w} \frac{dv}{dt} \quad (3.26)$$

Where ζ stands for the gear ratio.

So the function for the acceleration torque T_{at} on wheel can be derived.

$$T_{at} = (T_m - I_m \frac{d\omega_m}{dt}) \zeta \cdot \eta_{at} \quad (3.27)$$

Where T_m is the torque from the motor; I_m is the moment of inertia of the rotational part in motor; η_{at} is the energy conversion efficiency of the driving motor.

In this case, the corresponding force is expressed as below:

$$\begin{aligned}
 F_{at} &= \frac{T_{at}}{r_w} = \frac{T_m \zeta \eta_{at}}{r_w} - \frac{I_m \zeta \eta_{at}}{r_w} \frac{d\omega_m}{dt} \\
 &= \frac{T_m \zeta \eta_{at}}{r_w} - \frac{I_m \zeta^2 \eta_{at}}{r_w^2} \frac{dv}{dt}
 \end{aligned}
 \tag{3.28}$$

Last step is the analysis of the inertia of the scooter and rider. As introduced before, the rider shifts the mass center of his body to tilt the platform at certain angles, so that the sensing system can feed the angles and angular changes to the controller, thus the drive torque can be supplied by the motor, and the scooter moves forwards or backwards. Figure 3.8 describes the applied force and torque on the cart and rider under acceleration, with the forward tilt angle of θ .

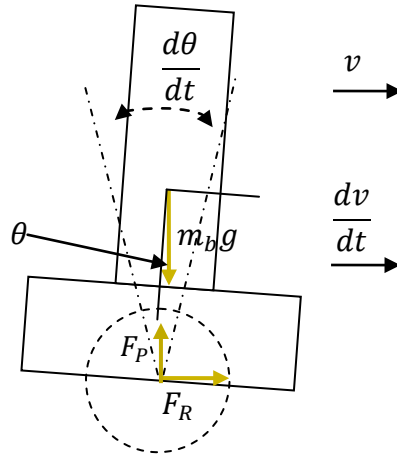


Figure 3.8 Force and torque at acceleration moment of cart and rider

As a result, the balance equations for both force and torque are calculated in the following ways.

$$\begin{aligned}
F_R &= m_b \frac{dv}{dt} + m_b \frac{d^2}{dt^2} (r_b \sin \theta) \\
&= m_b \frac{dv}{dt} + (m_b r_b \cos \theta) \ddot{\theta} \\
&\quad - (m_b r_b \sin \theta) \dot{\theta}^2
\end{aligned} \tag{3.29}$$

$$\begin{aligned}
F_P &= m_b g + m_b \frac{d^2}{dt^2} (r_b \cos \theta) \\
&= m_b g - (m_b r_b \sin \theta) \ddot{\theta} \\
&\quad - (m_b r_b \cos \theta) \dot{\theta}^2
\end{aligned} \tag{3.30}$$

$$\begin{aligned}
I_b \ddot{\theta} &= F_P r_b \sin \theta - F_R r_b \cos \theta = [m_b g - \\
&\quad (m_b r_b \sin \theta) \ddot{\theta} - (m_b r_b \cos \theta) \dot{\theta}^2] r_b \sin \theta - \\
&\quad \left[m_b \frac{dv}{dt} + (m_b r_b \cos \theta) \ddot{\theta} - \right. \\
&\quad \left. (m_b r_b \sin \theta) \dot{\theta}^2 \right] r_b \cos \theta = m_b g r_b \sin \theta - \\
&\quad m_b r_b \frac{dv}{dt} \cos \theta - m_b r_b^2 \ddot{\theta}
\end{aligned} \tag{3.31}$$

where m_b is the total weight of inertia of cart and rider; I_b is the total moment of inertia of cart and rider; r_b is the distance between the center of mass m_b and center of wheel.

From Equations (3.25), (3.28) and (3.29), the balance equation of force and torque for the whole scooter-rider system can be derived as:

$$\begin{aligned}
F_{at} &= m_b \frac{dv}{dt} + (m_b r_b \cos \theta) \ddot{\theta} - (m_b r_b \sin \theta) \dot{\theta}^2 \\
&\quad + 2(m_w + \frac{I_w}{r_w^2}) \frac{dv}{dt} + F_r
\end{aligned} \tag{3.32}$$

$$\begin{aligned}
& \frac{T_m \zeta \eta_{at}}{r_w} - \frac{I_m \zeta^2 \eta_{at}}{r_w^2} \frac{dv}{dt} \\
& = m_b \frac{dv}{dt} + (m_b r_b \cos \theta) \ddot{\theta} \\
& - (m_b r_b \sin \theta) \dot{\theta}^2 + 2(m_w \\
& + \frac{I_w}{r_w^2}) \frac{dv}{dt} + F_r
\end{aligned} \tag{3.33}$$

Finally, combining the terms including the same components of $\frac{dv}{dt}$, the function becomes as below:

$$\begin{aligned}
\frac{T_m \zeta \eta_{at}}{r_w} & = (2m_w + m_b) \frac{dv}{dt} + (\frac{I_m \zeta^2 \eta_{at}}{r_w^2} \\
& + 2 \frac{I_w}{r_w^2}) \frac{dv}{dt} + F_r + (m_b r_b \cos \theta) \ddot{\theta} \\
& - (m_b r_b \sin \theta) \dot{\theta}^2
\end{aligned} \tag{3.34}$$

Denoting $m = 2m_w + m_b$, m is the total weight of the whole system,

$$\begin{aligned}
\frac{T_m \zeta \eta_{at}}{r_w} & = (1 + \frac{I_m \zeta^2 \eta_{at}}{m r_w^2} + 2 \frac{I_w}{m r_w^2}) m \frac{dv}{dt} + F_r \\
& + (m_b r_b \cos \theta) \ddot{\theta} - (m_b r_b \sin \theta) \dot{\theta}^2
\end{aligned} \tag{3.35}$$

Denoting $\delta = 1 + \frac{I_m \zeta^2 \eta_{at}}{m r_w^2} + 2 \frac{I_w}{m r_w^2}$, δ is called the rotational inertia

coefficient, and this equation shows that the rotational inertia coefficient is the function of wheel radius, wheel moment of inertia motor moment of inertia, the total weight of the motion system, etc. At low speeds, which are the cases for scooter driving, the typical value of δ can be as high as 1.5.

The above analysis gives the general form of dynamic equation of motion for the whole scooter system on a level road:

$$F_t = \delta m \frac{dv}{dt} + F_r + (m_b r_b \cos \theta) \ddot{\theta} - (m_b r_b \sin \theta) \dot{\theta}^2 \quad (3.36)$$

When the scooter is rolling uphill with the slope angle of β , the set of the functions are as below.

$$F_t - F_R - m_w g \sin \beta = 2m_w \frac{dv}{dt} \quad (3.37)$$

$$F_R = m_b g \sin \beta + m_b \frac{dv}{dt} + (m_b r_b \cos \theta) \ddot{\theta} - (m_b r_b \sin \theta) \dot{\theta}^2 \quad (3.38)$$

$$F_P = m_b g \cos \beta - (m_b r_b \sin \theta) \ddot{\theta} - (m_b r_b \cos \theta) \dot{\theta}^2 \quad (3.39)$$

$$I_b \ddot{\theta} = m_b g r_b (\sin \theta \cos \beta - \sin \beta \cos \theta) - m_b r_b \frac{dv}{dt} \cos \theta - m_b r_b^2 \ddot{\theta} \quad (3.40)$$

$$F_t = \delta m \frac{dv}{dt} + F_r + (m_b r_b \cos \theta) \ddot{\theta} - (m_b r_b \sin \theta) \dot{\theta}^2 + m g \sin \beta \quad (3.41)$$

It must be pointed out that Equations (3.35) and (3.41) are only used for simple analysis, representing the relationship of values, and some of the terms are equivalent ones which don't exist in real, such as the rolling resistance force F_r . Likewise, the resistance to acceleration is only proposed for the dynamic influence analysis from the rotational motion.

3.2 Dynamic modeling by variational method

Through the study of force and torque, the dynamic equation of motion is derived previously. But the aim of the paper is building up a completed model for the mechatronic system of the scooter, the general dynamic equation of motion in Equation (3.35) is only limited to be used in mechanical field, thus the variational method of modeling has to be utilized.

From Figure 3.8, it is not hard to find out that the combined shape of cart and rider is just like an inverted T shape. As mentioned before, there is an assumption that no relative movement exists between the rider legs and the cart, thus the cart and rider can be modeled as one piece. A further simplified mechanical model of the scooter rider system is depicted in Figure 3.9. In this figure, the inverted T of scooter platform and rider is reduced into a bar connected through with a joint hinge in the center of the wheel, and the whole system is climbing up with the speed of \dot{x} on the roadway at the slope angle of θ . This figure also indicated that this mechanical system have two degree of freedom, which are the tilt angle θ of the cart and rider, and the scooter rolling distance x . In this case, when applying the variational method for the mechanical system modeling, the generalized coordinate is chosen as (θ, x) . The forces and torques act on the system is analyzed in Figures 3.7 and 3.8, then the following analysis can be based on these two figures.

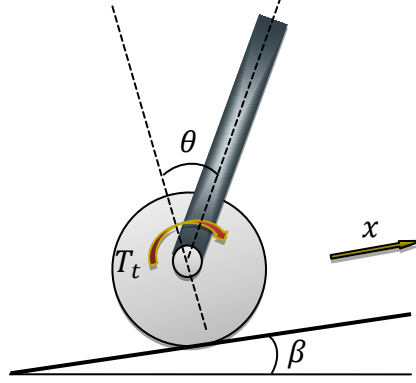


Figure 3.9 Modeling of scooter-rider system on slope

The previous analysis shows that the scooter is under a set of resistance forces, which are considered as non-conservative forces, thus the scooter system should follow the variational method for non-conservative mechanical system, whose equation is in the form as below:

$$\frac{d}{dt} \left(\frac{\partial L(p_i, \dot{p}_i)}{\partial \dot{p}_i} \right) - \frac{\partial L(p_i, \dot{p}_i)}{\partial p_i} + \frac{\partial J}{\partial \dot{p}_i} = F_i \quad (3.42)$$

Where J is the total co-content of the system dissipators.

The potential energy of the system can be calculated as below:

$$T = 2m_w g r_w \cos \beta + m_b g (r_b \cos \beta \cos \theta + r_w \cos \beta) \quad (3.43)$$

The definitions of the terms are the same as used in previous equations. The co-kinetic energy U_b^* for cart and rider can be found out as:

$$U_b^* = \frac{1}{2} m_b [\dot{x}^2 + (r_b \dot{\theta})^2 + 2r_b \dot{x} \dot{\theta} \cos \theta] + \frac{1}{2} I_b \dot{\theta}^2 \quad (3.44)$$

The co-kinetic energy U_w^* for the two driving wheels is:

$$U_w^* = \frac{1}{2} \cdot 2m_w \dot{x}^2 + \frac{1}{2} \cdot 2I_w \frac{\dot{x}^2}{r^2} = m_w \dot{x}^2 + I_w \frac{\dot{x}^2}{r^2} \quad (3.45)$$

Then the total co-kinetic energy U^* of the system is the sum of the above two co-kinetic energies.

$$\begin{aligned}
 U^* = U_b^* + U_w^* = & \frac{1}{2}m_b[\dot{x}^2 + (r_b\dot{\theta})^2 \\
 & + 2r_b\dot{x}\dot{\theta}\cos\theta] + \frac{1}{2}I_b\dot{\theta}^2 + m_w\dot{x}^2 \\
 & + I_w\frac{\dot{x}^2}{r_w^2}
 \end{aligned} \tag{3.46}$$

Finally, the system Lagrangian can be determined:

$$\begin{aligned}
 L = U^* - T = & \frac{1}{2}m_b[\dot{x}^2 + (r_b\dot{\theta})^2 + 2r_b\dot{x}\dot{\theta}\cos\theta] \\
 & + \frac{1}{2}I_b\dot{\theta}^2 + m_w\dot{x}^2 + I_w\frac{\dot{x}^2}{r_w^2} \\
 & - 2m_wgr_w\cos\beta \\
 & - m_bg(r_b\cos\beta\cos\theta + r_w\cos\beta)
 \end{aligned} \tag{3.47}$$

For the coordinate θ , Lagrange's equation is as below:

$$\frac{d}{dt}\left(\frac{\partial L}{\partial \dot{\theta}}\right) - \frac{\partial L}{\partial \theta} = T_b \tag{3.48}$$

Where the torque T_b in the cart and rider.

$$T_b = 0 \tag{3.49}$$

Thus the Lagrange's equation can be derived as:

$$\begin{aligned}
 (I_b + m_br_b^2)\ddot{\theta} + m_br_b\cos\theta\ddot{x} - m_br_b(\sin\theta)\dot{x}\dot{\theta} - \\
 m_br_b(\sin\theta)\dot{x}\dot{\theta} - m_bg r_b\sin\theta\cos\beta = 0
 \end{aligned} \tag{3.50}$$

As a result, the simplified equation is:

$$\begin{aligned}
(I_b + 2m_b r_b^2) \ddot{\theta} + 2m_b r_b \cos \theta \ddot{x} \\
- 2m_b r_b (\sin \theta) \dot{x} \dot{\theta} \\
- m_b g r_b \sin \theta \cos \beta = 0
\end{aligned} \tag{3.51}$$

For the coordinate x , Lagrange's equation is:

$$\frac{d}{dt} \left(\frac{\partial L}{\partial \dot{x}} \right) - \frac{\partial L}{\partial x} = F_T \tag{3.52}$$

Where F_T is the force in the direction of x .

As a result,

$$\begin{aligned}
m_b \ddot{x} + (m_b r_b \cos \theta) \ddot{\theta} - (m_b r_b \sin \theta) \dot{\theta}^2 + 2m_w \ddot{x} \\
+ 2I_w \frac{\ddot{x}}{r^2} = F_T
\end{aligned} \tag{3.53}$$

In conclusion, Equations (3.51) and (3.53) are the equations of motion of the mechanical model in terms of the coordinate system (θ, x) under the variational method.

3.3 Electrical System Modeling

3.3.1 Modeling of motor drive

Typically, motor drive is utilized to boost the current, since the input control signal of the interface circuit is low-level control signal, which couldn't provide enough power to run the motor, in other words, motor drive is a current amplifier. Two forms of input control signal could be applied to control the motor speed, either an analog DC voltage input signal or a digital pulse-width modulation (PWM) signal. By varying the amplitude of the DC voltage signal, or the duty cycle of the PWM signal so as to adjust the average DC voltage, the speed of the motor changes

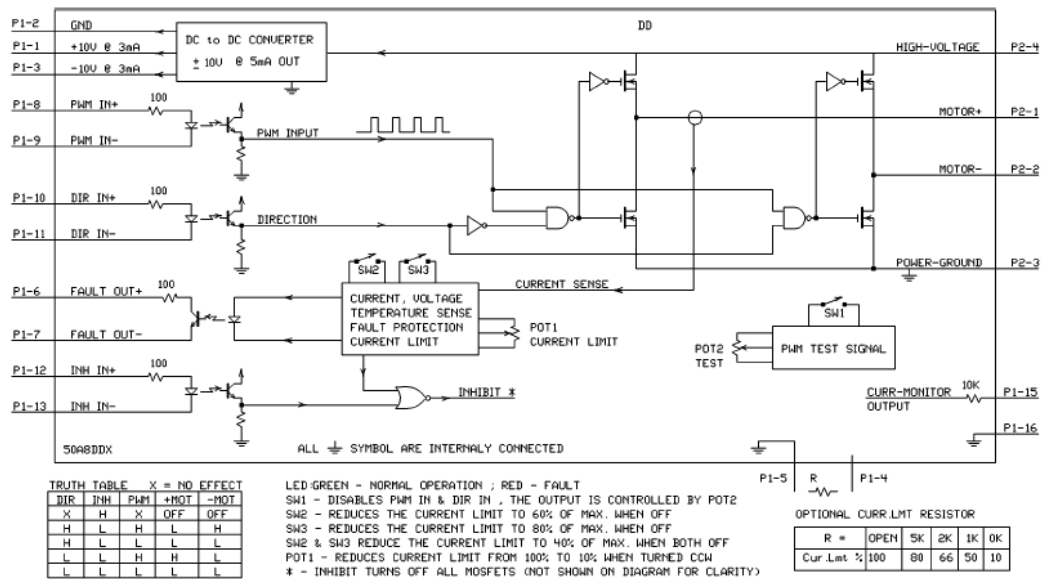


Figure 3.11 Block diagram of 30A8DD analog servo drive

In the block diagram, the PWM signal is connected to pin P1-8 and P1-9 while the direction signal is connected to pin P2-1 and P2-2. The circuit can be divided into three functional parts: phototransistor for generating reliable photocurrent signal, logic gates for deciding the on/off status of MOSFET in the H-bridge so as to determine the direction of the motor, and H-bridge for strengthening the signal to run the motor.

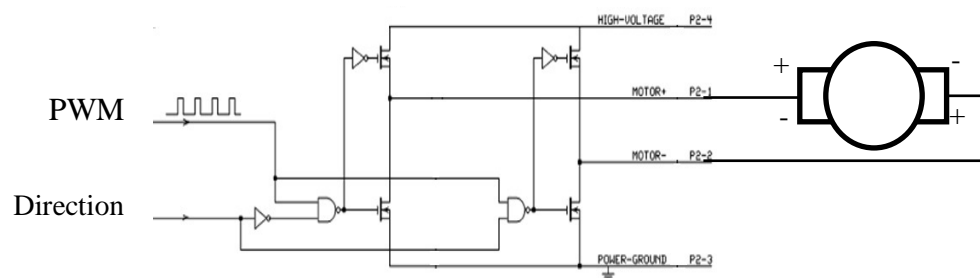


Figure 3.12 H-bridge motor drive circuit

From the brief description of the block diagram above, the H-bridge is in charge of signal amplification. Thus, the modeling of motor drive can be simplified as modeling of the H-bridge circuit, as is shown above. The H-bridge uses four n-channel enhancement type MOSFETs. Since only two of them would be on at the same time with one connected to the ground, this H-bridge modeling can be further simplified as the modeling of n-channel MOSFET.

Based on the relationship between the voltage and current flow in MOSFET, three distinct regions of operation can be concluded, and they are pointed in the curves in the figures below: the cutoff region in Figure 3.14, the triode region and the saturation region in Figure 3.13. If the relationship between the gate-to-source voltage V_{GS} and the threshold voltage V_t is $V_{GS} < V_t$, the MOSFET is cut off. When $V_{GS} \geq V_t$, the device can work in the triode region. And the value of the current is calculated as below.

$$i_D = k'_n \frac{W}{L} [(V_{GS} - V_t)V_{DS} - \frac{1}{2}V_{DS}^2] \quad (3.54)$$

Where $k'_n = \mu_n C_{ox}$ is the process transconductance parameter, with the unit of A/V^2 ; μ_n is electron mobility; C_{ox} is oxide capacitance; W is the channel width; L is the channel length. Besides, W and L are considered as the aspect ratio of the MOSFET.

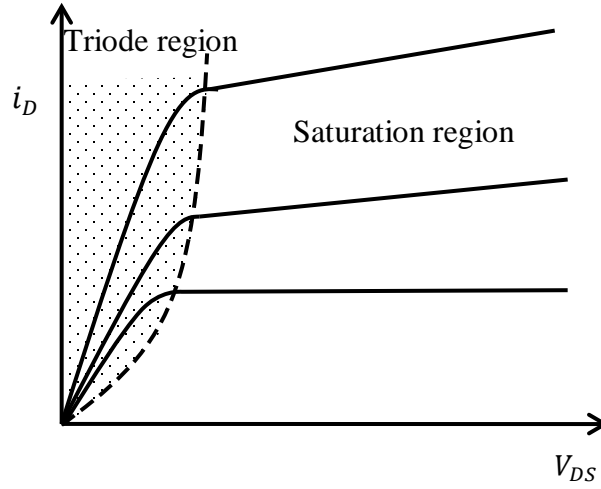


Figure 3.13 The drain current flow i_D VS the drain-to-source voltage V_{DS}

As an amplifier, the MOSFET must work under the saturation region. In order to make sure the MOSFET is operated in the saturation region, certain conditions must be satisfied.

$$V_{GS} \geq V_t \quad (3.55)$$

$$V_{DS} \geq V_{GS} - V_t \quad (3.56)$$

When the MOSFET switches from triode region into saturation region, it must pass the boundary condition, where $V_{DS} = V_{GS} - V_t$. By applying the boundary condition into Equation (3.1), the value of drain current i_D can be expressed as the function of gate-to-source voltage V_{GS} .

$$i_D = \frac{1}{2} k'_n \frac{W}{L} (V_{GS} - V_t)^2 \quad (3.57)$$

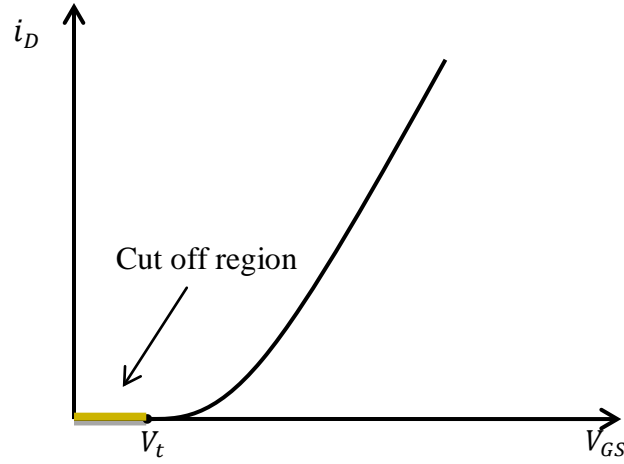


Figure 3.14 The drain current flow i_D versus the gate-to-source voltage V_{GS}

According to Equation (3.4), the MOSFET can be treated as current source, under the control of V_{GS} because of the nonlinear relationship between them.

Because of the channel-length modulation, the factor $(1 + \lambda V_{DS})$ needs to be counted in the i_D equation.

$$i_D = \frac{1}{2} k'_n \frac{W}{L} (V_{GS} - V_t)^2 (1 + \lambda V_{DS}) \quad (3.58)$$

where the λ is a positive constant MOSFET parameter, whose typical value is between 0.005 to 0.03 V⁻¹.

Finally, using equivalent circuit model, the MOSFET can be modeled as below. Since the value of i_G is almost zero under the saturation status, the resistance r_∞ with infinite value is used in the model.

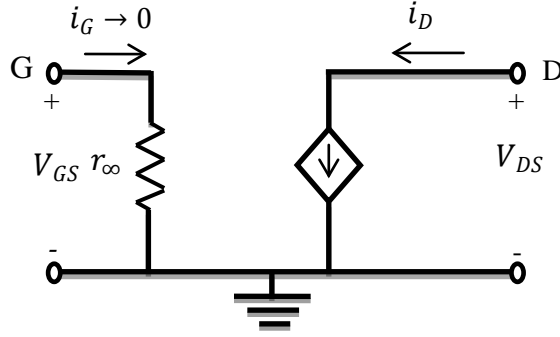


Figure 3.15 Large-signal equivalent circuit model of n-channel MOSFET in saturation region

As a conclusion, the amplitude of the n-channel MOSFET is the function of V_{GS} .

$$\beta = \frac{1}{2} k'_n \frac{W}{L} (1 + \lambda V_{DS}) (V_{GS} - V_t) \quad (3.59)$$

3.3.2 Modeling of motor

In mechatronic systems, motor is the device responsible for converting electrical energy into mechanical energy, therefore, the modeling of motor needs to apply both basic electromagnetic principles and fundamental physical laws. There are several types of motor that could be chosen for various applications, and DC motor is commonly chosen as servo motor for position or speed feedback control. In the two-wheeling self-balancing scooter, the T-64 NPC DC motor is used for speed feedback control, which is shown in the following figure. This motor is installed through a fixed gear ratio $Gr = 20:1$ of scooter wheel, transforming into rotational motion.



Figure 3.16 T-64 NPC DC motor

Generally speaking, motors include two main parts, stator and rotor, which are separated by air gap. Moreover, the armature windings on the rotor are supplied by input voltage through commutator. The modeling of DC motor should focus on the balancing relation between the voltages and torques. The schematic diagram of DC motor is displayed in Figure 3.16.

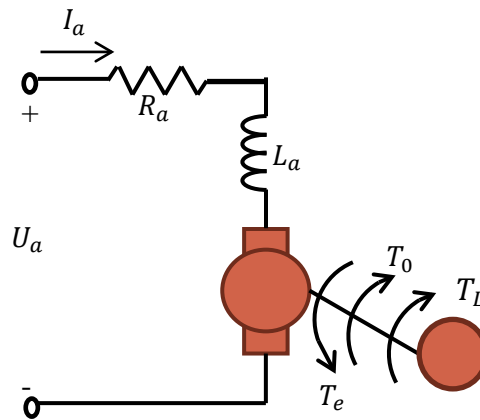


Figure 3.17 Schematic diagram of DC motor

For any electrical motion devices operating in magnetic field, the induced electromotive force (emf) and magnetomotive forces (mmf) are given as:

$$emf = \oint_l \vec{E} \cdot d\vec{l} = \oint_l (\vec{v} \times \vec{B}) \cdot d\vec{l} - \oint_s \frac{\partial \vec{B}}{\partial t} \cdot d\vec{s} \quad (3.60)$$

$$mmf = \oint_l \vec{H} \cdot d\vec{l} = \oint_l \vec{J} \cdot d\vec{s} + \oint_s \frac{\partial \vec{D}}{\partial t} \cdot d\vec{s} \quad (3.61)$$

Where \vec{E} is the electric field intensity; \vec{v} is speed of the motor; \vec{l} is the displacement; \vec{B} is the magnetic flux density; \vec{H} is the magnetic field intensity; \vec{D} is the electric flux density; \vec{J} is the volume charge density.

Assuming that in the linear magnetic system, the magnetic field is fixed and magnetic susceptibility is constant in the DC motor, the equations for deriving the back emf and electromagnetic torque calculation can be simplified as linear functions of angular speed ω_r and electrical current I_a respectively:

$$E_a = k_a \omega_r \quad (3.62)$$

$$T_e = k_a I_a \quad (3.63)$$

Where k_a is the back emf and torque constant.

From Kirchhoff's law, the steady state equation of the armature voltage can be concluded as:

$$U_a = E_a + R_a I_a \quad (3.64)$$

Where R_a is the armature resistance, which is below 0.2 Ohm

The dynamic equation of the armature voltage needs to take effect of the inductance into consideration, thus,

$$U_a = E_a + R_a I_a + L_a \frac{dI_a}{dt} \quad (3.65)$$

Similarly, from Newton's second law, the steady state equation of torque is:

$$T_e = T_L + T_0 \quad (3.66)$$

Where T_0 is the parasitic load.

Considering the moment of inertia of rotor, the dynamic equation of torque is:

$$T_e = T_L + T_0 + J_a \frac{d\omega_r}{dt} \quad (3.67)$$

Where J_a is the moment of inertia of the rotor; ω_r is the traveling angle speed of rotor.

Combining equations from Equation (3.64) to Equation (3.69),

$$\frac{dI_a}{dt} = -\frac{R_a}{L_a}I_a - \frac{k_a}{L_a}\omega_r + \frac{1}{L_a}U_a \quad (3.68)$$

$$\frac{d\omega_r}{dt} = \frac{k_a}{J}I_a - \frac{B_m}{J}\omega_r + \frac{1}{J}T_L \quad (3.69)$$

Thus, the state space function for motor modeling can be concluded:

$$\begin{bmatrix} \frac{dI_a}{dt} \\ \frac{d\omega_r}{dt} \end{bmatrix} = \begin{bmatrix} -\frac{R_a}{L_a} & -\frac{k_a}{L_a} \\ \frac{k_a}{J} & -\frac{B_m}{J} \end{bmatrix} \begin{bmatrix} I_a \\ \omega_r \end{bmatrix} + \begin{bmatrix} \frac{1}{L_a} \\ 0 \end{bmatrix} U_a + \begin{bmatrix} 0 \\ \frac{1}{J} \end{bmatrix} T_L \quad (3.70)$$

The most important characteristic of motor is the torque-speed relationship.

The steady state relationship can be derives from above equations.

$$\omega_r = \frac{U_a}{k_a} - \frac{R_a I_a}{k_a} = \frac{U_a}{k_a} - \frac{R_a}{k_a} T_e \quad (3.71)$$

Equation (3.66) shows that under a constant armature voltage U_a , the speed of motor ω_r will decrease as the electromagnetic torque T_e increases, and by adjusting the armature voltage U_a , the angular velocity ω_r would also changes correspondingly.

The details are illustrated in Figure 3.18.

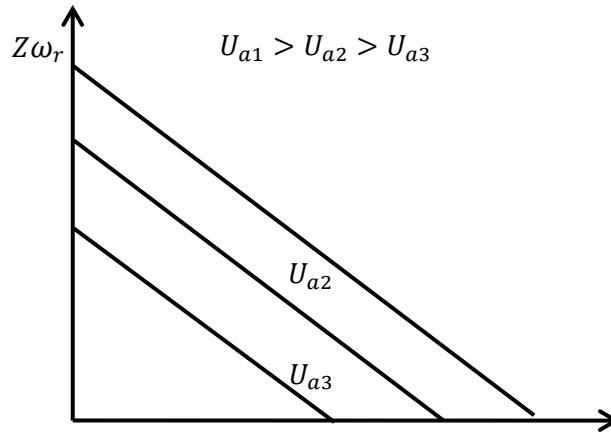


Figure 3.18 Torque-speed characteristic of DC motor

3.3.3 Modeling of Inertial Measurement Unit

Inertial Measurement Unit (IMU) is an electrical device composed of accelerometers detecting the current rate of acceleration and gyroscopes detecting the variations in the rotational attributes, such as pitch, roll and yaw. IMU has broad applications in various motion control devices or Global Positioning System (GPS) enabled devices, such as aircraft, robot and vehicles. In order to output accurate data, it is required to be installed on the center of gravity of motion devices.

The two-wheeled self-balancing scooter uses ADXL203/ADXRS300 Combo IMU board, which is showed in Figure 3.18. ADXL203 is a dual-axis accelerometer with signal conditioned voltage output while ADXRS300 follows the principles of resonator gyro to produce electrical rate signal.

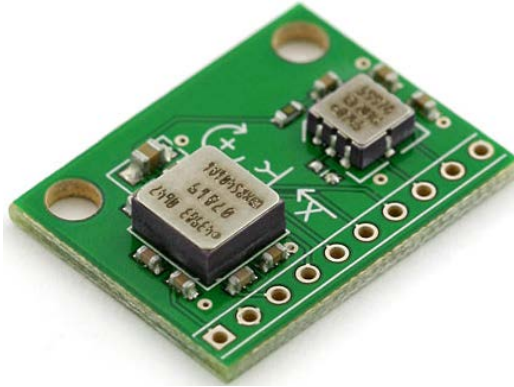


Figure 3.19 ADXL203/ADXRS300 Combo IMU board

3.3.3.1 Modeling of accelerometers

Accelerometers indirectly measures acceleration by detecting the inertial force or fictitious force. In general, the mechanical model of accelerometers can be illustrated in Figure 3.30, consisting of a spring of stiffness k , a mass M called seismic-mass or proof-mass, whose movement falls behind that of housing, and a mechanical damper with coefficient b . In this model, the mass is supported by the spring and damped by the damper, and both the spring and the damper are attached to the housing of the sensor.

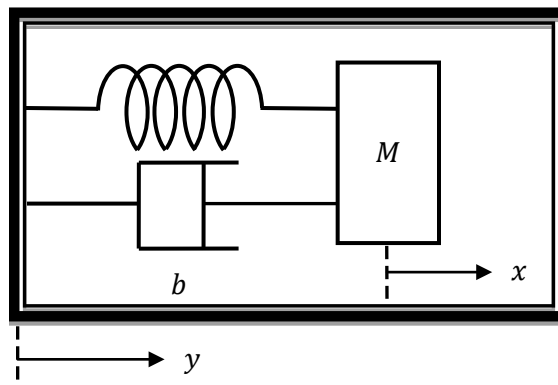


Figure 3.20 Mechanical model of accelerometer

When this damped mass-spring system is subject to acceleration, inertial force will act on the proof-mass. By applying Newton's second Law of motion, the equation of motion is derived as:

$$Ma = -kx - b \frac{dx}{dt} \quad (3.72)$$

Where a is the acceleration of the mass relative to the earth.

$$a = \frac{d^2x}{dt^2} + \frac{d^2y}{dt^2} \quad (3.73)$$

Where x is the relative displacement of the mass with respect to the housing; y is the displacement of the casing.

Replacing a with $\frac{d^2x}{dt^2} + \frac{d^2y}{dt^2}$, the equation for the mechanical model of accelerometer is as below:

$$M \frac{d^2x}{dt^2} + b \frac{dx}{dt} + kx = -M \frac{d^2y}{dt^2} \quad (3.74)$$

Through Laplace transformation, it yields

$$Ms^2X(s) + bsX(s) + kX(s) = -MY(s) \quad (3.75)$$

Where $X(s)$ and $Y(s)$ represent the Laplace transforms of output variable $x(t)$ and input variable $\frac{d^2y}{dt^2}$.

Thus,

$$X(s) = -\frac{MY(s)}{Ms^2 + bs + k} \quad (3.76)$$

By defining the variable $\omega_n = \sqrt{\frac{k}{M}}$ as natural frequency and $\zeta = \frac{b}{2\sqrt{kM}}$ as

damping ration, the transfer function can also be expressed as

$$G(s) = \frac{X(s)}{Y(s)} = -\frac{1}{s^2 + 2\zeta\omega_n s + \omega_n^2} \quad (3.77)$$

If the accelerometer is in under damped mode, in which $\zeta < 1$,

$$x(t) = \int_0^t -\frac{1}{\omega_n \sqrt{1 - \zeta^2}} e^{-\zeta\omega_n(t-\tau)} \sin(\omega_n(t-\tau)) y(t) d\tau \quad (3.78)$$

Whereas when it is under overdamped mode, in which $\zeta > 1$,

$$x(t) = \int_0^t -\frac{1}{\omega_n \sqrt{1 - \zeta^2}} e^{-\zeta\omega_n(t-\tau)} \sinh(\omega_n(t-\tau)) y(t) d\tau \quad (3.79)$$

In order to convert the displacement into corresponding voltage signal, a displacement transducer is in need, this transducer can be optical, capacitive, piezoresistive, or tunneling. For the ADXL203 sensor, there is a surface-micromachined polysilicon structure on top of its silicon wafer. This structure is held by polysilicon springs over the wafer, supplying a resistance against acceleration forces. A differential capacitor, whose stationary plates is connected to the housing and moving plates is attached to the moving mass, is employed to determine the deviation of the structure, since the capacitor value is the function of the distance. Finally, a voltage signal with amplitude proportional to acceleration can be derived. From the description of the structure, the ADXL203 is a capacitive sensor, and its functional block diagram is showed in Figure 3.20. In this diagram, two differential capacitors sense the displacements from x-axial and y-axial respectively, convert them into voltage signals. Besides, these signals are amplified and demodulated to supply the microprocessor.

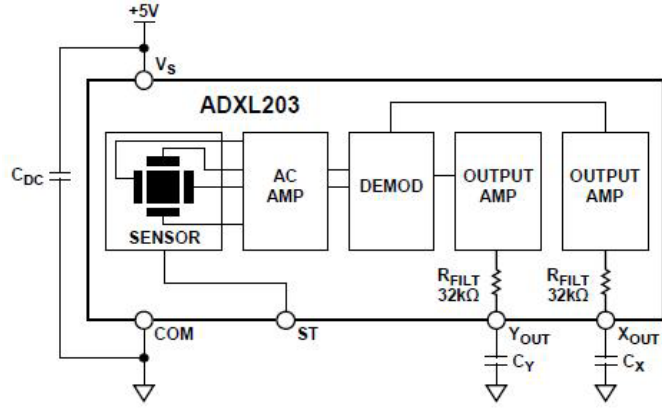


Figure 3.21 Functional block diagram of ADXL203

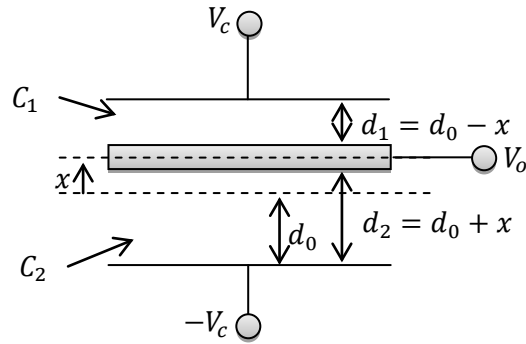


Figure 3.22 Structure of differential capacitor

In differential capacitor illustrated in Figure 3.21, the seismic mass is connected to the moving plates, changing the distance between the moving plate and the static plates, varying the capacitances C_1 and C_2 , whose values are the functions of d_1 and d_2 . Moreover, the moving distance of the mass is the difference between d_1 and d_2 . Thus the output of the capacitor is as below:

$$V_o = \frac{C_1 - C_2}{C_1 + C_2} V_c \quad (3.80)$$

The use of the ADXL203 in the scooter is for tilt angle measurement. In order to decide the orientation of the motion device, the force of gravity is applied as an

input vector. The installation of the accelerometer makes the x-axis and y-axis both parallel to the earth's surface so as to be able to measure the tilt angle around the roll axis and pitch axis. Conversion equation between the output voltage signal from the sensor and the acceleration signal A_x is needed.

$$A_x = \frac{V_{xout} - V_{off}}{S} \quad (3.81)$$

$$A_y = \frac{V_{yout} - V_{off}}{S} \quad (3.82)$$

Where $S = \frac{\Delta V}{\Delta g}$ is the sensitivity; V_{xout} and V_{yout} is the output signal; A_x and A_y is the acceleration; V_{off} is the accelerometer offset at 0g, and g is the earth's gravity.

As a result, the tilt angle can be calculated as

$$\theta_{pitch} = \arcsin\left(\frac{A_x}{R}\right) \quad (3.83)$$

$$\theta_{roll} = \arcsin\left(\frac{A_y}{R}\right) \quad (3.84)$$

Where R is half of the scale of the accelerometer.

In the case of ADXL203, $V_{off} = 2.5V$, $S = 1V/g$, and its output signal varies between $-1g$ and $1g$, thus,

$$A_x = \frac{V_{xout} - 2.5V}{1V/g} \quad (3.85)$$

$$A_y = \frac{V_{yout} - 2.5V}{1V/g} \quad (3.86)$$

$$\theta_{pitch} = \arcsin\left(\frac{A_x}{1g}\right) \quad (3.87)$$

$$\theta_{roll} = \arcsin\left(\frac{A_y}{1g}\right) \quad (3.88)$$

3.3.3.2 Modeling of Gyroscope

Gyroscope is the device for determining the rotation around one of the axes. Generally speaking, most microgyroscopes use vibrating element for angular rate sensing, based on the principles of Coriolis force. This can be further explained in the spring-mass-damping system with two degree of freedom as demonstrated in Figure 3.23.

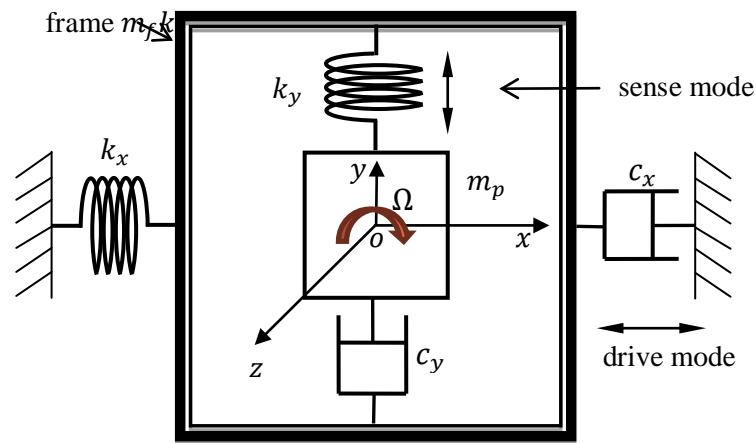


Figure 3.23 Mechanical model of vibrational gyroscope

This system consists of an inertial element m_p , which is usually called proof mass, a decoupling frame, and two orthogonal sets of springs and damper to suspend the proof mass and frame. When the proof mass is under the rotation about z axis and excited along x axis (drive direction) with prescribed amplitude, Coriolis force is induced in y direction, causing the proof mass to oscillate along this sense direction. In this way, the energy is transferred from the drive mode to sense mode, and the output is in proportion to the angular rate input. In addition, in order to reach maximum possible amplitude of oscillation, most microgyroscopes are driven and sensing at resonance.

The Coriolis force F_c on the proof mass is calculated by

$$a_c = 2 \frac{dx}{dt} \Omega \quad (3.89)$$

$$F_c = m_p a_c = 2m_p \frac{dx}{dt} \Omega \quad (3.90)$$

Where a_c is Coriolis acceleration; Ω is the angular speed of rotation.

If the external force $F(t) = F_0 \sin \omega_D t$, the dynamic equations of motion in driving direction x and sensing direction y are:

$$m_p \frac{d^2 x}{dt^2} + c_x \frac{dx}{dt} + k_x x = F_0 \sin \omega_D t \quad (3.91)$$

$$m_p \frac{d^2 y}{dt^2} + c_y \frac{dy}{dt} + k_y y = 2m_p \frac{dx}{dt} \Omega \quad (3.92)$$

Where c_x and c_y are the air damping coefficients; k_x and k_y are the stiffness of spring.

The solution of above equations are given as

$$x(t) = -\frac{F_0 Q_x}{k_x \omega_x} \cos \omega_x t \quad (3.93)$$

$$\begin{aligned} y(t) &= \frac{2m_p \Omega \omega_x F_0 Q_x}{k_x k_y} \frac{1}{\sqrt{(1 - (\omega_x/\omega_y)^2)^2 + (\omega_x/\omega_y)^2}} \sin(\omega_x t \\ &\quad - \varphi) \end{aligned} \quad (3.94)$$

Where $\varphi = \arctan \frac{c_y \omega_x / m_p}{\omega_y^2 - \omega_x^2}$; $Q_x = \frac{m_p \omega_x}{c_x}$; $Q_y = \frac{m_p \omega_y}{c_y}$; ω_x and ω_y are the

resonant frequencies; Q_x and Q_y are the frequency quality factors along corresponding x and y direction.

The dynamic equations show that the vibratory gyroscope is actually an accelerometer, since both of their sensing elements produce displacement signal. From the solution functions, it is obvious that if the drive amplitude of $x(t)$ remains constant, the amplitude of $y(t)$ as resulting oscillation signal in the sense mode is proportional to angular rate Ω .

The two-wheeled self-balancing scooter use ADXRS300 as rate sensor. The ADXRS300 is a Z-axis rate-sensing device, and it can be called yaw-rate sensing gyro. As a resonator gyro, it uses a two polysilicon sensing structures with an electrostatically driven to resonance dither frame each. Thus the Coriolis force can be produced and the corresponding proportional displacement signal is sensed by a capacitive pickoff structure, through which this mechanical signal is converted into electrical voltage signal. The principle of the capacitive conversion is very similar to that of the accelerometer explained before. The block diagram of it in Figure 3.23 gives the internal circuit structure of the IC.

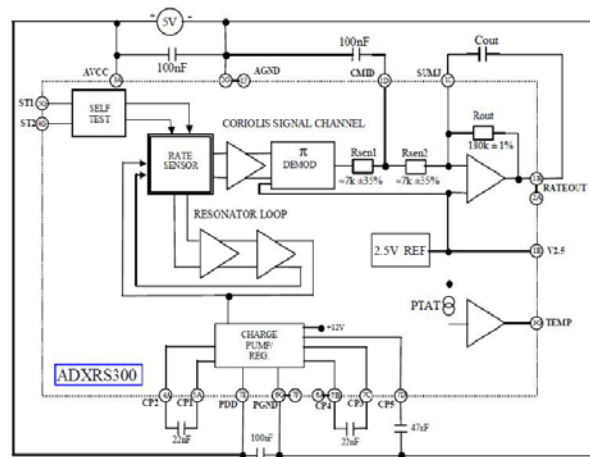


Figure 3.24 Block diagram with external components of ADXRS300

In the above block diagram, the signal from sense mode is amplified and demodulated to supply microprocessor. For clockwise rotation about the Z axis, it produces positive going voltage signal. The relationship between the rate in voltage and rate out voltage is showed below in Figure 3.25.

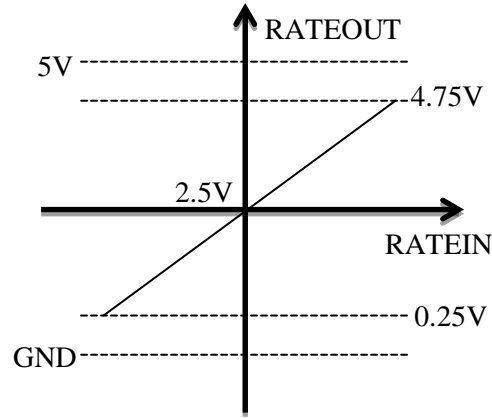


Figure 3.25 RATEOUT vs. RATEIN Curve for ADXRS300

Thus the transfer function between the angular rate and the voltage output is expressed as:

$$a_{\theta} = \frac{V_{Rout} - V_{null}}{S_g} \quad (3.95)$$

Where the offset at 0 rad/s $V_{null} = 2.5V$; and the sensitivity $S_g = 0.05V/^{\circ}/s$.

For the case of ADXRS300,

$$a_{\theta}(rad/s) = \frac{V_{Rout} - 2.5V}{0.05V/^{\circ}/s} * \frac{\pi}{180^{\circ}} \quad (3.96)$$

3.3.4 Sensor fusion

Accelerometer can directly output the proportional voltage data to derive the tilt angle, while gyroscope measures the tilt angular rate, and through integration over time, the tilt angle can also be calculated. Both of these sensors have their own advantages and disadvantages in tilt angle measurement. The signal from accelerometer is noisy, and its horizontal acceleration may be mistaken as an angular change. Even when a low-pass filter is added after the output of the accelerometer to make sure that the short-term horizontal acceleration signal is filtered out and only the long-term signal passes through it to the microprocessor, it still has slow response time because of the averaging, which is bad for stability. The gyroscope can generate fast and accurate angular rate signal, however, due to the bias drift of the sensor, a small error will keep adding to the angle data during integration to make it far away from the actual angle data. In conclusion, the accelerometer is preferred for long term measurement while the gyroscope is effective for short term.

In order to make the most of the best qualities of the accelerometer and gyroscope, their data needs to be combined in a smart way to achieve a more accurate, stable and faster performance of the system. Therefore, the sensor fusion technique is in need, by which the data is optimized through a certain adaptive algorithm to obtain dynamic results with accuracy and responsiveness. The simplest sensor fusion algorithm to use is the complementary filtering, which is designed to fuse both of the sensors to compensate the weaknesses of each other.

The basic idea of the algorithm is that the sum of the outputs from a time-varying signal passing through a low-pass filter and a high-pass filter exactly equals

to the input signal. Since the modeling functions of both accelerometer and the gyro are 2nd order equations, the 2nd order filters are chosen in sensor fusion calculation for the scooter. And the unity gain transfer function of the 2nd order low-pass and high-pass filters can be expressed as:

$$G_L(s) = \frac{1}{1 + 2\zeta \frac{s}{\omega_n} + (\frac{s}{\omega_n})^2} \quad (3.97)$$

$$G_H(s) = \frac{(\frac{s}{\omega_n})^2}{1 + 2\zeta \frac{s}{\omega_n} + (\frac{s}{\omega_n})^2} \quad (3.98)$$

Where ζ is damping ration; ω_n is the undamped natural frequency.

The pole are calculated as $\rho_{1,2} = (-\zeta \pm \sqrt{\zeta^2 - 1})\omega_n$.

The block diagram in Figure 3.25 explains how the data from accelerometer and gyroscope get fused together.

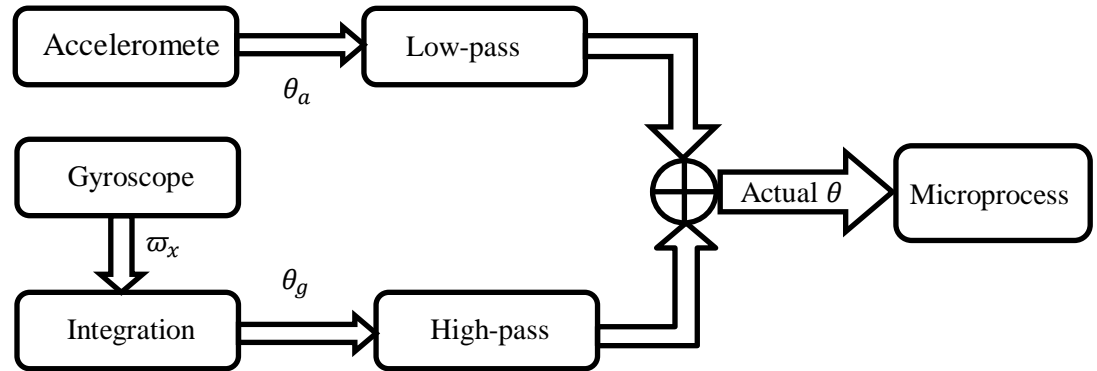


Figure 3.26 Block diagram of complementary filter for accelerometer and gyroscope

If the simple 2nd order filters are applied, the sum of the outputs is in the form showed below:

$$\begin{aligned}
\theta &= \theta_a G_L(s) + \theta_g G_H(s) \\
&= \theta_a \frac{1}{1 + 2\zeta \frac{s}{\omega_n} + (\frac{s}{\omega_n})^2} \\
&\quad + \theta_g \frac{(\frac{s}{\omega_n})^2}{1 + 2\zeta \frac{s}{\omega_n} + (\frac{s}{\omega_n})^2}
\end{aligned} \tag{3.99}$$

From the diagram, the low-pass filter allows long-term signals from accelerometer to pass through, filtering out short-term fluctuations. On the contrary, short-term signals from gyroscope remain through the high-pass filter, and steady signals are filtered out. The illustrations of bode plot and phase over frequency diagram of both 2nd order are showed in Figure 3.27.

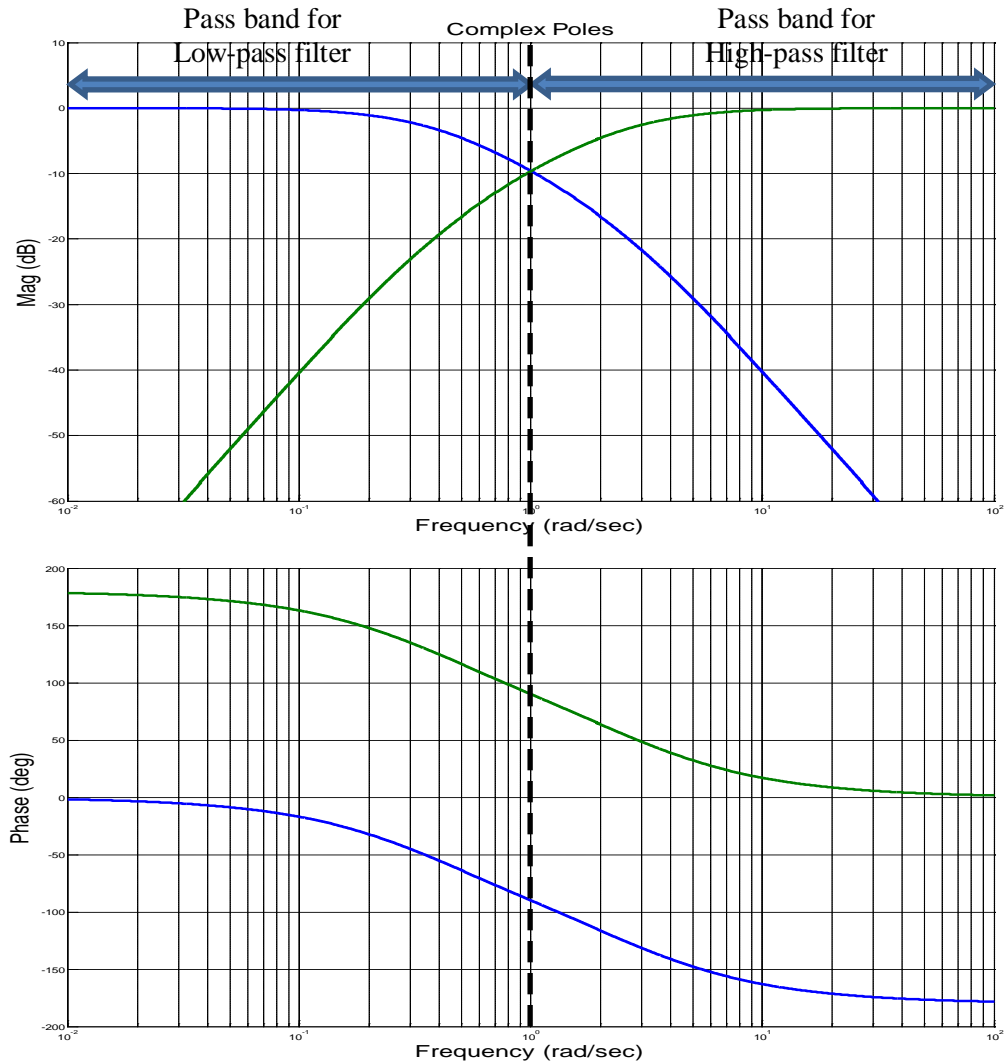


Figure 3.27 Bode plot and phase over frequency diagram for Low and high pass filter

This shows that when working at low frequency, which is lower than the cut off frequency f_c , the data from the accelerometer is weighted for the actual angle calculation, and when the frequency is higher than f_c , the calculation is mainly based on the signal from gyro. The algorithm of complementary filter can be assumed to be a weight function for accelerometer signal and gyroscope signal.

3.3.5 Modeling of electromagnetic relay

Generally speaking, relay is a communication carrier, which can be considered as on/off switches operated electromagnetically. It is intrigued by low power command signal to control the on/ off status of electrical devices, such as motors and valves. From this perspective, relay can be counted as digital (0/1) type amplifier instead of analog amplifier.

There are two types of electromagnetic relay, normally-closed (NC) relay and normally-open (NO) relay. The basic structure of the relay is simplified in Figure 3.27, mainly consisting of stationary member and moving plunger forming the flux path. The relay is energized when the voltage is applied to the winding to generate current flow in it. As a result, the plunger is moved by the corresponding electromagnetic force F_e towards the direction of minimizing the reluctance. The moving contacts are attached to the plunger, turning on or off the related electrical circuit. When the voltage to the winding is removed, the plunger goes back to its equilibrium position because of the returning spring k_a .

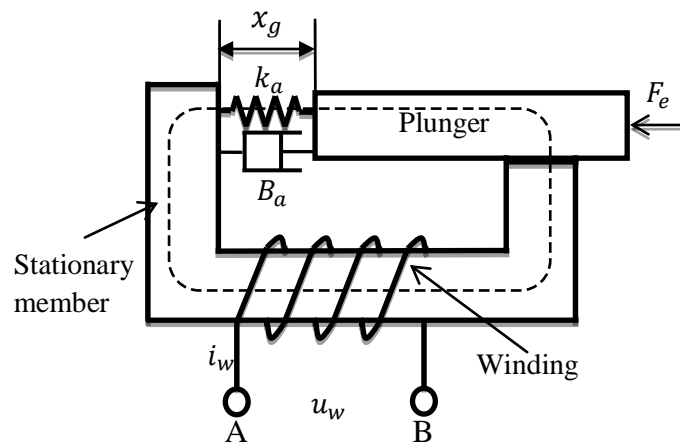


Figure 3.28 Simple schematics of electromagnetic relay schematics

The dynamic equation of the plunger can be developed by Newton's second law of motion,

$$m_{pl} \frac{d^2 x_g}{dt^2} = F_e(i, x_g) - B_a \frac{dx_g}{dt} - F_{sp}(k_a, x_g) \quad (3.100)$$

Where x_g is the width of the air gap; i is the current in the winding; m_{pl} is the mass of plunger; B_a is the damping coefficient; k_a is the spring constant for the returning spring.

Moreover, by Krichhoff's Law of $u = ri + \frac{d\psi}{dt}$ and $\psi = L(x)i$, one obtains u_w as:

$$u_w = r_R i_w + L(x_g) \frac{dr_R}{dt} + i \frac{dL(x_g)}{dx_g} \frac{dx_g}{dt} \quad (3.101)$$

Where u_w and i_w is the voltage and current applied to the winding; r_R is the resistance of the system.

The air-gap reluctance is,

$$\mathfrak{R}_a = \frac{x_g}{\mu_0 A_a} \quad (3.102)$$

Where A_a is the cross-sectional area of the air gap; μ_0 is the permeability of free space.

The reluctances of the ferromagnetic materials of stationary and moving parts \mathfrak{R}_s and \mathfrak{R}_m are given as below:

$$\mathfrak{R}_s = \frac{l_s}{\mu_0 \mu_{rs} A_s} \quad (3.103)$$

$$\mathfrak{R}_m = \frac{l_m}{\mu_0 \mu_{rm} A_m} \quad (3.104)$$

Where l_s and l_m are the equivalent lengths of the magnetic flux in the ferromagnetic stationary member and plunger respectively; μ_{rs} and μ_{rm} are the permeability of the stationary member and plunger material respectively; A_s and A_m are the effective cross-sectional area of the stationary member and plunger respectively.

Thus the magnetizing inductance of the relay is derived as below:

$$\begin{aligned} L(x_g) &= \frac{N^2}{\mathfrak{R}_a + \mathfrak{R}_s + \mathfrak{R}_m} \\ &= \frac{N^2}{\frac{x_g}{\mu_0 A_a} + \frac{l_s}{\mu_0 \mu_{rs} A_s} + \frac{l_m}{\mu_0 \mu_{rm} A_m}} \end{aligned} \quad (3.105)$$

Where N is the number of winding turns.

The electromagnetic force is obtained as below:

$$\begin{aligned} F_e(i, x_g) &= \frac{1}{2} i^2 \frac{\partial L(x_g)}{\partial x_g} \\ &= -i^2 \frac{N^2 \mu_{rs} \mu_{rm}}{2 \left(\frac{x_g}{\mu_0 A_a} + \frac{l_s}{\mu_0 \mu_{rs} A_s} + \frac{l_m}{\mu_0 \mu_{rm} A_m} \right)^2} \end{aligned} \quad (3.106)$$

Substitute the equation of $F_e(i, x_g)$ into the dynamic equation of the plunger, and the equation of $L(x_g)$ into the electrical equation of the plunger by neglecting the leakage, the dynamic of the plunger are:

$$\frac{dx_g}{dt} = v_{pl} \quad (3.107)$$

$$\begin{aligned} \frac{dv_{pl}}{dt} &= \frac{1}{m_{pl}} \left[i^2 \frac{N^2 \mu_{rs} \mu_{rm}}{2 \left(\frac{x_g}{\mu_0 A_a} + \frac{l_s}{\mu_0 \mu_{rs} A_s} + \frac{l_m}{\mu_0 \mu_{rm} A_m} \right)^2} \right. \\ &\quad \left. - B_a \frac{dx_g}{dt} - F_{sp}(k_a, x_g) \right] \end{aligned} \quad (3.108)$$

$$\begin{aligned}
& \frac{di}{dt} \\
&= \frac{\frac{x_g}{\mu_0 A_a} + \frac{l_s}{\mu_0 \mu_{rs} A_s} + \frac{l_m}{\mu_0 \mu_{rm} A_m}}{N^2} [u - ri \\
& \quad - \frac{N^2 \mu_{rs} \mu_{rm}}{2 \left(\frac{x_g}{\mu_0 A_a} + \frac{l_s}{\mu_0 \mu_{rs} A_s} + \frac{l_m}{\mu_0 \mu_{rm} A_m} \right)^2} i v_{pl}]
\end{aligned} \tag{3.109}$$

3.3.6 Modeling of optical encoder

An optical rotary encoder is electro-mechanical measurement device transferring angular position into digital signal. Compared to other counterparts, it is advanced in high resolution, high accuracy and direct digital output. Basically, there are two types of optical rotary encoder, absolute encoder and incremental encoder. Although both of the two types have very similar structure, composed of shaft, disk, light source and photo sensor, which could be photo cell, photo transistor or photo diode, the biggest difference between them is the pattern of tracks on the code disk.

Absolute encoder uses a pattern of concentric tracks on the disk, and each of the tracks is paired with individual photo sensor to receive the light signal and generate binary digit (0 or 1). By combining all the digits from the photo sensors in certain sequence into digital word, encoded binary output is produced. This method is straight forward, but it is limited to single revolution measurement, and generally used to determine fractions of a revolution.

On the other hand, incremental encoder has a single track equally spaced on the slotted disk, as is illustrated in Figure 3.29. As the disk rotates with the shaft

caused by the motion that is being measured, the light can pass through the slots and sensed by photo sensor to output pulse signal. By counting the number of pulses received, the angular displacement can be determined. Moreover, the angular speed can also be derived by timing the pulses.

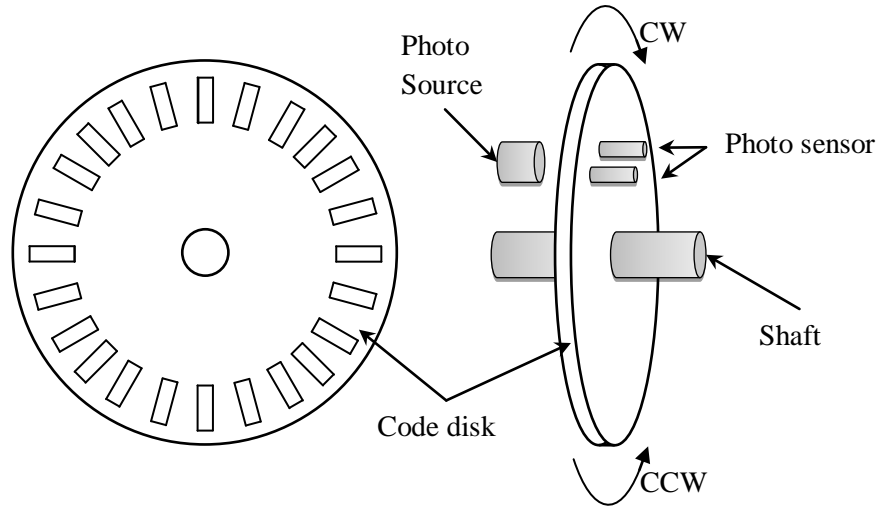


Figure 3.29 Basic structure of incremental encoder

The angular displacement θ_{en} is calculated as:

$$\theta_{en} = 2\pi \frac{\# \text{ of pulses}}{\text{pulses/revolution}} \text{ (rad)} \quad (3.110)$$

The angular speed $\dot{\theta}_{en}$ is calculated as:

$$\begin{aligned} \dot{\theta}_{en} &= \frac{\frac{\# \text{ of pulses}}{\text{pulses/revolution}}}{\text{fixed time interval(sec)}} \\ &\quad \times \frac{60\text{sec}}{1\text{min}} \text{ (RPM)} \end{aligned} \quad (3.111)$$

However, the direction of rotation can't be decided by single photo sensor, thus incremental encoder with two photo sensors called quadrature encoder is employed in measurement including both clockwise (CW) and counter clockwise

(CCW) rotation. By comparing the pulse signals from the two photo sensor, the direction of the rotation can be obtained. Figure 3.30 demonstrates the waveforms for the two photo sensor for certain cases. The two photo sensors are intentionally positioned so as to create two groups of pulse signals with 90 degrees of phase shift. If the signal from channel A is leading, then the rotation is clockwise, otherwise it is counter clockwise.

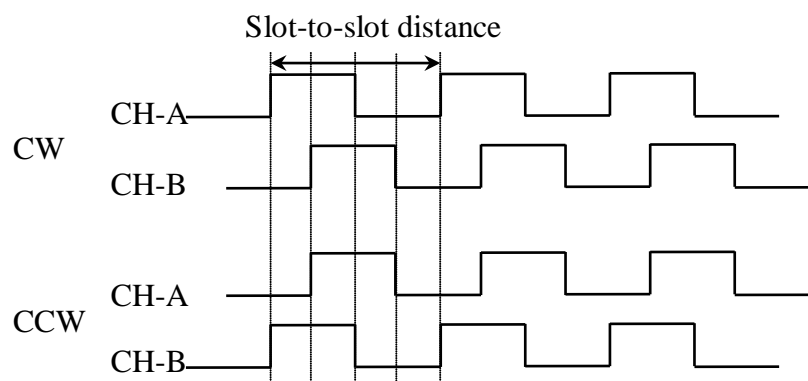


Figure 3.30 Encoder wave form for clockwise and counter-clockwise rotation

The optical encoder used in the two-wheeled self-balancing scooter is E4P module, which is offering two channel Quadrature TTL outputs. The two outputs are analyzed in microprocessor to decide the angular displacement and speed.

3.3.7 Modeling of microprocessor system

3.3.7.1 Modeling of microprocessor

Microprocessor, usually referring to the term of central processing unit (CPU), acts as the brain for mechatronic systems. It is typically a large scale integrated chip incorporated with digital arithmetic, logic, communication and control circuits to realize multipurpose performances.

Generally speaking, this programmable device may include CPU, which is composed of arithmetic logic unit (ALU) and control logic section as its subparts, memory and I/O devices. The structure of microprocessor varies depending on the requirements from different applications, and the minimal component for the device is CPU, performing the function of numerical and logic computing in ALU and data management in control logic section. The buses, such as address bus, control bus and data bus, carry corresponding information to enable the communication among CPU, memory and I/O devices. The basic structure and data exchange for general microprocessor is illustrated in Figure 3.31.

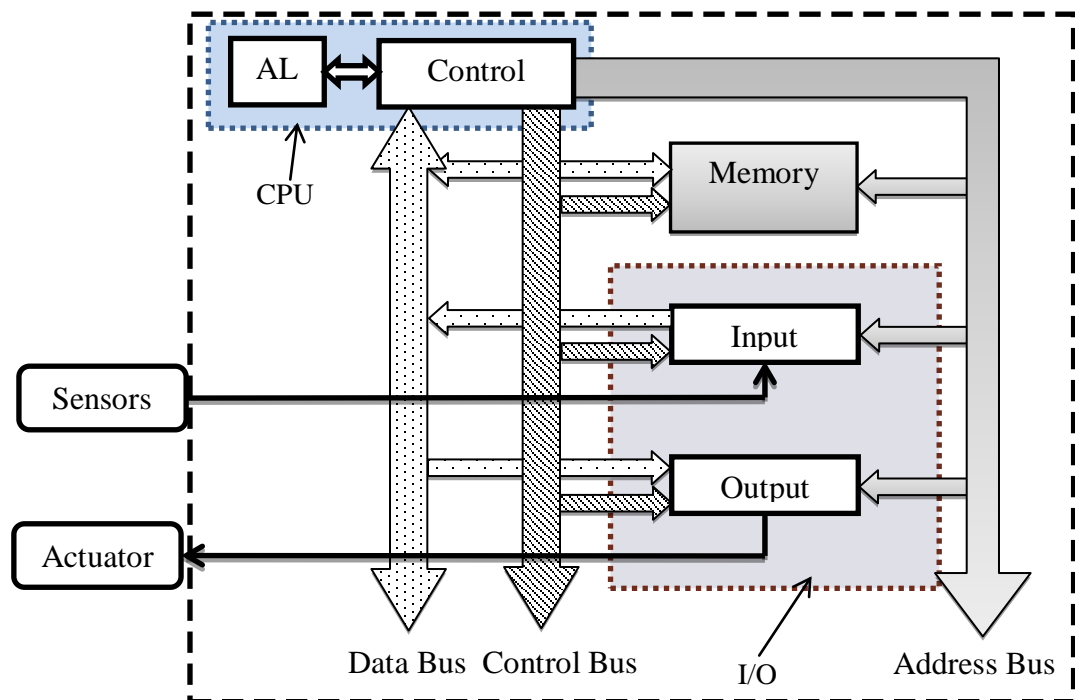


Figure 3.31 Basic structure and data exchange for general microprocessor

From Figure 3.31, it shows that the I/O section makes the data exchange possible between microprocessor and peripheral equipment through its interfaces,

such as various sensors and keyboard as input devices, and actuators and monitors as output devices. The I/O interface is also called port. Since microprocessor can only deal with digital data in words, composed of 8, 16 or 32 bits in binary form (0 or 1), the data may need analog-to-digital conversion through the input port and digital-to-analog conversion through the output port to make it matching with corresponding devices. All converted digital data is stored in the memory section, with a unique numeric address assigned to each byte. The memory can be divided into two kinds, random access memory (RAM) and read-only memory (ROM). In RAM, CPU can access any of its addresses to read or write data, while CPU is limited to read and cannot change the content in ROM. Besides, RAM is volatile memory, which is used for temporary program storage, whereas ROM is nonvolatile memory used for long term program storage. In the CPU, the ALU is in charge of all arithmetic operations of data from memory or I/O realized by the combination of logic gate and flip-flops, and it has accumulator as the principal register to hold data for mathematical operation and result storage. On the other hand, the control unit of the CPU executes the programs stored in memory in the form of instructions and data to give timing and control signals to other sections. The connection of I/O, memory and CPU are accomplished by the buses. Similar to memory address, the I/O ports are assigned with digital addresses. As a result, the address bus can treat the memory and I/O ports equally to map the data and carry their addresses from CPU to memory and I/O ports. The actual data are carried by the data bus in both directions after the address bus gets the designated address. At the same time, the control bus holding the timing and event-control signal from the control unit decides whether or not to read/write the

current data flow. All above processes are finished by the execution of the machine language program loaded into the memory sequentially beforehand. This program is written according to the specific microprocessor instruction set, in which each instruction is given distinctive operation code (op-code) of 8 bits long typically. The whole process is just like a series of fetch-executive cycles, with an address-storage register named program counter to track the current stage of the program.

As is said previously, the I/O section links the microprocessor with other input or output devices, and this can be done through parallel interface, transferring data of 8 bit or longer at the same time on eight or more wires, or serial interface, sending data 1 bit at a time on single wire. No matter which way is chosen, only digital signals are accepted by the microprocessor. Therefore, the rules for digital-to-analogy (DAC) and analog-to-digital (ADC) need to be set.

3.3.7.2 Modeling of DAC

A DAC is a circuit comprised of switches, op-amps and resistors in order to convert digital data, which is usually in binary form, into equivalent physical signals, such as voltage and current. It works as a decoder. Based on the circuit design, there are mainly two types of DAC devices, binary weighted resistor DAC and R-2R ladder DAC. A simplified block diagram of general n bits DAC is showed in Figure 3.31. The input in this figure is digital data D_n composed of n bits binary number from least significant bit (LSB) d_0 to most significant bit (MSB) d_{n-1} , while the output is analog voltage V_{out} , which is proportional to input value. The voltage V_{ref} supplied to the DAC is called reference voltage.

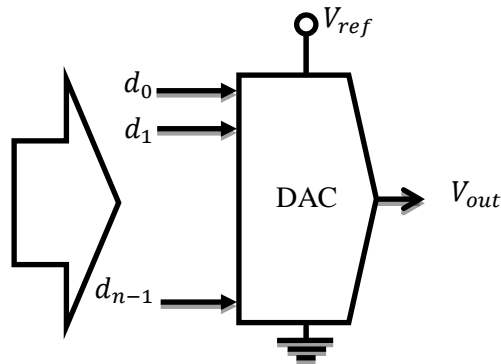


Figure 3.32 Simplified block diagram of n bits DAC

There are several factors that could affect the quality of conversion, such as reference voltage, resolution, speed, linearity, setting time and errors. Among these parameters, the reference voltage and resolution determine the main characteristics of a DAC. The reference voltage is the voltage used to decide the full scale voltage in output, whereas the resolution defines the voltage step increment in output corresponding to 1 LSB change in input. Under specified reference voltage V_{ref} and n bit digital input, the maximum voltage output V_{fs} and the resolution V_{LSB} of a DAC can be derived as below:

$$V_{fs} = \frac{2^n - 1}{2^n} V_{ref} \quad (3.112)$$

$$V_{LSB} = \frac{V_{ref}}{2^n} \quad (3.113)$$

The relationship between the digital input and analog output is illustrated in Figure 3.33. Ideally, they are linearly related, and the transfer curve is a set of discrete points as is shown in Figure 3.33 rather than continuous curve. The accuracy of the conversion suffers from various errors, such as the errors from differential non-

linearity, integral non-linearity and non-monotonicity, and the error because of gain and offset, bringing the deviation from the real value in output.

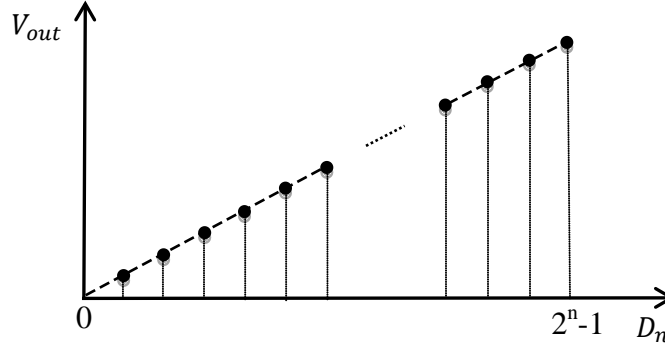


Figure 3.33 Ideal transfer curve of DAC

By converting the binary form digital data into decimal number through Equation (3.112), the transfer function for digital data D_n converting into analog voltage V_{out} is established in Equation (3.113).

$$D_n = d_{n-1} \cdot 2^{n-1} + d_{n-2} \cdot 2^{n-2} + \dots + d_1 \cdot 2^1 + d_0 \cdot 2^0 = \sum_{i=0}^{n-1} d_i \cdot 2^i \quad (3.114)$$

$$V_{out} = \frac{D_n V_{ref}}{2^n} = \frac{\sum_{i=0}^{n-1} d_i \cdot 2^i V_{ref}}{2^n} \quad (3.115)$$

3.3.7.3 Modeling of ADC

Compared to DAC, an ADC is a device that performs reverse operation, converting continuous analog signal into discrete digital code. The design of most ADC is based on the comparator principle to determine the on/off status of a particular bit in the binary form output. There are difference types of ADC circuit

design, such as digital ramp ADC, successive approximation ADC and flash ADC.

The simplified block diagram of general n bits ADC is showed in Figure 3.34.

Compared to the DAC in Figure 3.31, the ADC has more control signals to monitor the conversion process, such as the sampling clock, the star of conversion(SOC), and end of conversion (EOC).

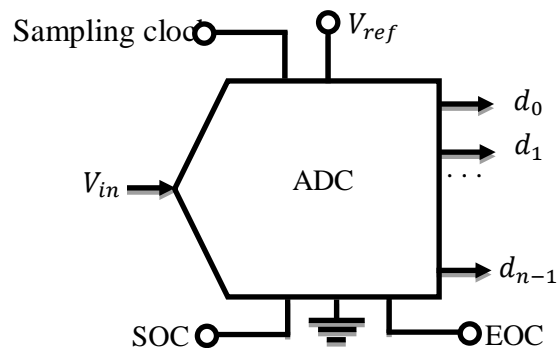


Figure 3.34 Simplified block diagram of n bits ADC

Generally speaking, the ADC conversion is a more complicated process, which cannot be finished instantaneously, and it is divided into two stages: sample and hold (S/H), quantization and binary encoding. Before the analog input is ready for conversion, it has to be stabilized, which is done by sample and hold stage. Sampling is the process of selecting a sequence of instantaneous values from continuously varying analog signal at regular time interval. Since the conversion destroys information, this process needs to choose appropriate sampling frequency and capture the key signal to avoid aliasing in later reconstruction. The result of the process is a sequence of discrete-time impulses, whose value equals to the amplitude of corresponding analog signal at the instant time of capturing. In order to eliminate variations, these values are locked for a specified period of time for interpolation

between samples to create stair step shape continuous signal through S/H circuit for quantization and binary encoding stage. Quantization is the process of mapping various input values into a set of discrete codes. By quantization, the stair step shape continuous signal will be rounded off to the nearest discrete values. Furthermore, the step size of the quantization interval is determined by the input dynamic range and perceptual sensitivity. At last, the quantized value can be converted into binary form through binary encoding for final output.

Similar to DAC, the performance metrics of ADC conversion are resolution, speed, and errors. The resolution of an ADC is crucial to its performance since it defines the sensitivity of the ADC. In an n -bit ADC supplied with reference voltage V_{ref} , the resolution can be expressed as:

$$V_{LSB} = \frac{V_{ref}}{2^n - 1} \quad (3.116)$$

The speed parameters in ADC include the conversion speed, aperture time, and transfer time. Besides the similar errors as DAC, there are quantization error in ADC resulted from the round off during the process. The ideal ADC transfer curve is illustrated in Figure 3.34, in which the analog input and digital output are also linearly related. The difference from the DAC transfer curve is that it is in the staircase shape without the vertical rising lines, indicating that the digital output from ADC jumps from code to code and the transition voltage is the same size as the resolution.

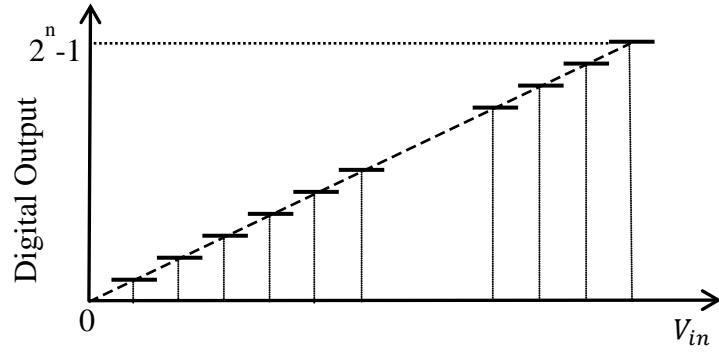


Figure 3.35 Ideal transfer curve of ADC

Finally, the transfer function for analog voltage V_{in} conversing into n bit digital data D_n is established in Equation (3. 117)

$$D_n = \frac{V_{in}}{V_{ref}} \times (2^n - 1) \quad (3.117)$$

In addition, the D_n is in decimal form from above conversion, and the binary code needs to be converted from this decimal number.

3.3.7.4 CompactRio system

The microprocessor system used in the two-wheeled self-balancing scooter is the advance reconfigurable embedded control and acquisition system—CompactRio from National Instrument. This processor includes a real-time controller, a reconfigurable chassis, and I/O modules, and those used in the scooter are showed in Figure 36, Figure 37 and Figure 38.



Figure 3.36 NI cRIO-9014 Real-time controller



Figure 3.37 Reconfigurable FPGA chassis



Figure 3.38 I/O modules

The NI cRIO-9014 real-time controller is equipped with an industrial 400 MHz Freescale MPC5200 processor. Besides, it contains a real-time clock, hardware watchdog timers, and dual 10/100 Mbits/s Ethernet ports enabling the direct communication between computer program and the controller, etc. Its 128 MB of DRAM memory and 2 GB of nonvolatile storage make it able to download and run the LabVIEW program so as to realize various control functions, such as multi-rate control, data exchange, and onboard data logging. The FPGA works as the bridge to enable the communication between the real-time processor and the I/O modules for data exchange and control of the peripheral devices. Furthermore, the FPGA chassis can be either four-slot or eight-slot, depending on the number of required I/O modules. It allows the I/O module directly connected to the FPAG for customized timing, triggering, synchronization and signal conditioning. Because of the direct FPGA connection instead of data bus connection and processing program code in hardware, both the speed and reliability of control are increased. The processed data in FPGA are from various sensors and actuators, which must go through the I/O modules for signal isolation, conversion and conditioning before processing by the controller. Based on the data types, a variety of I/O modules are available to receive analog current, voltage input, digital inputs or thermocouple inputs, etc. The I/O modules in Figure 39 are NI 9201 for analog input from accelerometer and gyro input, NI 9505 for digital input from encoders and scooter motor control.

The overall architecture of the CompactRIO control system for two-wheeled self-balancing system is shown in Figure 3.38, illustrating a more detailed internal relationship between the real-time controller, FPGA and peripheral devices. The

high-speed PCI bus carries the data for exchange between the real-time controller and FPGA, while the I/O modules directly linked to the FPGA are in charge of the communication between FPGA and peripheral devices. In the I/O modules, the signals can be input through screw terminals, D-sub, BNC or other customized connector block, and they are attenuated and filtered during signal conditional process. At last, they are isolated and digitalized in ADC/DAC conversion. Because of the embedded FPGA, this control and data acquisition system is at low-cost and with open access to low-level hardware resources. Especially with the built-in data transfer mechanisms in the RIO core, the real-time analysis, post processing, data logging, or communication to a networked host computer can be realized by transferring data from the I/O modules to the FPGA or from the FPGA to the embedded processor.

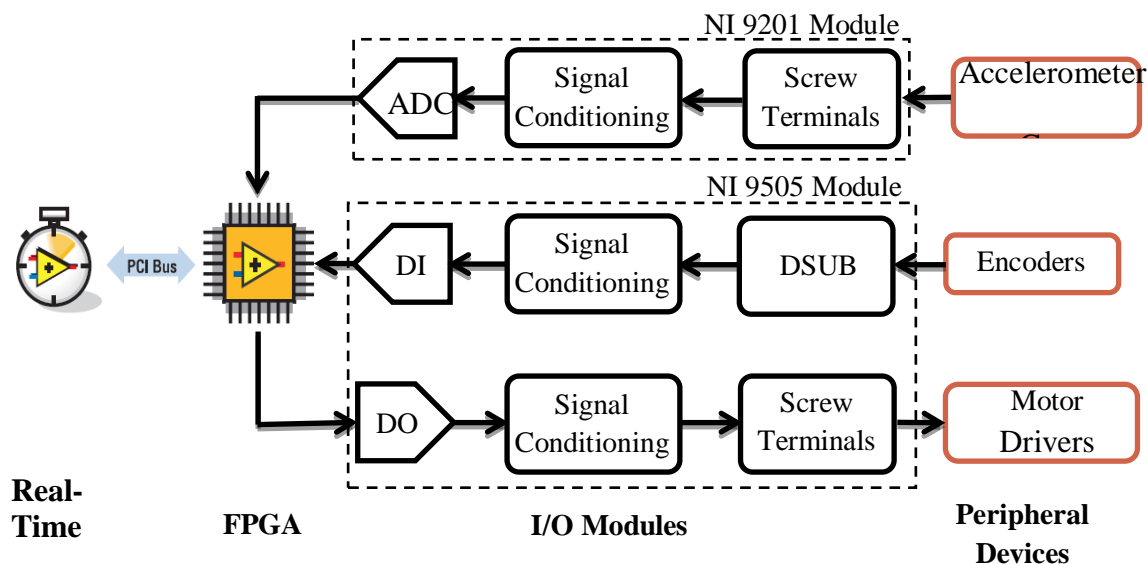


Figure 3.39 Architecture of the CompactRIO system of two-wheeled self-balancing scooter

3.4 State space modeling for scooter drivetrain system

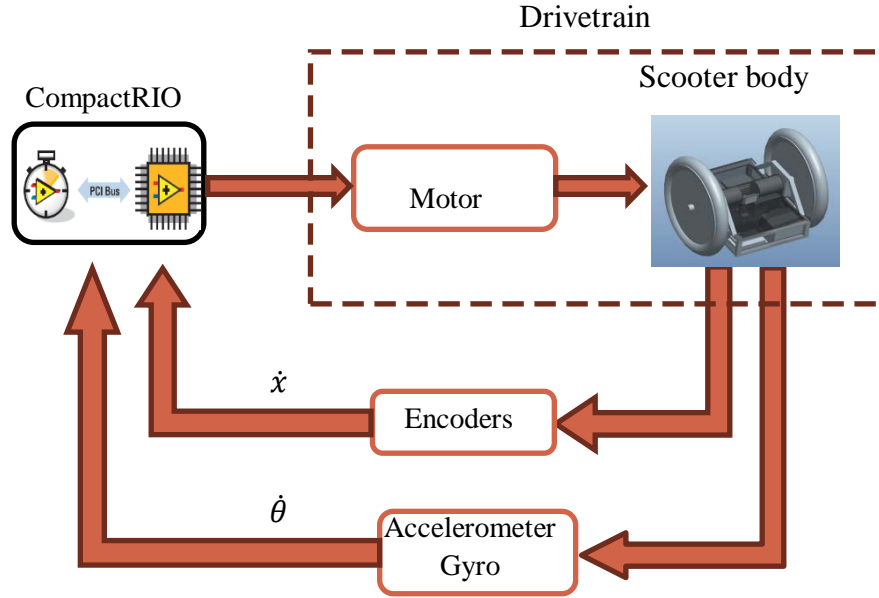


Figure 3.40 Architecture of the Comprehensive system of two-wheeled self-balancing scooter

Figure 3.40 illustrate the whole system structure of the two-wheeled self-balancing scooter, and the scooter drivetrain system is showed in the dash line frame, consisting of scooter body and motor drivers.

In order to build the state space modeling, the linearization of mechanical modeling of scooter body is needed. As previous given, they are given in two equations as below:

$$\begin{aligned}
 & (I_b + 2m_b r_b^2) \ddot{\theta} + 2m_b r_b \cos\theta \ddot{x} \\
 & - 2m_b r_b (\sin\theta) \dot{x} \dot{\theta} \\
 & - m_b g r_b \sin\theta \cos\beta = 0
 \end{aligned} \tag{3.118}$$

$$\begin{aligned}
& m_b \ddot{x} + (m_b r_b \cos \theta) \ddot{\theta} - (m_b r_b \sin \theta) \dot{\theta}^2 + 2m_w \ddot{x} \\
& + 2I_w \frac{\ddot{x}}{r^2} = F_T
\end{aligned} \tag{3.119}$$

Since θ is considered to be very small angle, by making $\sin \theta = \theta$ and $\cos \theta = 1$, they can be derived as:

$$\begin{aligned}
& (I_b + 2m_b r_b^2) \ddot{\theta} + 2m_b r_b \ddot{x} - 2m_b r_b \theta \dot{x} \dot{\theta} \\
& - m_b g r_b \theta \cos \beta = 0
\end{aligned} \tag{3.120}$$

$$\begin{aligned}
& (I_b + 2m_b r_b^2) \ddot{\theta} + 2m_b r_b \ddot{x} - 2m_b r_b \theta \dot{x} \dot{\theta} \\
& - m_b g r_b \theta \cos \beta = 0
\end{aligned} \tag{3.121}$$

In order to decouple θ , $\dot{\theta}$ and \dot{x} , taylor expansion is used.

$$(\sin \theta) \dot{\theta}^2 = \dot{\theta}_0^2 \theta \tag{3.122}$$

$$\theta \dot{x} \dot{\theta} = \dot{x}_0 \dot{\theta}_0 \theta \tag{3.123}$$

$$\begin{aligned}
& (I_b + 2m_b r_b^2) \ddot{\theta} + 2m_b r_b \ddot{x} - (2m_b r_b \dot{x}_0 \dot{\theta}_0 \\
& + m_b g r_b \cos \beta) \theta = 0
\end{aligned} \tag{3.124}$$

$$\begin{aligned}
& (m_b r_b) \ddot{\theta} + (2m_w + 2I_w \frac{1}{r^2} + m_b) \ddot{x} \\
& - (m_b r_b \dot{\theta}_0^2) \theta = F_T
\end{aligned} \tag{3.125}$$

As a result, 4-dimentional state space function can be built based on the linearized equations above.

$$\begin{aligned}
& \begin{bmatrix} \ddot{x} \\ \dot{x} \\ \ddot{\theta} \\ \dot{\theta} \end{bmatrix} \\
& = \begin{bmatrix} 0 & 0 & 0 & \frac{\dot{\theta}_0^2 - \frac{2m_b r_b \dot{x}_0 \dot{\theta}_0 + m_b g r_b \cos \beta}{I_b + 2m_b r_b^2}}{2m_w + 2I_w \frac{1}{r^2} + m_b} \\ 1 & 0 & \frac{2m_b r_b}{m_b r_b} - \frac{2m_b r_b}{I_b + 2m_b r_b^2} & \\ & 0 & 0 & \\ & \dot{x}_0 \dot{\theta}_0 + \frac{g}{2} \cos \beta - \frac{m_b r_b \dot{\theta}_0^2}{2m_w + 2I_w \frac{1}{r^2} + m_b} & \\ 0 & 0 & 0 & \frac{I_b + 2m_b r_b^2}{2m_b r_b} - \frac{m_b r_b}{2m_w + 2I_w \frac{1}{r^2} + m_b} \\ 0 & 0 & & \\ & 1 & 0 & \end{bmatrix} \begin{bmatrix} \dot{x} \\ x \\ \dot{\theta} \\ \theta \end{bmatrix} \\
& + \begin{bmatrix} -\frac{1}{m_b r_b} \\ \frac{2m_w + 2I_w \frac{1}{r^2} + m_b}{m_b r_b} - \frac{2m_b r_b}{I_b + 2m_b r_b^2} \\ 0 \\ -\frac{1}{2m_w + 2I_w \frac{1}{r^2} + m_b} \\ \frac{I_b + 2m_b r_b^2}{2m_b r_b} - \frac{m_b r_b}{2m_w + 2I_w \frac{1}{r^2} + m_b} \\ 0 \end{bmatrix} F_T
\end{aligned} \tag{3.126}$$

Combing the state space function of motor, which is:

$$\begin{bmatrix} \dot{I}_a \\ \dot{\omega}_r \end{bmatrix} = \begin{bmatrix} -\frac{R_a}{L_a} & -\frac{k_a}{L_a} \\ \frac{k_a}{J} & -\frac{B_m}{J} \end{bmatrix} \begin{bmatrix} I_a \\ \omega_r \end{bmatrix} + \begin{bmatrix} \frac{1}{L_a} \\ 0 \end{bmatrix} U_a + \begin{bmatrix} 0 \\ \frac{1}{J} \end{bmatrix} T_L \tag{3.127}$$

The state space function of the drivetrain can be derived in 6-dimentional.

$$\begin{aligned}
& \begin{bmatrix} \ddot{x} \\ \dot{x} \\ \ddot{\theta} \\ \dot{\theta} \\ \dot{I}_a \\ \dot{\omega}_r \end{bmatrix} \\
& = \begin{bmatrix} \frac{\dot{\theta}_0^2 - \frac{2m_b r_b \dot{x}_0 \dot{\theta}_0 + m_b g r_b \cos \beta}{I_b + 2m_b r_b^2}}{2m_w + 2I_w \frac{1}{r^2} + m_b} - \frac{2m_b r_b}{I_b + 2m_b r_b^2} & 0 & 0 \\ 0 & 0 & 0 \\ 1 & 0 & 0 \\ 0 & 0 & 0 \\ \frac{\dot{x}_0 \dot{\theta}_0 + \frac{g}{2} \cos \beta - \frac{m_b r_b \dot{\theta}_0^2}{2m_w + 2I_w \frac{1}{r^2} + m_b}}{\frac{I_b + 2m_b r_b^2}{2m_b r_b} - \frac{m_b r_b}{2m_w + 2I_w \frac{1}{r^2} + m_b}} & 0 & 0 \\ 0 & 0 & 0 \\ 0 & 0 & 1 \\ 0 & 0 & 0 \\ 0 & 0 & 0 \end{bmatrix} \begin{bmatrix} \dot{x} \\ x \\ \dot{\theta} \\ \theta \\ I_a \\ \omega_r \end{bmatrix} \\
& \quad + \begin{bmatrix} 0 \\ 0 \\ 0 \\ 0 \\ 1 \\ \frac{1}{L_a} \\ 0 \end{bmatrix} U_a + \begin{bmatrix} -\frac{1}{m_b r_b} \\ \frac{2m_w + 2I_w \frac{1}{r^2} + m_b}{m_b r_b} - \frac{2m_b r_b}{I_b + 2m_b r_b^2} \\ 0 \\ -\frac{1}{2m_w + 2I_w \frac{1}{r^2} + m_b} \\ \frac{I_b + 2m_b r_b^2}{2m_b r_b} - \frac{m_b r_b}{2m_w + 2I_w \frac{1}{r^2} + m_b} \\ 0 \\ 0 \\ 0 \end{bmatrix} F_T + \begin{bmatrix} 0 \\ 0 \\ 0 \\ 0 \\ 0 \\ 1 \\ \frac{1}{J} \end{bmatrix} T_L
\end{aligned} \tag{3.128}$$

If the scooter is running on level road, F_T can be calculated as below:

$$F_T = F_t - F_r \tag{3.129}$$

If the scooter is running uphill, since the rolling resistance is in a complicated expression,

$$F_r = \begin{cases} \text{sgn}[v_T] F_P \cos \beta (C_0 + C_1 v_T^2) & \text{if } v_T \neq 0 \\ F_t - F_{PT} & \text{if } v_T = 0 \text{ and } |F_t - F_{PT}| \leq C_0 F_P \cos \beta \\ \text{sgn}[F_t - F_{PT}] C_0 F_P \cos \beta & \text{if } v_T = 0 \text{ and } |F_t - F_{PT}| > C_0 F_P \cos \beta \end{cases}, \text{ the third}$$

case is only considered here by assuming that the scooter is rolling at slope with percent grade. As a result,

$$\begin{aligned} F_T &= 2 \frac{T_t}{r_w} - \text{sgn}[F_t - F_{PT}] C_0 (2m_w + \\ m_b) \cos \beta &= 2 \frac{T_L \cdot \zeta \cdot \eta_t}{r_w} - \text{sgn}[F_t - F_{PT}] C_0 (2m_w + \\ m_b) \cos \beta \end{aligned} \quad (3.130)$$

T_L is defined as the torque applied to the load, in the two-wheeled self-balancing scooter system, it is the torque applied to the wheels. Thus,

$$T_L = T_{tm} \quad (3.131)$$

Thus,

$$\begin{aligned} F_T &= 2 \frac{T_L \cdot \zeta \cdot \eta_t}{r_w} - \text{sgn}[F_t - F_{PT}] C_0 (2m_w + \\ m_b) \cos \beta \end{aligned} \quad (3.132)$$

As a result,

$$\begin{aligned} F_T &= 2 \frac{T_L \cdot \zeta \cdot \eta_t}{r_w} - \text{sgn}[F_t - F_{PT}] C_0 (2m_w \\ &+ m_b) \cos \beta \end{aligned} \quad (3.133)$$

Replacing F_T with Equation (3.133), the state space function can be rewritten as below:

$$\begin{bmatrix} \ddot{x} \\ \dot{x} \\ \ddot{\theta} \\ \dot{\theta} \\ \dot{I}_a \\ \dot{\omega}_r \end{bmatrix} = \begin{bmatrix} \frac{\dot{\theta}_0^2 - \frac{2m_b r_b \dot{x}_0 \dot{\theta}_0 + m_b g r_b \cos \beta}{I_b + 2m_b r_b^2}}{2m_w + 2I_w \frac{1}{r^2} + m_b} - \frac{2m_b r_b}{I_b + 2m_b r_b^2} & 0 & 0 \\ 0 & 0 & 0 \\ 1 & 0 & 0 \\ 0 & 0 & 0 \\ \dot{x}_0 \dot{\theta}_0 + \frac{g}{2} \cos \beta - \frac{m_b r_b \dot{\theta}_0^2}{2m_w + 2I_w \frac{1}{r^2} + m_b} & 0 & 0 \\ \frac{I_b + 2m_b r_b^2}{2m_b r_b} - \frac{m_b r_b}{2m_w + 2I_w \frac{1}{r^2} + m_b} & 0 & 0 \\ 0 & 0 & 0 \\ 0 & 0 & 1 \\ 0 & 0 & 0 \\ 0 & 0 & 0 \end{bmatrix} \begin{bmatrix} \dot{x} \\ x \\ \dot{\theta} \\ \theta \\ I_a \\ \omega_r \end{bmatrix} \quad (3.134)$$

$$\begin{bmatrix} 0 & 0 & 0 \\ 0 & 0 & 0 \\ 0 & 0 & 0 \\ 0 & 0 & 0 \\ 0 & 0 & 0 \\ 0 & 0 & 0 \\ 0 & 0 & 1 \\ 0 & 0 & 0 \\ 0 & 0 & 0 \end{bmatrix} \begin{bmatrix} 0 & 0 & 0 \\ -\frac{R_a}{L_a} & -\frac{k_a}{L_a} & \frac{k_a}{J} \\ \frac{k_a}{J} & -\frac{B_m}{J} & 0 \end{bmatrix} \begin{bmatrix} \dot{x} \\ x \\ \dot{\theta} \\ \theta \\ I_a \\ \omega_r \end{bmatrix}$$

$$\begin{aligned}
& + \begin{bmatrix} 0 \\ 0 \\ 0 \\ 0 \\ 1 \\ \frac{1}{L_a} \\ 0 \end{bmatrix} U_a + \begin{bmatrix} -\frac{1}{m_b r_b} \\ \frac{2m_w + 2I_w \frac{1}{r^2} + m_b}{m_b r_b} - \frac{2m_b r_b}{I_b + 2m_b r_b^2} \\ 0 \\ -\frac{1}{2m_w + 2I_w \frac{1}{r^2} + m_b} \\ \frac{I_b + 2m_b r_b^2}{2m_b r_b} - \frac{m_b r_b}{2m_w + 2I_w \frac{1}{r^2} + m_b} \\ 0 \\ 0 \\ 0 \end{bmatrix} \left\{ 2 \frac{T_L \cdot \zeta \cdot \eta_t}{r_w} \right. \\
& \left. - \operatorname{sgn}[F_t - F_{PT}] C_0 (2m_w + m_b) \cos \beta \right\} + \begin{bmatrix} 0 \\ 0 \\ 0 \\ 0 \\ 0 \\ 1 \\ \frac{1}{J} \end{bmatrix} T_L
\end{aligned}$$

Combing the coefficient with the same parameter, the state space function is represented as:

$$\begin{bmatrix} \ddot{x} \\ \dot{x} \\ \ddot{\theta} \\ \dot{\theta} \\ \dot{I}_a \\ \dot{\omega}_r \end{bmatrix} = \begin{bmatrix} \frac{\dot{\theta}_0^2 - \frac{2m_b r_b \dot{x}_0 \dot{\theta}_0 + m_b g r_b \cos \beta}{I_b + 2m_b r_b^2}}{0} & 0 & 0 \\ \frac{2m_w + 2I_w \frac{1}{r^2} + m_b}{m_b r_b} - \frac{2m_b r_b}{I_b + 2m_b r_b^2} & 0 & 0 \\ 0 & 0 & 0 \\ 1 & 0 & 0 \\ 0 & 0 & 0 \\ \dot{x}_0 \dot{\theta}_0 + \frac{g}{2} \cos \beta - \frac{m_b r_b \dot{\theta}_0^2}{2m_w + 2I_w \frac{1}{r^2} + m_b} & 0 & 0 \\ \frac{I_b + 2m_b r_b^2}{2m_b r_b} - \frac{m_b r_b}{2m_w + 2I_w \frac{1}{r^2} + m_b} & 0 & 0 \\ 0 & 0 & 0 \\ 0 & -\frac{R_a}{L_a} & -\frac{k_a}{L_a} \\ 0 & \frac{k_a}{J} & -\frac{B_m}{J} \end{bmatrix} \begin{bmatrix} \dot{x} \\ x \\ \dot{\theta} \\ \theta \\ I_a \\ \omega_r \end{bmatrix} \quad (3.135)$$

$$\begin{aligned}
& + \begin{bmatrix} 2 \frac{\zeta \cdot \eta_t}{r_w} \frac{-\frac{1}{m_b r_b}}{2m_w + 2I_w \frac{1}{r^2} + m_b} - \frac{2m_b r_b}{I_b + 2m_b r_b^2} \\ 0 \\ 0 \\ 0 \\ 0 \\ \frac{1}{L_a} \\ 0 \end{bmatrix} \begin{bmatrix} U_a \\ T_L \end{bmatrix} \\
& + \begin{bmatrix} -\frac{1}{m_b r_b} \\ \frac{2m_w + 2I_w \frac{1}{r^2} + m_b}{m_b r_b} - \frac{2m_b r_b}{I_b + 2m_b r_b^2} \\ 0 \\ -\frac{1}{2m_w + 2I_w \frac{1}{r^2} + m_b} \\ \frac{I_b + 2m_b r_b^2}{2m_b r_b} - \frac{m_b r_b}{2m_w + 2I_w \frac{1}{r^2} + m_b} \\ 0 \\ 0 \\ 0 \end{bmatrix} \{-sgn[F_t - F_{PT}]C_0(2m_w + m_b) \cos \beta\}
\end{aligned}$$

Noticing that besides matrix A and B , there is a constant in the state space matrix in the expression, which is introduced by the tractive force T_r . Since both of the coefficient C_0 and the roadway percent grade β changes as the change in the road condition, furthermore, $sgn[F_t - F_{PT}]$ is also changing based on running uphill or downhill, the function of $sgn[F_t - F_{PT}]C_0 \cos \beta$ can be treated as the input of the scooter, making

$$R_c = -sgn[F_t - F_{PT}]C_0 \cos \beta \quad (3.136)$$

The objective of the scooter modeling is to control the scooter speed and direction as required, thus, the output y is expressed as:

$$y = \dot{x} = \begin{bmatrix} 1 & 0 & 0 & 0 & 0 & 0 \end{bmatrix} \begin{bmatrix} \dot{x} \\ x \\ \dot{\theta} \\ \theta \\ I_a \\ \omega_r \end{bmatrix} \quad (3.137)$$

As a result, The final representation of the state space function can be written as below:

$$\begin{bmatrix} \ddot{x} \\ \ddot{x} \\ \ddot{\theta} \\ \dot{\theta} \\ \dot{I}_a \\ \dot{\omega}_r \end{bmatrix} = \begin{bmatrix} \frac{\dot{\theta}_0^2 - \frac{2m_b r_b \dot{x}_0 \dot{\theta}_0 + m_b g r_b \cos \beta}{I_b + 2m_b r_b^2}}{2m_w + 2I_w \frac{1}{r^2} + m_b} - \frac{2m_b r_b}{I_b + 2m_b r_b^2} & 0 & 0 \\ 0 & 0 & 0 \\ 1 & 0 & 0 \\ 0 & 0 & 0 \\ \frac{\dot{x}_0 \dot{\theta}_0 + \frac{g}{2} \cos \beta - \frac{m_b r_b \dot{\theta}_0^2}{2m_w + 2I_w \frac{1}{r^2} + m_b}}{\frac{I_b + 2m_b r_b^2}{2m_b r_b} - \frac{m_b r_b}{2m_w + 2I_w \frac{1}{r^2} + m_b}} & 0 & 0 \\ 0 & 0 & 0 \\ 0 & 0 & 1 \\ 0 & 0 & 0 \\ 0 & 0 & 0 \end{bmatrix} \begin{bmatrix} \dot{x} \\ x \\ \dot{\theta} \\ \theta \\ I_a \\ \omega_r \end{bmatrix} + \begin{bmatrix} \frac{\zeta \cdot \eta_t}{r_w} \frac{-\frac{1}{m_b r_b}}{2m_w + 2I_w \frac{1}{r^2} + m_b} - \frac{2m_b r_b}{I_b + 2m_b r_b^2} \\ 0 \\ 0 \\ 0 \\ 0 \\ 1 \\ \frac{L_a}{0} \end{bmatrix} \begin{bmatrix} (2m_w + m_b) \frac{-\frac{1}{m_b r_b}}{2m_w + 2I_w \frac{1}{r^2} + m_b} - \frac{2m_b r_b}{I_b + 2m_b r_b^2} \\ 0 \\ -\frac{1}{2m_w + 2I_w \frac{1}{r^2} + m_b} \\ (2m_w + m_b) \frac{\frac{1}{I_b + 2m_b r_b^2} - \frac{m_b r_b}{2m_w + 2I_w \frac{1}{r^2} + m_b}}{2m_b r_b} \\ 0 \\ 0 \\ 0 \end{bmatrix} \begin{bmatrix} U_a \\ T_L \\ R_c \end{bmatrix} \quad (3.138)$$

$$y = [1 \quad 0 \quad 0 \quad 0 \quad 0 \quad 0] \begin{bmatrix} \dot{x} \\ x \\ \dot{\theta} \\ \theta \\ I_a \\ \omega_r \end{bmatrix} \quad (3.139)$$

According to the standard form of state space function showed below,

$$\dot{x}(t) = Ax(t) + Bu(t) \quad (3.140)$$

$$y(t) = Cx(t) + Du(t) \quad (3.141)$$

For the scooter case,

$$A = \begin{bmatrix} \frac{\dot{\theta}_0^2 - \frac{2m_b r_b \dot{x}_0 \dot{\theta}_0 + m_b g r_b \cos \beta}{I_b + 2m_b r_b^2}}{2m_w + 2I_w \frac{1}{r^2} + m_b} - \frac{2m_b r_b}{I_b + 2m_b r_b^2} & 0 & 0 \\ 0 & 0 & 0 \\ 1 & 0 & 0 \\ 0 & 0 & 0 \\ \frac{\dot{x}_0 \dot{\theta}_0 + \frac{g}{2} \cos \beta - \frac{m_b r_b \dot{\theta}_0^2}{2m_w + 2I_w \frac{1}{r^2} + m_b}}{\frac{I_b + 2m_b r_b^2}{2m_b r_b} - \frac{m_b r_b}{2m_w + 2I_w \frac{1}{r^2} + m_b}} & 0 & 0 \\ 0 & 0 & 0 \\ 0 & 0 & 1 \\ 0 & 0 & 0 \\ 0 & 0 & 0 \end{bmatrix} \quad (3.142)$$

B

$$= \begin{bmatrix} 0 & 2 \frac{\zeta \cdot \eta_t}{r_w} \frac{-\frac{1}{m_b r_b}}{\frac{2m_w + 2l_w \frac{1}{r^2} + m_b}{m_b r_b} - \frac{2m_b r_b}{l_b + 2m_b r_b^2}} & (2m_w + m_b) \frac{-\frac{1}{m_b r_b}}{\frac{2m_w + 2l_w \frac{1}{r^2} + m_b}{m_b r_b} - \frac{2m_b r_b}{l_b + 2m_b r_b^2}} \\ 0 & 0 & 0 \\ 0 & -\frac{1}{2m_w + 2l_w \frac{1}{r^2} + m_b} & -\frac{1}{2m_w + 2l_w \frac{1}{r^2} + m_b} \\ 0 & 2 \frac{\zeta \cdot \eta_t}{r_w} \frac{\frac{2m_w + 2l_w \frac{1}{r^2} + m_b}{l_b + 2m_b r_b^2} - \frac{m_b r_b}{2m_w + 2l_w \frac{1}{r^2} + m_b}}{\frac{2m_b r_b}{2m_b r_b} - \frac{m_b r_b}{2m_w + 2l_w \frac{1}{r^2} + m_b}} & (2m_w + m_b) \frac{\frac{2m_w + 2l_w \frac{1}{r^2} + m_b}{l_b + 2m_b r_b^2} - \frac{m_b r_b}{2m_b r_b} - \frac{m_b r_b}{2m_w + 2l_w \frac{1}{r^2} + m_b}}{\frac{2m_b r_b}{2m_b r_b} - \frac{m_b r_b}{2m_w + 2l_w \frac{1}{r^2} + m_b}} \\ \frac{1}{L_a} & 0 & 0 \\ 0 & 0 & 0 \\ & 0 & 0 \\ & \frac{1}{j} & 0 \end{bmatrix} \quad (3.143)$$

$$C = [1 \quad 0 \quad 0 \quad 0 \quad 0 \quad 0] \quad (3.144)$$

$$D = 0 \quad (3.145)$$

CHAPTER 4. MODEL ORDER REDUCTION TECHNIQUE

4.1 Introduction

With the development of modern technology, products become more and more integrated from multidisciplinary fields, making the modeling of system highly complex and large in dimension. There is no accepted definition for large scale system, but it all agreed that the large scale system is high in dimensions that the computational efforts for system modeling, analysis and control design are time consuming or even the solutions are beyond the conventional techniques.

The characteristics of the large scale system are in their hierarchical structures and decentralized control. They can be decoupled into a number of subsystems, and most of them are MIMO systems. From this point of view, the two-wheeled self-balancing scooter can be defined as large scale system, since it contains both mechanical system and electrical system with multiple inputs of angular speed, tilt angle and wheel speed. In chapter 3, the mathematical model of such large scale system has been built up, which turns out to be a 6 dimensional MIMO state space model.

Any modeling task always needs to make a compromise between simplicity and accuracy. For large scale system, their complicated mathematical model commands heavy computational efforts, making it is hard to work with their original form. Therefore, a simpler model is more practical.

There are several methods created based on estimating the dominant part of the original system, approximating the mathematical model by its dominant pole-zero in the complex plane to make simpler system representation. Examples of such model reduction techniques are Davison Technique, Chidambara Technique and Marshall Technique. Davison technique is to retain dominant eigenvalues while neglect those far from the origin; but it doesn't provide accurate steady-state response result. Chidambara technique considers the steady-state of the ignored parts in Davison techniques and only ignores the transient response of them, in order to decrease the steady-state error. Marshall technique is similar to Chidambara technique but it uses different way to obtain the reduced order state equation.

There are also some other of approaches based on various criterion. For example, aggregation methods, frequency domain based methods, including moment matching, Pade approximation methods, Routh approximation techniques and continued fraction method, and norm based methods, including model reduction by balanced truncation, model reduction by impulse/step error minimization and optimal model order reduction using Wilson's technique, and pole placement techniques.

Based on the state space model obtained from the previous chapter, Routh approximation technique is chosen to reduce model order for the two-wheeled self-balancing scooter.

4.2 Continued fraction expansions

Consider the linear time-invariant multivariable system described by:

$$\dot{x}(t) = Ax(t) + Bu(t) \quad (4.1)$$

$$y(t) = Cx(t) + Du(t) \quad (4.2)$$

Where $x \in R^n$, $u \in R^m$ and $y \in R^p$.

The transfer function matrices are given as below:

$$H(s) = C(sI - A)^{-1}B + D \quad (4.3)$$

$$H(z) = C(zI - A)^{-1}B + D \quad (4.4)$$

Equation (4.3) is used for continuous time system while Equation(4.4) is used for discret time system.

There are two concepts associating with the system, which are time moments m_i and

Markov parameters h_i . Equation (4.5) shows the expression for time moments m_i .

And the Markov parameters h_i for continuous time system, can be derived from

Equation (4.6) and equation (4.7).

$$m_i = \int_0^{\infty} t^{i+1} h(t) dt \quad (4.5)$$

Where $h(t) = Ce^{At}B$ is the impulse response of the system.

$$h_i = CA^{i-1}B \quad (4.6)$$

$$H(s) = D + \sum_{i=1}^{\infty} h_i s^{-i} \quad (4.7)$$

Notice that,

$$h(0) = [Ce^{At}B]_{t=0} = CB \quad (4.8)$$

$$\left[\frac{d^i h(t)}{dt^i} \right]_{t=0} = \left[\frac{d^i}{dt^i} [CAe^{At}B] \right]_{t=0} = CA^i B \quad (4.9)$$

Therefore, the Markov parameters are values of $h(t)$ and its derivatives evaluated at $t = 0$.

It can be expanded about $s = 0$.or $s = \infty$ in order to get the following forms.

Expansion about $s = 0$:

$$\begin{aligned}
 H(s) &= \frac{b_0 s^0 + b_1 s^1 + b_2 s^2 + \dots + b_{n-1} s^{n-1}}{a_0 s^0 + a_1 s^1 + a_2 s^2 + \dots + a_n s^n} \\
 &= \frac{A_{20} s^0 + A_{21} s^1 + A_{22} s^2 + \dots + A_{2,n-1} s^{n-1}}{A_{10} s^0 + A_{11} s^1 + A_{12} s^2 + \dots + A_{1,n} s^n} \\
 &= \frac{1}{h_1 + \frac{s}{h_2 + \frac{s}{h_3 + \frac{s}{\ddots}}}}
 \end{aligned} \tag{4.10}$$

Expansion about $s = \infty$,

$$\begin{aligned}
 G(s) &= \frac{A_{20} s^{n-1} + A_{21} s^{n-2} + A_{22} s^{n-3} + \dots + A_{2,n-1} s^0}{A_{10} s^n + A_{11} s^{n-1} + A_{12} s^{n-2} + \dots + A_{1,n} s^0} \\
 &= \frac{1}{sh_1 + \frac{1}{sh_2 + \frac{1}{sh_3 + \frac{1}{\ddots}}}}
 \end{aligned} \tag{4.11}$$

In addition, the above methods can be combined together for the same transfer function in order to get a mixed form. There are two types of it: Caucer First Form and Caucer Second Form.

4.2.1 Caucer First Form

Caucer First Form is obtained by removing poles at infinity. Suppose that

$H_1(s) = \frac{n(s)}{d(s)}$, with $\deg[n(s)] > \deg[d(s)]$. Then, $H_1(s)$ must have a pole at infinity.

Removing this pole at infinity yields,

$$H_2(s) = \frac{n_1(s)}{d(s)} = H_1(s) - h_1s \quad (4.12)$$

With $H_2(s)$ having a zero at infinity. Thus, to remove a pole at infinity invert $H_2(s)$ to get,

$$H_3(s) = \frac{d_2(s)}{n_1(s)} = \frac{1}{H_2(s)} - h_2s \quad (4.13)$$

Therefore, the process to obtain the Caucer First Form involves a repetition of the following pattern: step one is to remove a pole at infinity; step two is to invert and remove a pole at infinity; step three is to go back to step two and repeat it until done

This process yields:

$$H_1(s) = h_1(s) + \frac{1}{sh_1 + \frac{1}{sh_2 + \frac{1}{sh_3 + \frac{1}{\ddots}}}} \quad (4.14)$$

4.2.2 Caucer Second Form

Caucer Second Form is obtained by successively removing poles at the origin. This can be done using the previous technique but doing synthetic division in terms of $1/s$.

4.2.3 Routh approximation technique

By using the Routh approximation technique, the reduced order model is obtained by developing a Routh-like table for the full order system. Then the reduced order model is constructed such that the coefficients of its Routh table match those of the Routh table of the original system up to the desired order. The stability of the

system is preserved. Let $H(s)$, the full order model, be asymptotically stable, linear and given as

$$H(s) = \frac{b_1 s^{n-1} + b_2 s^{n-2} + b_3 s^{n-3} + \dots + b_n}{a_0 s^n + a_1 s^{n-1} + a_2 s^{n-2} + \dots + a_n} \quad (4.15)$$

Then, the α - β expansion of $H(s)$ is defined as:

$$H(s) = \beta_1 F_1(s) + \beta_2 F_1(s)F_2(s) + \dots + \beta_n F_1(s)F_2(s) \dots F_n(s) \quad (4.16)$$

This implies the equation as below.

$$H(s) = \sum_{i=1}^n \beta_i \prod_{j=1}^i F_j(s) \quad (4.17)$$

Where $\beta_i \equiv \text{constants for } i = 1, 2, \dots, n$.

$$F_1(s) = \frac{1}{1 + s\alpha_1 + \frac{1}{s\alpha_2 + \frac{1}{s\alpha_3 + \frac{1}{\ddots s\alpha_{n-1} + \frac{1}{s\alpha_n}}}}} \quad (4.18)$$

$$F_j(s) = \frac{1}{s\alpha_j + \frac{1}{s\alpha_{j+1} + \frac{1}{s\alpha_{j+2} + \frac{1}{\ddots s\alpha_{n-1} + \frac{1}{s\alpha_n}}}}} \quad (4.19)$$

The α_i 's are determined from the Routh table (Table 4.1) of the original system, which is the same as the stability analysis,

$$a_0^{i+2} = a_2^{i-1} - \alpha_i a_2^i \quad (4.20)$$

$$a_2^{i+1} = a_4^{i-1} - \alpha_i a_4^i \quad (4.21)$$

$$a_{n-i-2}^{i+1} = a_{n-i}^{i-1} - \alpha_i a_{n-i}^i \quad (4.22)$$

For $i = 1, 2, \dots, n-1$; $n-i$ even

If $n-i$ is odd, then

$$a_{n-i-1}^{i+1} = a_{n-i+1}^{i-1} \quad (4.23)$$

And the α_i 's are given as:

$$\alpha_i = \frac{a_0^{i-1}}{a_0^i} \quad (4.24)$$

Table 4.1 α (Routh) Table

	$a_0^0 = a_0$	$a_2^0 = a_2$	$a_4^0 = a_4$	$a_6^0 = a_6$
	$a_1^0 = a_1$	$a_3^0 = a_3$	$a_5^0 = a_5$...
$\alpha_1 = a_0^0/a_0^1$	a_0^2 $= a_2^0 - \alpha_1 a_2^1$	a_2^2 $= a_4^0 - \alpha_1 a_4^1$	a_0^2 $= a_4^2 - \alpha_1 a_6^1$...
$\alpha_2 = a_0^1/a_0^2$	a_0^3 $= a_2^1 - \alpha_2 a_2^2$	a_2^3 $= a_4^1 - \alpha_2 a_4^2$...	
$\alpha_3 = a_0^2/a_0^3$	a_0^4 $= a_2^2 - \alpha_3 a_2^3$	a_2^4 $= a_4^2 - \alpha_3 a_4^3$...	
$\alpha_4 = a_0^3/a_0^4$	a_0^5 $= a_2^3 - \alpha_4 a_2^4$...		
$\alpha_5 = a_0^4/a_0^5$	a_0^6 $= a_2^4 - \alpha_5 a_2^5$...		
$\alpha_6 = a_0^5/a_0^6$...			
...	...			

The β_i 's can be determined from the Routh table (Table 4.2) of the numerator of $H(s)$ with

$$b_{j-2}^{i+2} = b_j^i - \beta_i a_j^i \quad (4.25)$$

Where $i = 1, 2, \dots, n - 2$ and if $n - i$ is even, $j = 2, 4, 6, \dots, n - i$; if not, $j = 2, 4, 6, \dots, n - i - 1$.

$$\beta_i = \frac{b_0^i}{b_0^i} \quad (4.26)$$

Table 4.2 β (Routh) Table

	$b_0^1 = b_1$	$b_2^1 = b_3$	$b_4^1 = b_5$
	$b_0^2 = b_2$	$b_2^2 = b_4$	$b_4^2 = b_6$
$\beta_1 = b_0^1/a_0^1$	$b_0^3 = b_2^1 - \beta_1 a_2^1$	$b_2^3 = b_4^1 - \beta_1 a_4^1$...
$\beta_2 = b_0^2/a_0^2$	$b_0^4 = b_2^2 - \beta_2 a_2^2$	$b_2^4 = b_4^2 - \beta_2 a_4^2$...
$\beta_3 = b_0^3/a_0^3$	$b_0^5 = b_2^3 - \beta_3 a_2^3$...	
$\beta_4 = b_0^4/a_0^4$	$b_0^6 = b_2^4 - \beta_4 a_2^4$...	
$\beta_5 = b_0^5/a_0^5$...		
$\beta_6 = b_0^6/a_0^6$...		
...			

Because that the Routh approximation method for obtaining reduced order models consists in truncating the last $n-k$ terms in the continued fraction expansion of F_i ; $i = 1, 2, \dots, n$. Denote the functions that result from truncating F_i by G_{1k} ; that is,

$$G_{1k}(s) = \frac{1}{1 + s\alpha_1 + \frac{1}{s\alpha_2 + \frac{1}{s\alpha_3 + \frac{1}{\ddots s\alpha_{n-1} + \frac{1}{s\alpha_n}}}}} \quad (4.27)$$

$$G_{ik}(s) = \frac{1}{s\alpha_i + \frac{1}{s\alpha_{i+1} + \frac{1}{s\alpha_{i+2} + \frac{1}{\ddots s\alpha_{k-1} + \frac{1}{s\alpha_k}}}}} \quad (4.28)$$

Where $k < n$. Then $H(s)$ can be approximated by the truncated alpha-beta expansion which results from replacing F_i by G_{1k} for $i = 1, 2, \dots, k$,

$$R_k(s) = \beta_1 G_{1k}(s) + \beta_2 G_{1k}(s) G_{2k}(s) + \dots + \beta_k G_{1k}(s) G_{2k}(s) \dots G_{kk}(s) \quad (4.29)$$

Thus,

$$R_k(s) = \sum_{i=1}^k \beta_i \prod_{j=1}^i G_{jk}(s) \quad (4.30)$$

Rearranging the k th Routh convergent of $H(s)$ as a rational function of s it follows that the denominator $A_k(s)$ and the numerator $B_k(s)$ of $R_k(s)$ are

$$R_1(s) = \beta_1 G_{11}(s) = \frac{\beta_1}{1 + \alpha_1 s} = \frac{B_1(s)}{A_1(s)} \quad (4.31)$$

$$R_2(s) = \sum_{i=1}^2 \beta_i \prod_{j=1}^i G_{jk}(s) \quad (4.32)$$

$$= \beta_1 G_{12}(s) + \beta_2 G_{12}(s) G_{22}(s)$$

$$G_{12}(s) = \frac{1}{1 + \alpha_1 s + \frac{1}{\alpha_2 s}} = \frac{\alpha_2 s}{1 + \alpha_1 s + \alpha_1 \alpha_2 s^2} \quad (4.33)$$

$$G_{22}(s) = \frac{1}{\alpha_2 s} \quad (4.34)$$

As a result,

$$\begin{aligned} R_2(s) &= \frac{\beta_1 \alpha_2 s}{1 + \alpha_1 s + \alpha_1 \alpha_2 s^2} \\ &\quad + \frac{\beta_2 \alpha_2 s}{(1 + \alpha_1 s + \alpha_1 \alpha_2 s^2) \alpha_2 s} \\ &= \frac{\beta_1 \alpha_2 s + \beta_2}{1 + \alpha_1 s + \alpha_1 \alpha_2 s^2} = \frac{B_2(s)}{A_2(s)} \end{aligned} \quad (4.35)$$

In general it can be shown that $A_k(s)$ and $B_k(s)$ are given as,

For $k = 1, 2, \dots$

$$A_k(s) = \alpha_k s A_{k-1}(s) + A_{k-2}(s) \quad (4.36)$$

Where $A_{-1}(s) = 1$ and $A_0(s) = 1$.

$$B_k(s) = \alpha_k s B_{k-1}(s) + B_{k-2}(s) + \beta_k \quad (4.37)$$

Where $B_{-1}(s) = 0$ and $B_0(s) = 0$.

Equation (4.36) and (4.37) shows that the calculation of $A_k(s)$ and $B_k(s)$ are very similar to α - β expansion.

Besides, using initial value theorem,

$$\lim_{t \rightarrow 0} \{f(t)\} = \lim_{s \rightarrow \infty} \{sF(s)\} \quad (4.38)$$

$$\lim_{t \rightarrow \infty} \{f(t)\} = \lim_{s \rightarrow 0} \{sF(s)\} \quad (4.39)$$

It can be shown that $R_k(s)$ maintains the fast components (high frequency behaviours) be of the original system. Therefore, to obtain a low-frequency approximation it is necessary to use the reciprocate of $H(s)$, $\hat{H}(s)$.

$$\widehat{H}(s) = \frac{1}{s} H\left(\frac{1}{s}\right) = \frac{1}{s} \frac{b_1 \frac{1}{s^{n-1}} + b_2 \frac{1}{s^{n-2}} + \cdots + b_n}{a_0 \frac{1}{s^n} + a_1 \frac{1}{s^{n-1}} + \cdots + a_n} \quad (4.40)$$

$$= \frac{b_n s^{n-1} + b_{n-1} s^{n-2} + \cdots + b_1}{a_n s^n + a_{n-1} s^{n-1} + \cdots + a_1} \quad (4.41)$$

In effect, the reciprocal of $H(s)$ is obtained by reversing the order of the polynomial coefficient. Also, note that if $H(s)$ has a pole (zero) at $s = s_i$, then $\widehat{H}(s)$ has a pole at $s = 1/s_i$. The alpha-beta expansion can be written as:

$$\widehat{H}(s) = \sum_{i=1}^n \widehat{\beta}_i \prod_{j=1}^i \widehat{F}_j(s) \quad (4.42)$$

Therefore, if $\widehat{R}_k(s) = \sum_{i=1}^k \widehat{\beta}_i \prod_{j=1}^i \widehat{G}_{jk}(s)$ is a Routh approximant of $\widehat{H}(s)$, it follows that a k th order approximant for $H(s)$ is given by the reciprocal of $\widehat{R}_k(s)$.

$$R_k(s) = \frac{1}{s} \widehat{R}_k\left(\frac{1}{s}\right) \quad (4.43)$$

Furthermore, it is not hard to tell that:

$$H(s) = \frac{1}{s} \widehat{H}\left(\frac{1}{s}\right) \quad (4.44)$$

The most attractive characteristic of Routh approximation technique is in the single set of computations for obtaining the derivation of simplified models and the maintenance of stability. Moreover, it not only preserves the stability but it also applicable to unstable system by forming a new asymptotically stable transfer function by shifting the imaginary axis, which is showed in Equation (4.39). In this equation, a is chosen to make the newly formed transfer function $\widetilde{H}(s)$ asymptotically stable to replace the unstable $H(s)$.

$$\tilde{H}(s) = H(s + a), a \in R_+ \quad (4.45)$$

Therefore, it is valuable to find the time-domain representation analogous through the Routh approximation technique.

4.3 Generalized Routh Algorithm

Cauer first form requires reduced order matches Markow parameters and yields a high frequency approximation while Cauer second form requires reciprocal transformation and its reduced order model matches time moments by yielding a low frequency approximation.

In order to obtain a better approximation for both the transient and steady-state responses of the original system a mixed form, Cauer third is developed. In this approach, to obtain a kth order reduced order model, the first k time moments of the impulse response and the first k Markov parameters of the system are matched. In general, the Cauer third form can be written as below:

$$H(s) = \frac{1}{k_1 + k'_1 s + \frac{1}{\frac{k_2}{s} + k'_2 + \frac{1}{k_3 + k'_3 s + \frac{1}{\frac{k_4}{s} + k'_4 + \frac{1}{\ddots}}}}} \quad (4.46)$$

Here, h_i and h'_i are obtained using the Routh algorithm, while k_i and k'_i are obtained from the generalized Routh algorithm, given next.

Given the usual $H(s)$, rearranging the numerator and denominator polynomials in increasing powers of s yields:

$$H(s) = \frac{A_{21}s^0 + A_{22}s^1 + A_{23}s^2 + \dots + A_{2,n}s^{n-1}}{A_{11}s^0 + A_{11}s^1 + A_{12}s^2 + \dots + A_{1,n+1}s^n} \quad (4.47)$$

Next, using long division $H(s)$ can be written as,

$$H(s) = \frac{1}{\frac{A_{11}}{A_{21}} + \frac{A_{1,n+1}}{A_{2,n}}s + \frac{A_{12} - \frac{A_{11}A_{22}}{A_{21}} - \frac{A_{1,n+1}A_{21}}{A_{2,n}}}{A_{21}s^0 + A_{22}s^1 + A_{23}s^2 + \dots + A_{2,n}s^{n-1}} + \dots + (*)s^{n-1}} \quad (4.48)$$

Let $k_p = \frac{A_{p,1}}{A_{p+1,1}}$, and $k'_p = \frac{A_{p,n+2-p}}{A_{p+1,n+1-p}}$ for $p = 1, 2, \dots, n$,

$$\begin{aligned} H(s) &= \frac{1}{k_1 + k'_1s + \frac{(A_{12} - k_1A_{22} - k'_1A_{21})s + \dots + Ms^{n-1}}{A_{21}s^0 + A_{22}s^1 + A_{23}s^2 + \dots + A_{2,n}s^{n-1}}} \\ &= \frac{1}{k_1 + k'_1s + \frac{A_{31}s + A_{32}s^2 \dots + A_{3,n-1}s^{n-1}}{A_{21}s^0 + A_{22}s^1 + A_{23}s^2 + \dots + A_{2,n}s^{n-1}}} \\ &= \frac{1}{k_1 + k'_1s + H'(s)} \end{aligned} \quad (4.49)$$

This process can be repeated for $H'(s)$ until the expansion is complete.

In general, the quotients in this expansion can be obtained by using the generalized Routh algorithm and the modified Routh array.

Table 4.3 Modified Routh Array

A_{11}	A_{12}	A_{13}	A_{14}	...	$A_{1,n-3}$	$A_{1,n-2}$	$A_{1,n-1}$	$A_{1,n}$
A_{21}	A_{22}	A_{23}	A_{24}	...	$A_{2,n-3}$	$A_{2,n-2}$	$A_{2,n-1}$	$A_{2,n}$
A_{31}	A_{32}	A_{33}		...	$A_{3,n-3}$	$A_{3,n-2}$	$A_{3,n-1}$	
A_{41}	A_{42}	A_{43}		...	$A_{4,n-4}$	$A_{4,n-3}$	$A_{4,n-2}$	
			\ddots			\ddots		

$A_{n-1,1} \quad A_{n-1,2} \quad A_{n-1,3}$
$A_{n,1} \quad A_{n,2}$
$A_{n+1,1}$

From the above table,

Table 4.4 Quotients for Generalized Routh algorithm

$k_1 = \frac{A_{11}}{A_{21}}$	$k'_1 = \frac{A_{1,n+1}}{A_{2,n}}$
$k_2 = \frac{A_{21}}{A_{31}}$	$k'_1 = \frac{A_{2,n}}{A_{3,n-1}}$
\vdots	\vdots
$k_{n-1} = \frac{A_{n-1,1}}{A_{n,1}}$	$k'_{n-1} = \frac{A_{n-1,3}}{A_{n,2}}$
$k_n = \frac{A_{n,1}}{A_{n+1,1}}$	$k'_n = \frac{A_{n,2}}{A_{n+1,1}}$

Where $A_{-}(i, j) = A_{-}(i - 2, j + 1) - k_{-}(i - 2) A_{-}(i - 1, j + 1) - k_{-}(n - 2) A_{-}(i - 1, j)$ for $i = 1, 2, 3, \dots, n + 1$ and $j = 1, 2, 3 \dots$

Once the expansion has been completed and the reduced order model has been determined by truncation, the next step would be to invert the truncated continued fraction to obtain the corresponding transfer function. An algorithm for carrying out this continued fraction inversion follows below.

From the modified Routh array,

$A_{n,1} = k_n A_{n+1,1}$

$$\begin{aligned}
A_{n-1,1} &= k_{n-1}A_{n,1} = k_{n-1}k_nA_{n+1,1} \\
&\dots \\
A_{2,1} &= k_2A_{3,1} = k_2k_3k_4 \dots k_nA_{n+1,1} \\
A_{1,1} &= k_1A_{2,1} = k_1k_2k_3k_4 \dots k_nA_{n+1,1}
\end{aligned}$$

Without loss of generality, let $A_{n+1,1} = 1$,

$$A_{i,j} = \prod_{j=1}^n k_j \quad (4.50)$$

For $j = i, i + 1, \dots, n$

On the other hand, similar form can be generalized as below:

$$A_{i,n+2-i} = \prod_{j=1}^n k'_j \quad (4.51)$$

Where i is the row number in the modified array for the equation above.

The generalized expression used to obtain the $A_{i,j}$'s in the modified Routh array can be used to determine the intermediate terms, starting with the last row up to the first row. This can be seen by letting $i = n + 1$ and $j = 1$ in this expression to get:

$$\begin{aligned}
A_{n+1,1} &= A_{n-1,2} - k_{n-1}A_{n,2} - k'_{n-1}A_{n,1} \\
A_{n-1,2} &= A_{n+1,1} + k_{n-1}A_{n,2} + k'_{n-1}A_{n,1} \\
A_{n,1} &= A_{n-2,2} - k_{n-2}A_{n-1,2} - k'_{n-2}A_{n-1,1} \\
A_{n-2,2} &= A_{n,1} + k_{n-2}A_{n-1,2} + k'_{n-2}A_{n-1,1} \\
&\vdots \quad \quad \quad \vdots \\
A_{i,j} &= A_{i+2,j-1} + k_iA_{i+1,j} + k'_iA_{i+1,j-1}
\end{aligned}$$

Where $i = n - 1, n - 2, \dots, 1$ and $j = 2, 3, \dots, n + 1 - i$.

4.4 State space formulation of routh algorithm and other related forms

Consider the following feedback system:

$$\begin{aligned}
 H(s) &= \frac{Y(s)}{U(s)} = \frac{G(s)}{1 + R(s)G(s)} + D \\
 &= \frac{1}{R(s) + \frac{1}{G(s)}} + D
 \end{aligned}
 \tag{4.52}$$

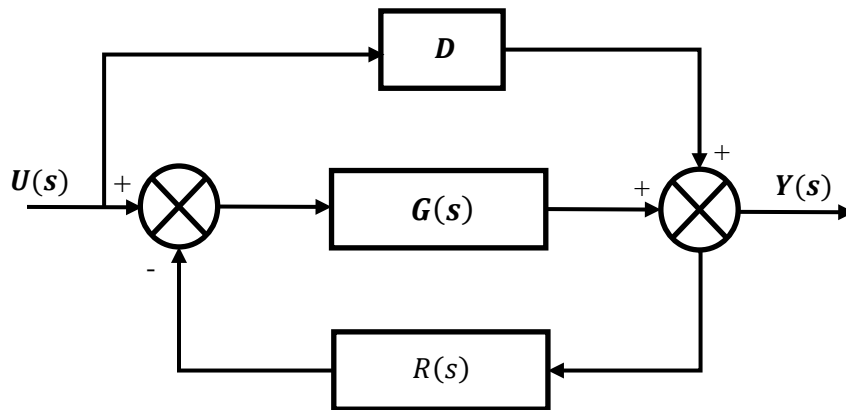


Figure 4.1 Block diagram of feedback system

The above expression resembles the form of a continued fraction expansion.

So it is possible to generalize the block diagram representation give above for the mixed or Cauer third form discussed before. Incidentally, the Cauer first and second forms are special cases of the mixed form. Since the Cauer third form can be written as follows:

$$\begin{aligned}
 H(s) &= [k_1 + k'_1 s + [\frac{k_2}{s} + k'_2 + [k_3 + k'_3 s \\
 &\quad + [\dots]^{-1}]^{-1}]^{-1}
 \end{aligned}
 \tag{4.53}$$

Next, consider a first order approximation of $H(s)$, namely

$$H_1(s) = [k_1 + k'_1 s]^{-1} = [(1 + \frac{k'_1 s}{k_1})k_1]^{-1} \quad (4.54)$$

$$\begin{aligned} H_2(s) &= [k_1 + k'_1 s + [\frac{k_2}{s} + k'_2]^{-1}]^{-1} \\ &= [(k_1 + k'_1 s) (\frac{k_2}{s} + k'_2) \\ &\quad + 1] [\frac{k_2}{s} + k'_2]^{-1} \\ &= (\frac{k_2}{s} + k'_2) [(k_1 + k'_1 s) (\frac{k_2}{s} \\ &\quad + k'_2) + 1]^{-1} \end{aligned} \quad (4.55)$$

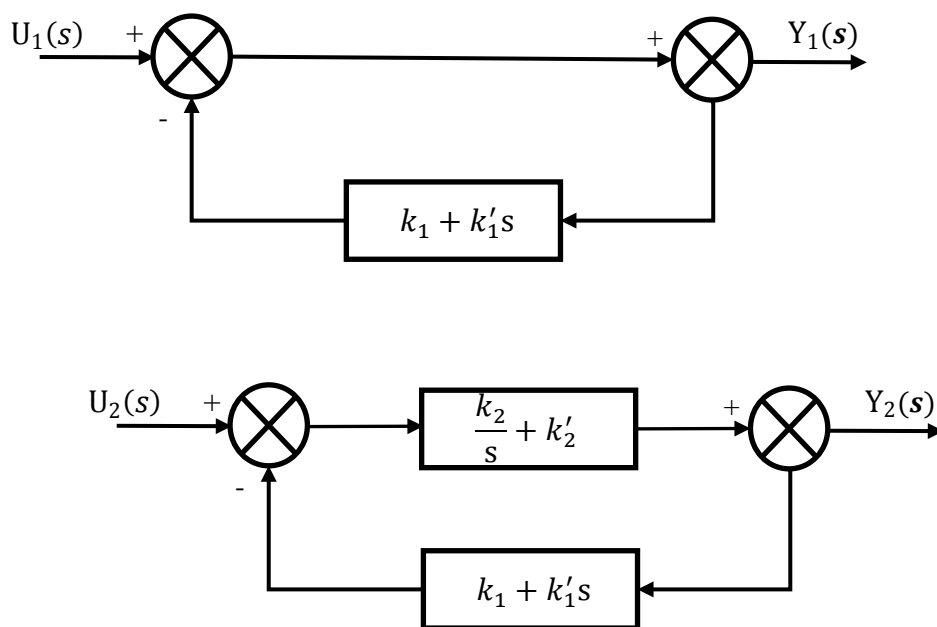


Figure 4.2 Detailed block diagram of feedback system

Hence, in general, the Cauer third form of $H(s)$ can be represented in a block diagram as follows,

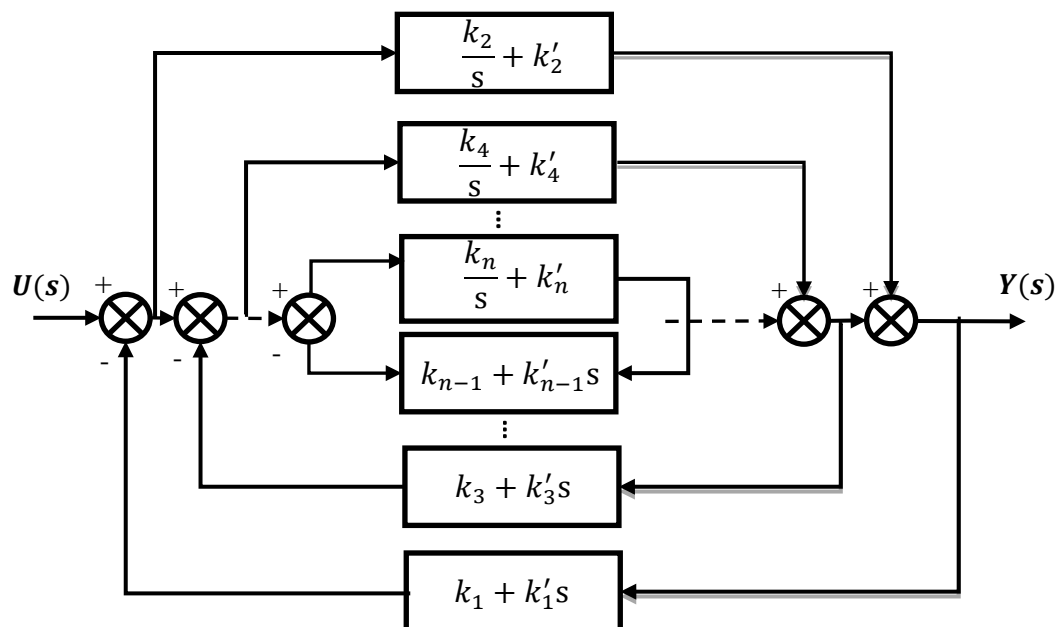


Figure 4.3 Generalized block diagram in Cauer third form

Considering the case of $n=4$, the corresponding block diagram is shown in the following figure,

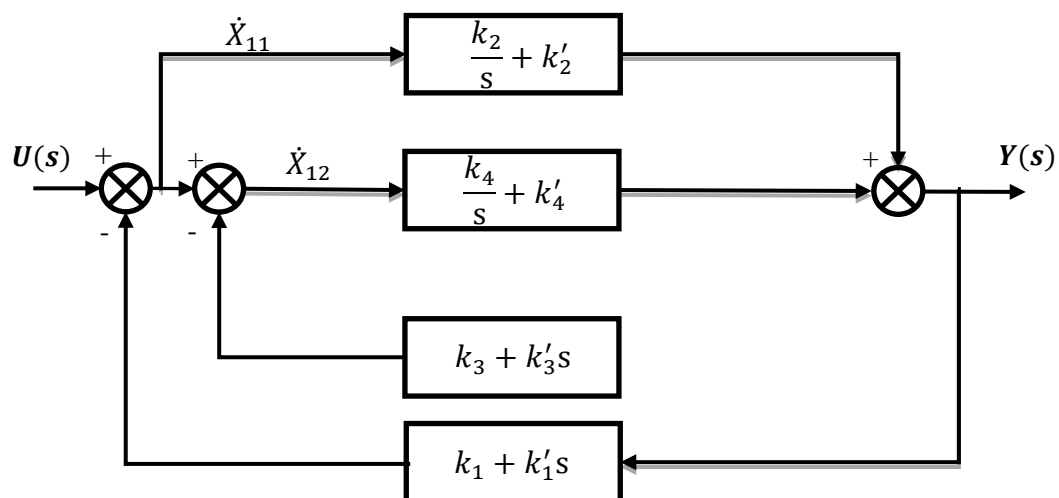


Figure 4.4 Block diagram for $n=4$

$$\dot{X}_{11}(t) = Iu(t) - k_1 y(t) - k'_1 \dot{y}(t) \quad (4.56)$$

$$\begin{aligned} Iy(t) &= k_2 X_{11}(t) + k'_2 \dot{X}_{11}(t) + k_4 X_{12}(t) \\ &\quad + k'_4 \dot{X}_{12}(t) \end{aligned} \quad (4.57)$$

$$\begin{aligned} \dot{I}y(t) &= k_2 \dot{X}_{11}(t) + k'_2 \ddot{X}_{11}(t) + k_4 \dot{X}_{12}(t) \\ &\quad + k'_4 \ddot{X}_{12}(t) \end{aligned} \quad (4.58)$$

Thus,

$$\begin{aligned} \dot{X}_{11}(t) &= Iu(t) - k_1 k_2 X_{11}(t) - k_1 k'_2 \dot{X}_{11}(t) \\ &\quad - k'_1 k_2 \dot{X}_{11}(t) - k'_1 k'_2 \ddot{X}_{11}(t) \\ &\quad - k_1 k_4 X_{12}(t) - k_1 k'_4 \dot{X}_{12}(t) - k'_1 k_4 \dot{X}_{12}(t) \\ &\quad - k'_1 k'_4 \ddot{X}_{12}(t) \end{aligned} \quad (4.59)$$

Similarly, $\dot{X}_{12}(t)$ can be obtained.

$$\begin{aligned} \dot{X}_{12}(t) &= \dot{X}_{11}(t) - k_3 k_4 X_{12}(t) - k_3 k'_4 \dot{X}_{12}(t) \\ &\quad - k'_3 k_4 \dot{X}_{12}(t) - k'_3 k'_4 \ddot{X}_{12}(t) \end{aligned} \quad (4.60)$$

Therefore, combining above two equations,

$$\begin{aligned} X_{12}(t) &= Iu(t) - k_1 k_2 X_{11}(t) \\ &\quad - (k_1 k'_2 + k'_1 k_2) \dot{X}_{11}(t) \\ &\quad - k'_1 k'_2 \ddot{X}_{11}(t) \\ &\quad - (k_1 k_4 + k_3 k_4) X_{12}(t) \\ &\quad - (k_1 k'_4 + k'_1 k_4 + k_3 k'_4 \\ &\quad + k'_3 k_4) \dot{X}_{12}(t) - (k'_1 k'_4 \\ &\quad + k'_3 k'_4) \ddot{X}_{12}(t) \end{aligned} \quad (4.61)$$

By grouping similar terms,

$$\begin{aligned}
& \begin{bmatrix} k'_1 k'_2 & k'_1 k'_4 \end{bmatrix} \begin{bmatrix} \ddot{X}_{11}(t) \\ \ddot{X}_{12}(t) \end{bmatrix} \\
& + \begin{bmatrix} 1 + k_1 k'_2 + k'_1 k_2 & k_1 k'_4 + k'_1 k_4 \end{bmatrix} \begin{bmatrix} \dot{X}_{11}(t) \\ \dot{X}_{12}(t) \end{bmatrix} \\
& + \begin{bmatrix} k_1 k_2 & k_1 k_4 \end{bmatrix} \begin{bmatrix} X_{11}(t) \\ X_{12}(t) \end{bmatrix} = Iu(t)
\end{aligned} \tag{4.62}$$

$$\begin{aligned}
& \begin{bmatrix} k'_1 k'_2 & k'_1 k'_4 + k'_3 k'_4 \end{bmatrix} \begin{bmatrix} \ddot{X}_{11}(t) \\ \ddot{X}_{12}(t) \end{bmatrix} \\
& + \begin{bmatrix} k_1 k'_2 + k'_1 k_2 & 1 + k_1 k'_4 + k'_1 k_4 + k_3 k'_4 + k'_3 k_4 \end{bmatrix} \begin{bmatrix} \dot{X}_{11}(t) \\ \dot{X}_{12}(t) \end{bmatrix} \\
& + \begin{bmatrix} k_1 k_2 & k_1 k_4 + k_3 k_4 \end{bmatrix} \begin{bmatrix} X_{11}(t) \\ X_{12}(t) \end{bmatrix} = Iu(t)
\end{aligned} \tag{4.63}$$

Thus a compact form is showed below,

$$\begin{aligned}
& \begin{bmatrix} k'_1 k'_2 & k'_1 k'_4 \\ k'_1 k'_2 & k'_1 k'_4 + k'_3 k'_4 \end{bmatrix} \begin{bmatrix} \ddot{X}_{11}(t) \\ \ddot{X}_{12}(t) \end{bmatrix} \\
& + \begin{bmatrix} 1 + k_1 k'_2 + k'_1 k_2 & k_1 k'_4 + k'_1 k_4 \\ k_1 k'_2 + k'_1 k_2 & 1 + k_1 k'_4 + k'_1 k_4 + k_3 k'_4 + k'_3 k_4 \end{bmatrix} \begin{bmatrix} \dot{X}_{11}(t) \\ \dot{X}_{12}(t) \end{bmatrix} \\
& + \begin{bmatrix} k_1 k_2 & k_1 k_4 \\ k_1 k_2 & k_1 k_4 + k_3 k_4 \end{bmatrix} \begin{bmatrix} X_{11}(t) \\ X_{12}(t) \end{bmatrix} = Ij(t)
\end{aligned} \tag{4.64}$$

Therefore, the following state-space like matrix equation results,

$$A_1 \ddot{X}(t) + A_2 \dot{X}(t) + A_3 X(t) = Bu(t) \tag{4.65}$$

And the output equation can be obtained as:

$$\begin{bmatrix} k_2 & k_4 \end{bmatrix} \begin{bmatrix} X_{11}(t) \\ X_{12}(t) \end{bmatrix} + \begin{bmatrix} k'_2 & k'_4 \end{bmatrix} \begin{bmatrix} \dot{X}_{11}(t) \\ \dot{X}_{12}(t) \end{bmatrix} = Y(t) \tag{4.66}$$

$$C_1 X(t) + C_2 \dot{X}(t) = Y(t) \tag{4.67}$$

The above results can be generalized to give

$$A_1 \ddot{X}(t) + A_2 \dot{X}(t) + A_3 X(t) = Bu(t) \tag{4.68}$$

$$C_1 X(t) + C_2 \dot{X}(t) = Y(t) \quad (4.69)$$

Where

$$A_1 = \begin{bmatrix} k'_1 k'_2 & k'_1 k'_4 & \cdots & k'_1 k'_n \\ k'_1 k'_2 & (k'_1 + k'_3) k'_4 & \cdots & (k'_1 + k'_3) k'_n \\ \vdots & \vdots & \cdots & \vdots \\ k'_1 k'_2 & (k'_1 + k'_3) k'_4 & \cdots & (k'_1 + \cdots + k'_n) k'_{n-1} \end{bmatrix} \quad (4.70)$$

And A_3 is the same as A_1 except that k'_i should be replaced by k_i where $i = 1, 2, \dots, n$.

$$A_2 = \begin{bmatrix} 1 + k_1 k'_2 + k'_1 k_2 & k_1 k'_4 + k'_1 k_4 & \cdots & k_1 k'_n + k'_1 k_n \\ k_1 k'_2 + k'_1 k_2 & 1 + (k'_1 + k'_3) k_4 + (k_1 + k_3) k'_4 & \cdots & (k'_1 + k'_3) k_n + (k_1 + k_3) k'_n \\ k_1 k'_2 + k'_1 k_2 & (k'_1 + k'_3) k_4 + (k_1 + k_3) k'_4 & \cdots & \vdots \\ \vdots & \vdots & \cdots & \vdots \\ k_1 k'_2 + k'_1 k_2 & (k'_1 + k'_3) k_4 + (k_1 + k_3) k'_4 & \cdots & (k'_1 + \cdots + k'_{n-1}) k'_n + (k_1 + \cdots + k_{n-1}) k'_n \end{bmatrix} \quad (4.71)$$

$$B = \begin{bmatrix} I \\ I \\ \vdots \\ I \end{bmatrix} \quad (4.72)$$

$$C_1 = [k_2 \quad k_4 \quad \cdots \quad k_n] \quad (4.73)$$

$$C_1 = [k'_2 \quad k'_4 \quad \cdots \quad k'_n] \quad (4.74)$$

$$X = \begin{bmatrix} X_{11} \\ X_{12} \\ \vdots \\ X_{1,n/2} \end{bmatrix} \quad (4.75)$$

$$\text{Where } X_{11} = \begin{bmatrix} X_1 \\ X_2 \\ \vdots \\ X_m \end{bmatrix}, X_{12} = \begin{bmatrix} X_{m+1} \\ X_{m+2} \\ \vdots \\ X_{2m} \end{bmatrix}, \dots, X_{1,n/2} = \begin{bmatrix} X_{(n-1)m+1} \\ X_{(n-1)m+1} \\ \vdots \\ X_{nm/2} \end{bmatrix}$$

In order to represent Equation (4.68) and (4.69) in the usual state-space form,

first let

$$X(t) = P_1(t) \quad (4.76)$$

$$\dot{P}_1(t) = P_2(t) \quad (4.77)$$

Thus,

$$\ddot{X}(t) = \ddot{P}_1(t) = \dot{P}_2(t) \quad (4.78)$$

$$\dot{X}(t) = \dot{P}_1(t) = P_2(t) \quad (4.79)$$

Hence, after a little algebra, the state-space expression can be obtained as below:

$$\begin{aligned} \begin{bmatrix} \dot{P}_1(t) \\ \dot{P}_2(t) \end{bmatrix} &= \begin{bmatrix} 0 & 1 \\ -A_1^{-1}A_3 & -A_1^{-1}A_2 \end{bmatrix} \begin{bmatrix} P_1(t) \\ P_2(t) \end{bmatrix} \\ &+ \begin{bmatrix} 0 \\ -A_1^{-1}B \end{bmatrix} u(t) \end{aligned} \quad (4.80)$$

Also, A_1^{-1} exists provided that $|K_i| \neq 0$ for all i 's.

The Cauer third form gives a good approximation for both the transient and the steady state responses. This is easily seen by means of the initial and final value theorems, namely,

$$\lim_{t \rightarrow \infty} [Y(t)] = \lim_{s \rightarrow 0} [sH(s)U(s)] \Big|_{\left(\frac{1}{s}I=U(s)\right)} = K_1^{-1} \quad (4.81)$$

$$\lim_{t \rightarrow 0} [Y(t)] = \lim_{s \rightarrow \infty} [sH(s)U(s)] \Big|_{(I=U(s))} = (K_1')^{-1} \quad (4.82)$$

Equation (4.81) shows that K_1 dominates the steady-state response while

Equation (4.82) shows that K_1' dominates the initial response. Therefore, the first approximation $K_1 + K_1'$ is the most important one, which implies that to obtain a reduced model, the inner terms in the block diagram representation of the Cauer third form can be discarded, starting with the one corresponding to n.

4.5 Model Reduction for Two-wheeled Self-balancing Scooter

From Chapter 3, the matrices for the state space function of the two-wheeled self-balancing scooter has been obtained as the expression below:

$$A = \begin{bmatrix} \frac{\dot{\theta}_0^2 - \frac{2m_b r_b \dot{x}_0 \dot{\theta}_0 + m_b g r_b \cos \beta}{I_b + 2m_b r_b^2}}{2m_w + 2I_w \frac{1}{r^2} + m_b} - \frac{2m_b r_b}{I_b + 2m_b r_b^2} & 0 & 0 \\ 0 & 0 & 0 \\ 1 & 0 & 0 \\ 0 & 0 & 0 \\ \dot{x}_0 \dot{\theta}_0 + \frac{g}{2} \cos \beta - \frac{m_b r_b \dot{\theta}_0^2}{2m_w + 2I_w \frac{1}{r^2} + m_b} & 0 & 0 \\ \frac{I_b + 2m_b r_b^2}{2m_b r_b} - \frac{m_b r_b}{2m_w + 2I_w \frac{1}{r^2} + m_b} & 0 & 0 \\ 0 & 0 & 0 \\ 0 & 0 & 1 \\ 0 & 0 & 0 \\ 0 & 0 & 0 \end{bmatrix} \quad (4.83)$$

B

$$= \begin{bmatrix} 2 \frac{\zeta \cdot \eta_t}{r_w} \frac{-\frac{1}{m_b r_b}}{2m_w + 2I_w \frac{1}{r^2} + m_b} - \frac{2m_b r_b}{I_b + 2m_b r_b^2} & (2m_w + m_b) \frac{-\frac{1}{m_b r_b}}{2m_w + 2I_w \frac{1}{r^2} + m_b} - \frac{2m_b r_b}{I_b + 2m_b r_b^2} \\ 0 & \frac{1}{2m_w + 2I_w \frac{1}{r^2} + m_b} \\ 0 & 0 \\ 0 & 0 \\ 0 & 2 \frac{\zeta \cdot \eta_t}{r_w} \frac{\frac{1}{I_b + 2m_b r_b^2} - \frac{m_b r_b}{2m_w + 2I_w \frac{1}{r^2} + m_b}}{2m_b r_b} & (2m_w + m_b) \frac{-\frac{1}{m_b r_b}}{I_b + 2m_b r_b^2} - \frac{m_b r_b}{2m_w + 2I_w \frac{1}{r^2} + m_b} \\ \frac{1}{L_a} & 0 \\ 0 & 0 \\ 0 & 0 \\ 0 & 0 \\ 0 & 0 \end{bmatrix} \quad (4.84)$$

$$C = [1 \quad 0 \quad 0 \quad 0 \quad 0 \quad 0] \quad (4.85)$$

In the expression for those matrices, there are several repeating elements.

Thus they can be further simplified. Denoting

$$2m_w + 2I_w \frac{1}{r^2} + m_b = M \quad (4.86)$$

$$I_b + 2m_b r_b^2 = M_b \quad (4.87)$$

$$m_b r_b = T_b \quad (4.88)$$

$$2m_w + m_b = W \quad (4.89)$$

$$\frac{\zeta \cdot \eta_t}{r_w} = R \quad (4.90)$$

As a result,

A

[illegible]

$$B = \begin{bmatrix} 0 & -\frac{2R}{T_b} & -\frac{W}{T_b} \\ 0 & \frac{M}{T_b} - \frac{2T_b}{M_b} & \frac{M}{T_b} - \frac{2T_b}{M_b} \\ 0 & 0 & 0 \\ 0 & -\frac{2R}{M} & -\frac{W}{M} \\ 1 & \frac{M_b}{2T_b} - \frac{T_b}{M} & -\frac{M_b}{2T_b} - \frac{T_b}{M} \\ \frac{1}{L_a} & 0 & 0 \\ 0 & 0 & 0 \\ & 0 & 0 \\ & 1 & 0 \\ & J & 0 \end{bmatrix} \quad (4.92)$$

In order to use Routh approximation for such system, the transfer function should be represented at first. Through the Matlab software, the transfer function can be obtained as below:

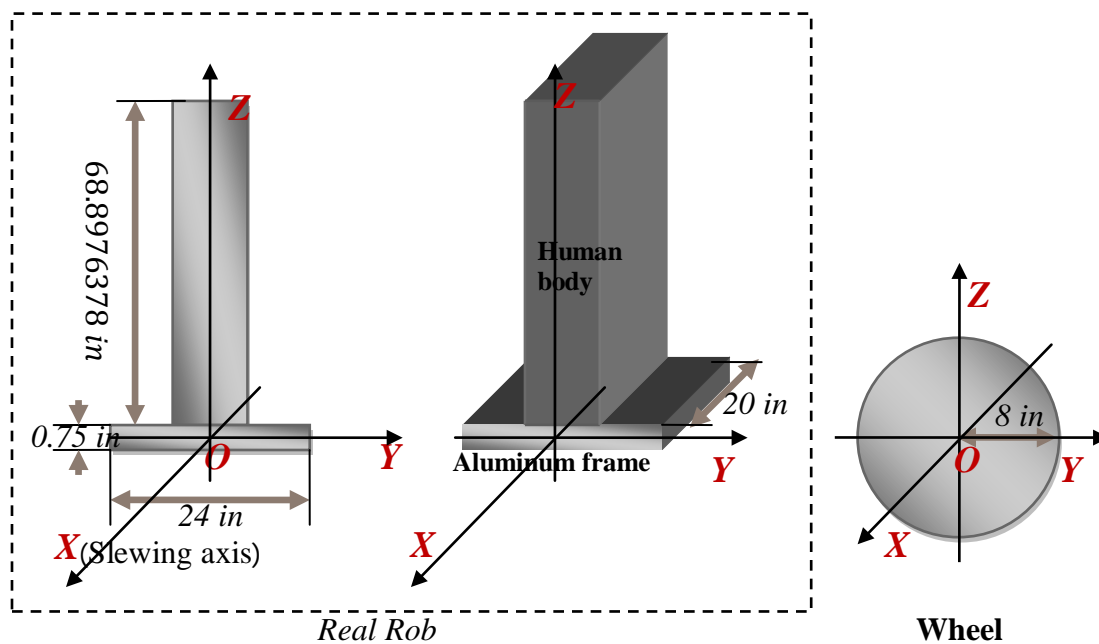
$$H(s) = \frac{0, (2*r*tb*(-mb*dtheta0^2 + 2*dx0*tb*dtheta0 + g*tb*cos(beta)))/(m*(tb/m - mb/(2*tb)))*(-2*dtheta0^2*s*tb^2 + 2*dx0*m*dtheta0*s*tb + 2*s^3*tb^2 - m*mb*s^3 + g*m*cos(beta)*s*tb)) - (2*r)/(s*tb*(m/tb - (2*tb)/mb)), (tb*w*(-mb*dtheta0^2 + 2*dx0*tb*dtheta0 + g*tb*cos(beta)))/(m*(tb/m - mb/(2*tb)))*(-2*dtheta0^2*s*tb^2 + 2*dx0*m*dtheta0*s*tb + 2*s^3*tb^2 - m*mb*s^3 + g*m*cos(beta)*s*tb)) - w/(s*tb*(m/tb - (2*tb)/mb))}{}$$

$$\frac{r \cdot \#1^2}{\#2} - \frac{w \cdot \#1}{\#2}$$

where

$$\begin{aligned} \#1 &= -4 dtheta0^2 mb tb^2 + 2 dx0 m dtheta0 mb tb + 4 dx0 dtheta0 tb^3 - m mb s^2 + 2 mb s^2 tb \\ &\quad + g m cos(beta) mb tb + 2 g cos(beta) tb^3 \\ \#2 &= s (m mb - 2 tb^2) (-2 dtheta0^2 tb^2 + 2 dx0 m dtheta0 tb + 2 s^2 tb^2 - m mb s^2 + g m cos(beta) tb) \end{aligned}$$

4.6 Determination of scooter parameters



4.5 Real structure and dimensions of rob and wheels (side views)

Table 4.5 Scooter Parameters

Average height of human body Z_h	$1.75\text{ m}=5.7414698\text{ ft}$
Height of aluminum frame Z_f	$0.75\text{ in}=0.0625\text{ ft}$
Width of aluminum frame X_f	$20\text{ in}=1.6666667\text{ ft}$
Length of aluminum frame Y_f	$24\text{ in}=2\text{ ft}$
Radius of wheel r_w	$8\text{ in}=0.6666667\text{ ft}$
Density of aluminum D_f	$2.7\text{ g/cm}^3=0.0972\text{ lb/in}^3$

Weight of wheels m_w	10 lb
Weight of motor m_m	15 lb
Average weight of human body m_H	150 lb
the moment of inertia for the wheels I_w	$I_w = \frac{1}{2} m_w r^2 = 0.5 \times 10 \times 0.6666667 \times 0.6666667 = 2.2222 lb \cdot ft^2$
Distance between center of mass m_b and center of wheel r_b	$Z_h/2$

The rob part in Figure 4.5 composed of four parts: the human body, the aluminum frame and the two motors in real case. So the moment of inertia for the rob equals to the sum of the four moments, whose slewing axis is OX. The next step is to calculate the moment of inertia about the OX of the whole parts.

For simplified case, the weight of motors and the frame are considered to be homogeneous distributed in the frame. Then they can be taken as a cubic of $0.75 \times 20 \times 24 \text{ in}^3$.

$$m_f = 0.0792 \times 0.75 \times 24 \times 20 = 28.5120 \text{ lb} \quad (4.93)$$

So the total weight of their part is calculated as:

For this total frame, its moment of inertia about OX axis is as below:

$$\begin{aligned} m_F &= m_f + m_m = 28.5120 + 15 \times 2 \\ &= 58.5120 \text{ lb} \end{aligned} \quad (4.94)$$

$$\begin{aligned}
I_F &= \frac{1}{3} m_F (X_f/2)^2 \\
&= \frac{1}{3} \times 58.2150 \times \left(\frac{1.6666667}{2}\right)^2 \\
&= 13.4757 \text{ lb} \cdot \text{ft}^2
\end{aligned} \tag{4.95}$$

For the human body part, the height of center of gravity is roughly taken as half of the human body height. Then its moment of inertia can be got as below:

$$\begin{aligned}
I_H &= I_G + m_H \cdot (Z_h/2)^2 \\
&= \frac{1}{3} m_H (Z_h/2)^2 + m_H \cdot (Z_h/2)^2 \\
&= \frac{1}{3} \times 150 \times \left(\frac{5.7414698}{2}\right)^2 + 150 \\
&\quad \times \left(\frac{5.7414698}{2}\right)^2 \\
&= 1648.2 \text{ lb} \cdot \text{ft}^2
\end{aligned} \tag{4.96}$$

From the above result, the total moment of inertia for the rob system can be derived, and the expression $I + mR^2$ in the former equation can be calculated as:

$$\begin{aligned}
I_b &= I_H + I_F = 13.4757 + 1648.2 \\
&= 1661.7 \text{ lb} \cdot \text{ft}^2
\end{aligned} \tag{4.97}$$

$$\begin{aligned}
m_b &= m_H + m_b = 58.5120 + 150 \\
&= 208.5120 \text{ lb}
\end{aligned} \tag{4.98}$$

$2m_w + 2I_w \frac{1}{r^2} + m_b = M$	$2 \times 10 + 2 \times \frac{320}{8^2} + 208.5120 =$ 238.5120
---------------------------------------	--

$I_b + 2m_b r_b^2 = M_b$	$1661.7 + 2 \times 208.5120$ $\times \left(\frac{5.7414698}{2} \right)^2$ $= 5098.4$
$m_b r_b = T_b$	$208.5120 \times 5.7414698 = 1197.2$
$2m_w + m_b = W$	$2 \times 10 + 208.5120 = 228.5120$
$\frac{\zeta \cdot \eta_t}{r_w} = R$	$20 \times \frac{0.95}{0.6666667} = 28.5$

$$\begin{aligned}
H(s) = & [0, (12765219825 * ((9628481 * \cos(\beta)) / 250 + (11972 * d\theta_0 * dx_0) / 5 \\
& - (25492 * d\theta_0^2 / 5)) / (128948914 * ((143531766267 * s * \cos(\beta)) / 15625 - \\
& (71664392 * d\theta_0^2 * s) / 25 + (1031591312 * s^3) / 625 + \\
& (356933208 * d\theta_0 * dx_0 * s) / 625)) + 45407625 / (257897828 * s), \\
& (127938855818 * ((9628481 * \cos(\beta)) / 250 + (11972 * d\theta_0 * dx_0) / 5 - \\
& (25492 * d\theta_0^2 / 5)) / (322372285 * ((143531766267 * s * \cos(\beta)) / 15625 - \\
& (71664392 * d\theta_0^2 * s) / 25 + (1031591312 * s^3) / 625 + \\
& (356933208 * d\theta_0 * dx_0 * s) / 625)) + 45509593 / (64474457 * s)]
\end{aligned}$$

Making $d\theta_0 = 0.1, dx_0 = 0.5 \text{ ft/s}^2$ and $\beta = 0$,

$$\begin{aligned}
H(s) = & [0, 985032272666469 / (257897828 * ((1031591312 * s^3) / 625 + \\
& (143530030327 * s) / 15625)) + 45407625 / (257897828 * s), \\
& 123405534370372897 / (8059307125 * ((1031591312 * s^3) / 625 + \\
& (143530030327 * s) / 15625)) + 45509593 / (64474457 * s)]
\end{aligned}$$

Thus the corresponding Routh table can be built.

α (Routh) Table

	$a_0^0 = 1.6628e + 18$	$a_2^0 = 0$
	$a_0^1 = 9.2541e + 18$	$a_2^1 = 0$
$\alpha_1 = \frac{a_0^0}{a_0^1} = 0.1797$	$a_0^2 = a_2^0 - \alpha_1 a_2^1 = 0$	$a_2^2 = a_4^0 - \alpha_1 a_4^1$
$\alpha_2 = a_0^1/a_0^2$	$a_0^3 = a_2^1 - \alpha_2 a_2^2$	$a_2^3 = a_4^1 - \alpha_2 a_4^2$

CHAPTER 5. SIMULATION, EXPERIMENT AND CONCLUSION

5.1 Simulation and experiment

Evaluation of the control design based on the modeling is required to make sure the practical application on real system. Figure 5.1 shows the inside structure of the two-wheeled self-balancing scooter. The wheels integrated with motor are installed in the middle of the scooter body. In the front side of the scooter body, the micro-controller lies in the middle with 4 modules installed. The two drives are installed at the back of the body on each side to provide current for the motors. There are basically two types of batteries are used, rechargeable battery in the middle of the drivers supplies the power in order to drive the system and 5 volt battery to support the usage of sensors and the modules in microcontroller.

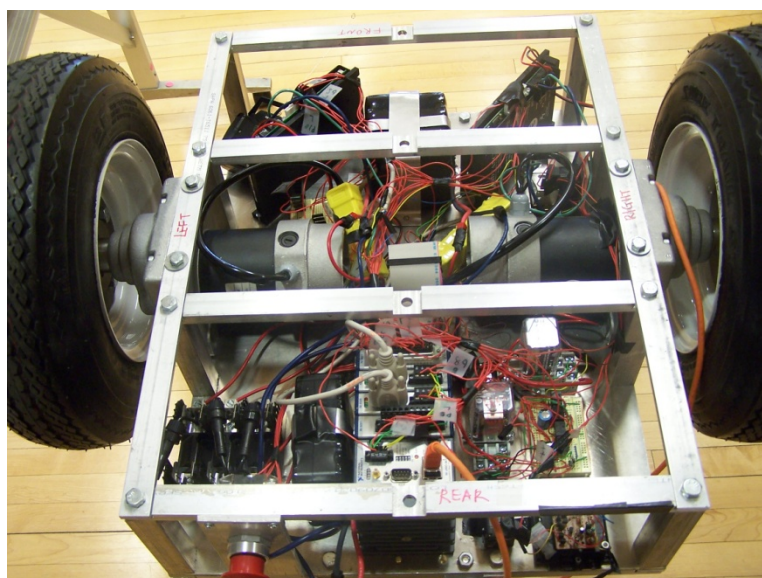


Figure 5.1 Inside structure of two-wheeled self-balancing scooter

The programming for such system can be design in Labview software, and from Figure 5.2 to Figure 5.7 give a brief view about this software. Labview has control panel and program panel, integrating the communication between the sensors and its FPGA modules.

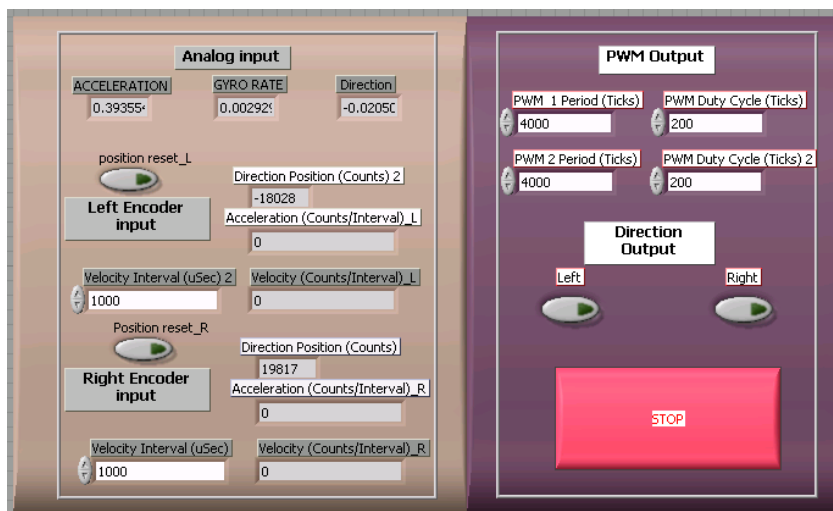


Figure 5.2 Scooter FPGA program panel on Labview

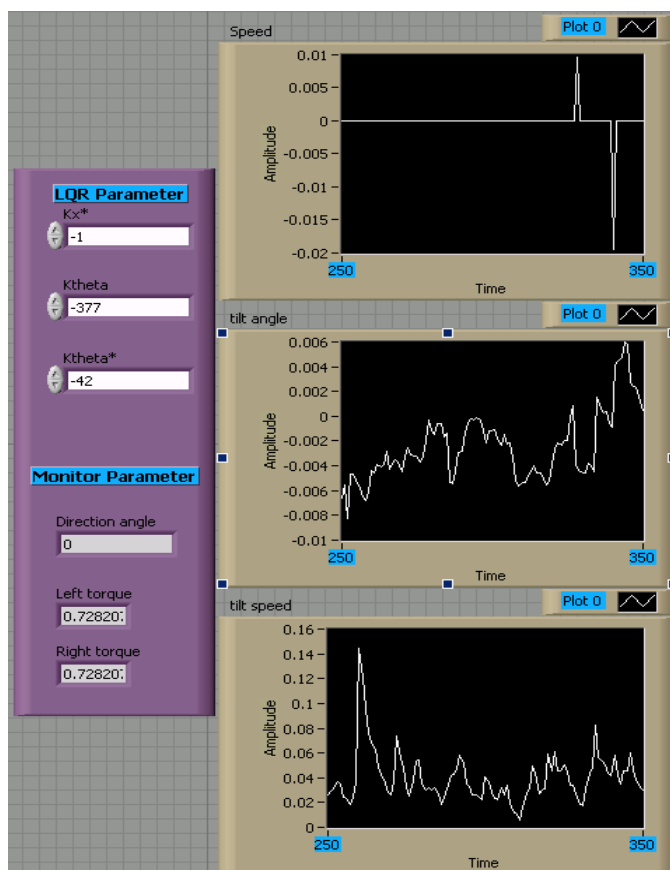


Figure 5.3 Scooter host program panel

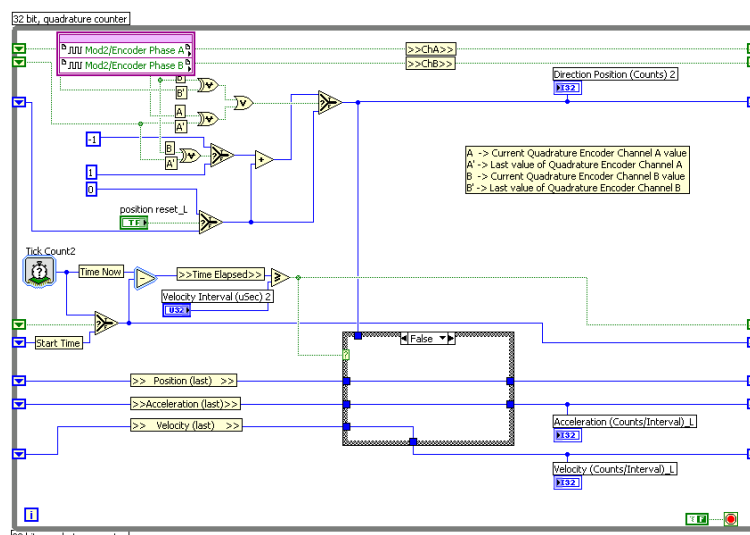


Figure 5.4 Encoder for wheels

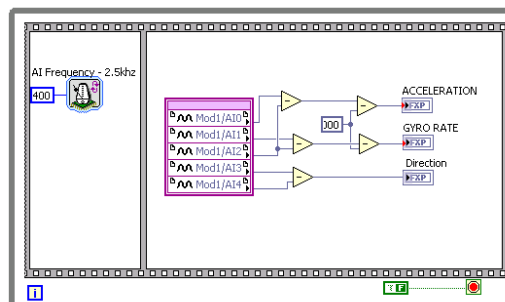


Figure 5.5 Gyro rate and acceleration input

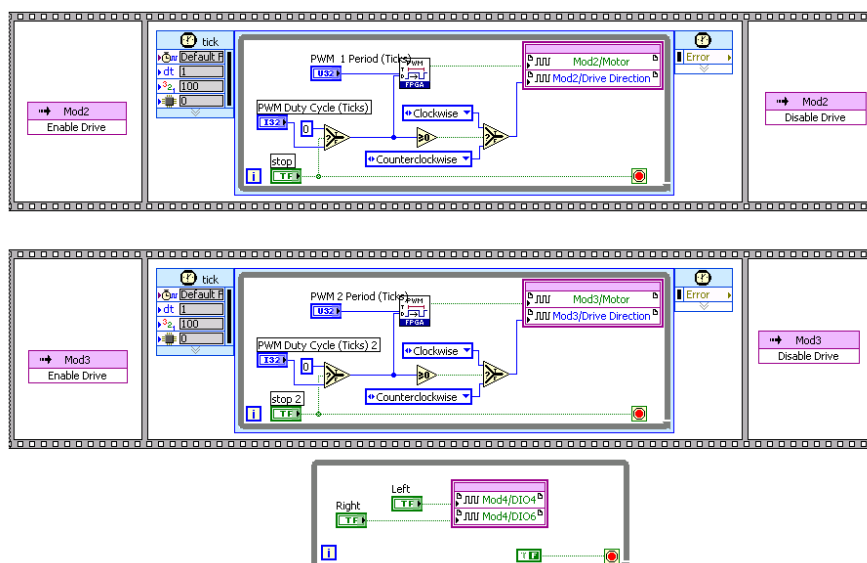


Figure 5.6 PWM output

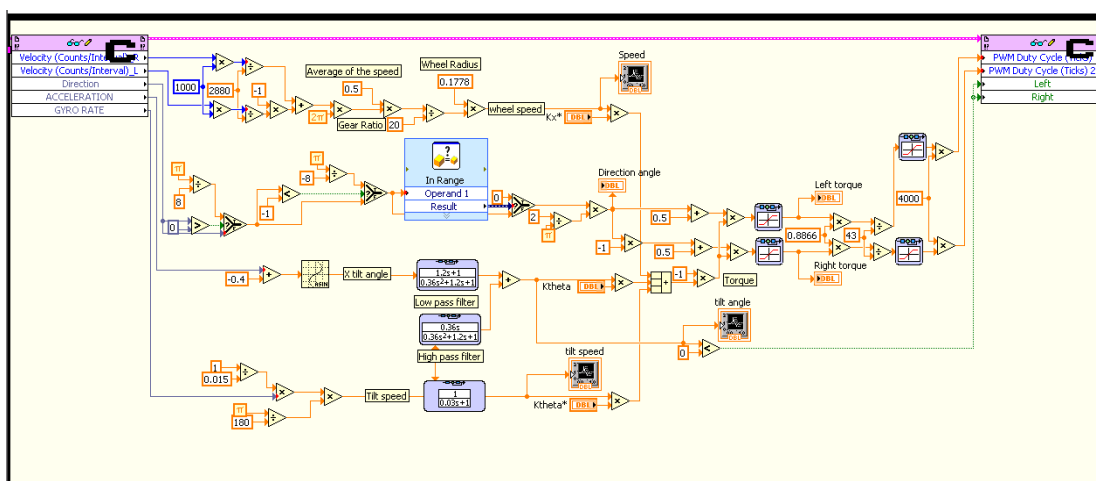


Figure 5.7 Host program block digram



Figure 5.8 Riding on the scooter

The Labview software is downloaded into the memory of the compactRio microprocessor, which enables the offline control for the scooter. Human can stand on it to ride for the experimental test, which is accomplished by applying the mathematical model built from previous chapter.

There are two aspects to be discussed from the result of such experiment. Firstly, the scooter shows a perfect decision making ability on the direction control required from the Tai Chi pose. Secondly, the response time is longer than predicted from simulation result.

5.2 Conclusion

From the experiment on the real mechatronic system, the simplified model of two-wheeled self-balancing scooter is proved to be applicable. But there are some problems need to be solved in future implementation of the system.

First of all, the battery life is too short to make long-term run for the system. The current battery can only support the system for only 20 minutes.

Secondly, although the scooter can response in the right direction, it always takes a delay of several seconds to activate the motor to drive. One of the reasons for this is because the largest torque the motor can provide is very limited to have enough power to drive a full load system. Thus during the design process of the system, corresponsive compensate should be made, such as using light weight material for body framing and optimization of the layouts of the physical element in the body.

Furthermore, the speed limitation for the scooter should be set by programme safety consideration.

At last, data acquisition system or programming should be implemented in order to make detailed real-time data analysis to understand more of the system.

For future work, the scooter should be equipped with more powerful motors, and the structure design and material selection of the physical framing system needs to be optimized. Real time data from physical system should be collected to make further analysis.

LIST OF REFERENCES

LIST OF REFERENCES

- Giurgiutiu, V. & Lyshevski, S.E. (2009). *Micromechatronics: Modeling, Analysis, and Design with Matlab*. CRC Press.
- Wellstead, P. (2005). *Introduction to physical system modeling*. Retrieved from <http://www.control-systems-principles.co.uk/>.
- Friedland, B. (1986). *Control system design* McGraw-Hill.
- Isermann, R. (2003). *Mechatronic systems fundamentals*. Springer.
- Strelow, D. & Singh, S. (2004). Motion estimation from image and inertial Measurements. *The International Journal of Robotics Research*, 23, 1157.
- Nasrallah, D., Michalska, H. & Angeles, J. (2007). Controllability and posture control of a wheeled pendulum moving on an inclined plane. *IEEE Transactions on Robotics*, 23(3).
- Hu, J. & Tsai, M. (2008). Design of robust stabilization and fault diagnosis for an auto-balancing two-Wheeled cart. *Advanced Robotics*, 22, 319–338.
- Kim, Y., Kim, S.H. & Kwak, Y. (2005). Dynamic analysis of a nonholonomic two-wheeled inverted pendulum robot. *Journal of Intelligent and Robotic Systems*, 44, 25–46.
- Wai R. (2006). Adaptive stabilizing and tracking control for a nonlinear inverted-pendulum system via sliding-mode technique. *IEEE Transactions on Industrial Electronics*, 53(2).
- Kim, Y., Kim, S.H. & Kwak, Y. K. (2006). Improving driving ability for a two-wheeled inverted-pendulum-type autonomous vehicle. *Proc. IMechE*, 220.
- Huang, L. (2005). Speed control of differentially driven wheeled mobile robots—model-based adaptive approach. *Journal of Robotic Systems*, 22(6), 323–332.
- Wai, R.J. (2006). Stabilizing and tracking control of nonlinear dual-Axis inverted-pendulum system using fuzzy neural network. *IEEE Transactions on Fuzzy Systems*, 14(1).

- Kugi, A. (2009). Some basics in modeling of mechatronic systems. *Control Systems, Robotics and Automation*, IV.
- Janardhanan, S. (2014). *Model order reduction and controller design techniques*. Retrieved from http://www.researchgate.net/publication/236166577_Model_Order_Reduction_and_Controller_Design_Techniques.
- Grasser, F., D'Arrigo, A. & Colombi, S. (2002). JOE: A mobile, inverted pendulum. *IEEE Transactions on Industrial Electronics*, 49(1).
- Wai, R.J. and Chang, L.J. (2006). Adaptive stabilizing and tracking control for a nonlinear Inverted-pendulum system via sliding-mode technique. *IEEE Transactions on Industrial Electronics*, 53(2).
- Jung, S. (2008). Control experiment of a wheel-driven mobile inverted pendulum using neural network *IEEE Transactions on Control Systems Technology*, 16(2).
- Nasrallah, D.S., Michalska, S. and Angeles, J. (2007). Controllability and posture control of a wheeled pendulum moving on an inclined plane, *IEEE Transactions on Robots*, 23(3).
- Awtar, S., King, N., Allen, T., Bang, I., Hagan, M., Skidmore, D., & Craig, K. (2002). Inverted pendulum systems: rotary and arm-driven-a mechatronic system design case study. *Mechatronics*, 12(2), 357-370.
- Antoulas, A.C., Sorensen, D.C. and Gugercin, S. (2001). A survey of model reduction methods for large-scale systems. *Contemporary Mathematics*, 280, 193-291.
- Hu, J.S. & Tsai, M.C. (2008). Design of robust stabilization and fault diagnosis for an auto-balancing two-wheeled cart, *Advanced Robotics*, 22, 319-338.
- Jung, S. & Kim, S.S. (2007). Hardware implementation of a real-Time neural network controller with a DSP and an FPGA for nonlinear systems. *IEEE Transactions on Industrial Electronics*, 54(1).
- Kim, Y., Kim, S. H. & Kwak, Y. K. (2006). Improving driving ability for a two-wheeled inverted-pendulum-type autonomous vehicle Proc. *J. Automobile Engineering*, 220.
- Filippa, M., Mi, C., Shen, J., & Stevenson, R. C. (2005). Modeling of a hybrid electric vehicle powertrain test cell using bond graphs. *Vehicular Technology, IEEE Transactions on*, 54(3), 837-845.
- Otter, M., & Grübel, G. (1993). Direct physical modeling and automatic code generation for mechatronics simulation. In *2nd Conference on Mechatronics and Robotics. Duisburg, 27-29 September, IMECH*.

- Mahfouz, A. A., Mohammed, M. K., & Salem, F. A. (2013). Modeling, simulation and dynamics analysis issues of electric motor, for mechatronics applications, using different approaches and verification by MATLAB/Simulink. *International Journal of Intelligent Systems and Applications (IJISA)*, 5(5), 39.
- Zi, B., Duan, B. Y., Du, J. L., & Bao, H. (2008). Dynamic modeling and active control of a cable-suspended parallel robot. *Mechatronics*, 18(1), 1-12.
- Kim, M. S., Shin, J. H., Hong, S. G., & Lee, J. J. (2003). Designing a robust adaptive dynamic controller for nonholonomic mobile robots under modeling uncertainty and disturbances. *Mechatronics*, 13(5), 507-519.
- Van Beek, T. J., Erden, M. S., & Tomiyama, T. (2010). Modular design of mechatronic systems with function modeling. *Mechatronics*, 20(8), 850-863.
- Kim, D.H. & Oh, J.H. (1999). Tracking control of a two-wheeled mobile robot using input-output linearization. *Control Engineering Practice*, 7, 369-373.
- Jung, S, Cho, H.T. & Hsia, T. C. (2007). Neural network control for position tracking of a two-axis inverted pendulum system: experimental studies. *IEEE Transactions on Neural Networks*, 18(4).
- TSAI, M.C. & HU, J.S. (2007). Pilot control of an auto-balancing two-wheeled cart. *Advanced Robotics*, 21(7), 817-827.
- Saifizul, A.A., Zainon, IZ. & Osman, N.A. (2006). Intelligent control for self-erecting inverted pendulum via adaptive neuro-fuzzy Inference system. *American Journal of Applied Sciences* 3 (4), 1795-1802.
- Huang, L. (2005). Speed control of differentially driven wheeled mobile robots—model-based adaptive approach. *Journal of Robotic Systems*, 22(6), 323-332.
- Yap, W. & Karri, Y. (2008). Modeling and simulation of a hybrid scooter. *Proceedings of World Academy of Science*, 2.
- Hang, H. J. L. (2005). Modeling and control simulation of developed coaxial two-wheeled electric scooter. *China Mechanical Engineering*, 8.
- Wai, R.J. & Chang, L.J. (2006). Stabilizing and tracking control of nonlinear dual-Axis inverted-pendulum system using fuzzy neural network. *IEEE Transactions on Fuzzy Systems*, 14(1).
- Hopkins, M.A. (2007). Improved selection of state-weighting matrices for LQR MIMO-controller design. *Intelligent Systems and Control*.
- Ouyang, P. R., Li, Q., Zhang, W. J., & Guo, L. S. (2004). Design, modeling and control of a hybrid machine system. *Mechatronics*, 14(10), 1197-1217.

- Gilbert, M. G., & Horner, G. C. (1998, June). Actuator concepts and mechatronics. *In 5th Annual International Symposium on Smart Structures and Materials* (pp. 214-222). International Society for Optics and Photonics.
- Weustink, P. B. T., De Vries, T. J. A., & Breedveld, P. C. (1998). Object-oriented modeling and simulation of mechatronic systems with 20-sim 3.0. *Mechatronics*, 98, 873-787.
- Emadi, A., Gao Y. and Ehsan M. (2009). *Modern Electric, Hybrid Electric, and Fuel Cell Vehicles*. CRC Press.
- Olson, B.J. (2001). *Nonlinear Dynamics of Longitudinal Ground Vehicle Traction*. Retrieved from http://www.egr.msu.edu/dvrl/pubs/Olson_MS01.pdf
- Zoroofi, S. (2008). *Modeling and Simulation of Vehicular Power Systems*. Retrieved from <http://citeseerx.ist.psu.edu/viewdoc/download?doi=10.1.1.518.450&rep=rep1&type=pdf>

VITA

VITA

Qiong Li received her master degree in Mechatronics in Beihang University, China in April, 2006. After that she went to Purdue graduate school to pursue Ph.D. degree.

At first she studied product lifecycle management for 2 years, later on she changed her interest of research by focusing on mathematical modeling and control design for mechatronic system.

Moreover, she also worked as a TA in college of technology, in charge of the labs for Controls and instrumentation for automation class and Materials and Processes.

Upon receiving her Ph.D. from Purdue University in May 2015, she will work in industry field as an engineer.